UNIVERSITY OF READING

Department of Meteorology

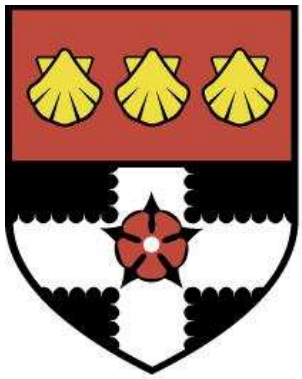

Why can't models simulate mixed-phase clouds correctly?

ANDREW BARRETT

A thesis submitted for the degree of Doctor of Philosophy

June 2012

DECLARATION

I confirm that this is my own work and the use of all material from other sources has been properly and fully acknowledged.

Andrew Barrett

ABSTRACT

Motivated by the importance of clouds for weather and climate due to their radiative impact, this thesis addresses the current poor representation of thin, stratiform mixed-phase clouds by state-of-the-art numerical weather prediction (NWP) models. Due to the supercooled liquid water present at cold temperatures near the cloud top, mixed-phase clouds strongly influence the amount of solar radiation reaching the surface and have a net cooling effect on the climate.

Supercooled liquid water content is underestimated, by a factor of 2 or more, in all 5 NWP models tested and ERA-Interim when compared with ground-based remote-sensing observations of mixed-phase clouds. The ice water content is better predicted, but ice cloud fraction is underestimated. A new ice cloud fraction parameterization is developed to correct this bias, based on radar observations.

EMPIRE, a new high-resolution single column model is developed and used to determine the most important processes for maintaining mixed-phase clouds. It is found that altering the model specification of ice particles (size, fall speed, concentration or habit) affected the liquid water content and most also affect the ice water content. A key reason why models underestimate liquid is an overestimate of ice growth rate but parameterizing N_0 as a function of ice water content based on aircraft measurements leads to a significant improvement.

A strong sensitivity to the model vertical resolution is identified. At coarse resolutions EMPIRE produces less than 2% of the liquid water content of high resolution simulations. This is because the coarse resolution model does not resolve the vertical profile of temperature, liquid and ice near the cloud top. By adding a parameterization of the vertical structure of the upper part of the cloud, the resolution sensitivity is largely removed suggesting that the implementation of such a parameterization in NWP models could improve their simulation of mixed-phase clouds.

ACKNOWLEDGEMENTS

There are many people to whom I owe thanks for their professional and/or personal input to my thesis. Firstly, I show my gratitude to my two supervisors **Robin Hogan** and **Richard Forbes** for their enthusiasm, help, support and guidance throughout the course of my work. I have thoroughly enjoyed working with both and hope to continue to do so in the future.

I also owe thanks to **Chris Westbrook** for interesting discussions about mixed-phase clouds and cloud microphysics, **Jon Shonk** for his understanding of radiative transfer and **Rob Thompson** and **Ewan O'Connor** for their MATLAB expertise.

I am very grateful to **Roel Neggers** for providing the ERA-Interim forcing dataset, without which much of the work for this thesis would not be possible, and to **Martin Kohler** for assisting me in understanding how to use it. I am also thankful to everybody working at **Chilbolton** who maintain the instruments that give us a dataset of cloud observations.

There are many other people in the department with whom I have interacted with for work or social purposes, but particularly the members of **2U06**, **radar group**, **the department cricket team** and **Abi van der Linden**, **Dan Peake**, **Dirk Cannon** and **Kim Bartholomew** for providing both welcome and unwelcome distractions.

- Andrew Barrett - June 2012

Contents

CHAPTER 1:
INTRODUCTION

1.1 Motivation

Clouds are unquestionably an important part of the weather that we experience. Their presence affects the amount of sunlight reaching the surface, and thus alters near-surface temperature as well as the liklihood of precipitation. For this reason it is important to understand clouds and cloud processes, their global coverage and their radiative impact. It is also important that these are all accurately predicted by numerical weather and climate prediction models if their output is to be believed.

From a climate perspective it is important to correctly simulate the radiative impact of clouds but not necessarily the clouds themselves. Because clouds interact with both solar (shortwave) and terrestrial (longwave) radiation they strongly modulate the amount of energy reaching the surface and leaving the atmosphere. During the day clouds reflect some of the incoming shortwave radiation and always, though most notably at night, they trap longwave radiation near the Earth's surface keeping it warm. There are considerable uncertainties in how clouds will change as the planet warms and comparisons of numerous climate simulations suggest that cloud feedbacks are the largest single cause of inter-model variability in predicted climate scenarios during CMIP3 (Dufresne and Bony, 2008; Bony et al., 2006) and this continues to be the case in CMIP5 (Andrews et al., 2012).

Mixed-phase clouds are those that contain both liquid and ice. There are multiple types of mixed-phase clouds which include convective, frontal, and layer clouds. Convective clouds are often mixed-phase with large liquid water contents in the main updraft and ice particles, or even hail, forming at higher altitudes and falling back through the cloud. Frontal clouds may contain both liquid and ice in a similar way (e.g. Hogan et al., 2002). If the large-scale ascent along the frontal surface is strong enough a whole layer of air may be brought to liquid saturation and ice

may form in this layer or higher in the cloud as the liquid gets advected to colder temperatures. On fronts with weaker ascent, not sufficient to bring air to liquid saturation, mixed-phase regions may still exist due to embedded regions of turbulence which locally give enough ascent to form liquid water within an otherwise ice cloud. Mixed-phase layer clouds exist in the Arctic boundary layer (e.g. Morrison et al., 2012) and in the mid-levels of the atmosphere at mid-latitudes as well as in the tropics (Riihimaki et al., 2012). Cloud systems are often complex and can contain multiple types of mixed-phase clouds, such as reported in Crosier et al. (2011).

This thesis is concentrated on mixed-phase, mid-level altocumulus clouds which are unusual in that they comprise a thin layer of liquid water a few hundred metres deep with ice particles falling beneath this layer (e.g. Rauber and Tokay, 1991). This means that the liquid water occupies the coldest part of the cloud and ice is present at warmer temperatures, contrary to our expectation that the amount of liquid water present in the atmosphere will be less at colder temperatures. These clouds are similar to those observed in the Arctic boundary layer, differing only in that they are physically distant from the surface and therefore unaffected by surface processes such as heat fluxes and their associated turbulence. Additionally their existence for many hours or sometimes days (e.g. Marsham et al., 2006; Shupe, 2011; Morrison et al., 2012) is unexpected as growth of ice by the Wegener-Bergeron-Findeison process would quickly remove the small liquid water contents of these clouds.

Stratiform mixed-phase clouds have a net cooling effect on the climate system (Hogan et al., 2003a) because of their structure and because of their lifetime and large areal extent their effect may be large. However, they are poorly simulated by current numerical weather and climate prediction models (Marsham et al., 2006). It is therefore likely that this cooling effect is mis-represented by climate models. The way in which mixed-phase clouds are prescribed in climate models has been shown to be important (e.g. Mitchell et al., 1989; Senior and Mitchell, 1993) and can significantly change the climate sensitivity of the models. As these clouds have the potential to be important in the climate system then they should be included correctly in numerical models.

1.2 Stratiform mixed-phase clouds

1.2.1 Observed frequency and structure

Stratiform mixed-phase clouds can occur in the mid-troposphere of the mid-latitudes and have been observed in the United States (Fleishauer et al., 2002; Carey et al., 2008), Canada (Korolev et al., 2003; Vaillancourt et al., 2003), the United Kingdom (Hogan et al., 2002, 2003a,b; Field et al., 2004; Marsham et al., 2006) and also in the Arctic boundary layer (Shupe et al., 2008a,b; Lawson and Zuidema, 2009; de Boer et al., 2009; Morrison et al., 2011a,b, 2012), over the Southern Ocean south of Australia (Morrison et al., 2011a) and in the tropics (Riihimaki et al., 2012).

Compilations of surface observations of clouds show that altocumulus and altostratus together cover 22% of the Earth's surface (Warren et al., 1986a,b) and mixed-phase clouds were observed 46% of the time during the Third Canadian Freezing Drizzle Experiment (Cober et al., 2001). Observations from a lidar mounted on the space shuttle in September 2004 detected supercooled liquid at temperatures as cold as -30°C and across all latitudes from 60°N to 60°S and found that 20% of clouds between -10 and -15 °C contained liquid water but with a larger fraction in the southern hemisphere (Hogan et al., 2004). A study using the spaceborne lidar CALIPSO by (Zhang et al., 2010) found that 33.6% of all mid-level clouds are liquid-topped stratiform clouds and they cover 7.8% of the Earth's surface at any time.

Typically, stratiform mixed-phase clouds consist of a thin layer of liquid water a few hundred metres deep in which ice particles form and fall out beneath (Rauber and Tokay, 1991; Shupe et al., 2008a). The liquid layer was observed to be between 500 and 800 metres deep in mixed-phase clouds observed over North America (Fleishauer et al., 2002) for a number of cases where the cloud top temperature was between -8 and -31 °C. In these clouds the largest mean liquid water content observed was 0.359 g m^{-3} in single layered clouds. The largest ice water content in the same clouds was 9×10^{-4} g m^{-3} with largest values near cloud base.

These are broadly similar to observations reported by Hogan et al. (2003a), where thinner liquid water clouds only 100–200 metres deep had a total liquid water path between 10 and 20 g m^{-2}. In these clouds the typical ice water path was a similar magnitude (10–30 g m^{-2}) but is spread over a considerably deeper layer than the liquid layer. The liquid layer has an almost

adiabatic profile of liquid water when the layer is less than 500 metres deep and less than half of liquid layer clouds observed by Korolev et al. (2007) exceeded this depth.

Aircraft observations by Korolev et al. (2003) and later by Vidaurre and Hallett (2009) show that on scales of 100 metres in the horizontal the fraction of condensed water in the cloud was typically greater than 90% liquid or 90% ice, with relatively little genuinely mixed-phase regions. This is in direct contrast with Field et al. (2004) who reported that mixed-phase conditions do exist on 100 metre scales, although did not state how often. Vaillancourt et al. (2003) also found a near constant number of aircraft samples at all liquid fractions between 0.05 and 0.95 from longer averages with samples approximately 1500 metres in length.

Recent studies by Westbrook and Illingworth (2011) found that almost all of the ice in clouds with a cloud top temperature warmer than $-27\ ^{\circ}\mathrm{C}$ originates from a pre-existing liquid water cloud and therefore it is likely that the liquid water layer at the top of mixed-phase clouds is the source of the ice found falling beneath the liquid layer. This is also true in Arctic mixed-phase clouds, where ice is not observed until after a liquid layer has formed (de Boer et al., 2011). Arctic clouds composed only of ice are less frequent than those topped by supercooled liquid at temperatures warmer than $-25\ ^{\circ}\mathrm{C}$ to $-30\ ^{\circ}\mathrm{C}$, suggesting ice formation generally occurs in conjunction with liquid.

1.2.2 Radiative impact

Because of their structure, large areal extent and long lifetime, stratiform mixed-phase clouds are a significant contributor to the cloud radiative effect. The liquid present within the cloud tends to be located at the top (e.g. Hogan et al., 2003a; Shupe et al., 2008a) and consists of a large concentration of small droplets with effective radii as small as 2 μm (Hogan et al., 2003a). Largely due to the large concentration of liquid droplets, this layer is very effective at reflecting solar radiation incident on the cloud. Because this layer is located at the top of the cloud there is little opportunity for the cloud to absorb the radiation before it is reflected back away from the Earth and therefore this layer increases the albedo of the cloud relative to an ice only cloud (Hogan et al., 2003a).

Mixed-phase clouds are an important contributor to the uncertainty in the magnitude and sign

of the cloud feedback. Typically they have a net cooling effect (Hogan et al., 2003a), although the magnitude of this effect for an individual cloud will depend on the time of day and other clouds that are present. The specification of mixed-phase clouds in GCMs is a large source of variability in climate simulations. This was first shown by Mitchell et al. (1989) who changed the cloud scheme in a GCM from a relative humidity to a cloud water scheme. The model cloud fraction in the relative humidity (RH) scheme is based on the grid-box mean relative humidity and the radiative properties such as albedo and emissivity are a fixed function of height. By contrast the cloud water scheme calculates the cloud fraction and water content within a grid-box, the ratio of liquid and ice within the grid-box is determined by temperature and the cloud ice precipitates towards the ground. The change from the RH scheme to the cloud water scheme resulted in a reduction from 5.2 K to 2.7 K in the annual average surface warming due to doubling CO_2 concentrations. This sensitivity of climate models to mixed-phase cloud specification has been confirmed by other papers; Senior and Mitchell (1993) used 4 different cloud schemes in a GCM and this gave values for the climate sensitivity parameter, λ, between 0.45 and 1.29 °C (W $m^{-2})^{-1}$. It was also reported that the simulation with the cloud water scheme had a negative cloud feedback as temperature increased as less cloud water was in the ice phase and therefore did not precipitate. This effect was further increased when an interactive radiation scheme was included that treated liquid and ice cloud separately (Senior and Mitchell, 1993). Also, by changing the range of temperature in which mixed-phase clouds can exist significantly changed the radiation budget (Gregory and Morris, 1996). GCMs are also sensitive to the cloud altitude and how the liquid and ice are assumed to be mixed within the cloud as the cloud albedo is very dependent on the phase of the cloud condensate (Sun and Shine, 1994, 1995).

The radiative impact of mixed-phase clouds is also felt at a more local scale. Because of the longwave emission from cloud top, a strong cooling is observed at the top of the cloud. This cooling was calculated to be more than 70 K day^{-1} in two cases observed by Pinto (1998) and cooling rates of 90 K day^{-1} were reported by both Jiang et al. (2000) and Hogan et al. (2003a). This cooling will have effects on both the microphysics within the cloud and the dynamics of the cloud, with the strength of cooling sufficient to destabilise the cloud top and drive turbulent eddies.

1.2.3 Cloud microphysics

The liquid phase is found at the top of stratiform mixed-phase clouds and therefore occupies the coldest part of the cloud. The layer of liquid water is often very thin, sometimes as little as 100 metres in depth (Hogan et al., 2003a) but can be deeper than 500 metres (Korolev et al., 2007). Concentrations of liquid droplets within altostratus have been observed at around 25–50 cm^{-3}, with sizes between 2 and 50 μm (Crosier et al., 2011). These particles are much smaller and many times more numerous than the ice particles present in mixed-phase clouds. Because a large number of droplets exist they can, collectively, react quickly to any changes in saturation of the air; they are able to grow in the presence of supersaturation and remove the excess vapour from the air and equally evaporate quickly when the air becomes subsaturated. As such the growth rate of liquid droplets is often neglected in model parameterization schemes (e.g. Wilson and Ballard, 1999), where it is impossible for the air to exceed liquid saturation.

Evidence indicates that ice formation is dependent on the presence of liquid at temperatures warmer than -40 °C (Hobbs and Rangno, 1985; Westbrook and Illingworth, 2011; de Boer et al., 2011). The ice in stratiform mixed-phase clouds forms within the liquid layer through heterogeneous nucleation where a liquid droplet freezes with the aid of an ice nucleus. Unlike cloud condensation nuclei, ice nuclei are rare and often limit the nucleation rate of ice particles. As a result there are many fewer ice particles observed in clouds than liquid droplets, with observed values in mixed-phase clouds around 0.2 L^{-1} at -12 °C (Crosier et al., 2011). The ice nuclei number concentration increases with decreasing temperature; a collection of previous observations collated by Meyers et al. (1992) showed an increase from less than 0.1 L^{-1} at -10 °C to more than 100 L^{-1} at temperatures colder than -25 °C. Because ice particles are less numerous than liquid droplets they grow to be significantly larger than, reaching hundreds of microns across. By the time they reach this size their terminal fall velocity has become large enough to allow the particles to fall from the liquid layer and begin forming an ice only layer below.

Once ice has been nucleated, the habit (shape) that ice particles acquire as they grow is determined by both the supersaturation and the temperature of the air in which they exist (Rogers and

Yau, 1988). The growth rate of a single ice particle can be calculated as

$$\frac{dm}{dt} = \frac{4\,\pi\,CFSS_i}{\left(\frac{L_s}{R_vT} - 1\right)\frac{L_s}{KT} + \frac{R_vT}{e_i(T)D}}, \tag{1.1}$$

where m is the mass of the ice crystal in kg, C is the capacitance of the ice particle in m, dependent on its size and shape, F is the ventilation coefficient, SS_i is the supersaturation of the air with respect to ice, L_s is the latent heat of sublimation, K is the thermal conductivity of air, D is the diffusivity of water vapour in air and e_i is the saturated vapour pressure over ice. The capacitance of the ice particle is dependent on the size and habit of the crystal, with larger particles and those with the largest aspect ratios (e.g. thin plates or dendrites) having larger capacitances (Westbrook et al., 2008), although when normalised by size, spheres have the greatest capacitance. The habit of the ice particles can affect the cloud structure by changing both the growth rate and the terminal fall velocity of the ice particles (Avramov and Harrington, 2010).

The terminal fall speed of the ice particles is also a function of their size and shape. Much work has been done to describe the fall speed of a number of different shapes of particle, often using power-law relationships with their mass (Mitchell, 1996). The relationships are often based on theoretical or lab-based experimental work as measuring the fall speed of ice particles in clouds would be very difficult. This is particularly the case because the effects of aggregation of numerous ice particles and riming of the particles can significantly alter the fall speed (Locatelli and Hobbs, 1974).

Ice clouds are made up of a collection of different ice particles of different sizes. It is of interest to describe the number of different sized particles observed within a particular volume of the cloud. This is described through the ice particle size distribution. Following from the early description of raindrop size distributions by Marshall and Palmer (1948) as inverse exponentials, similar expressions for snowflake size distributions followed (Gunn and Marshall, 1958). Houze et al. (1979) observed that most size distributions fitted this inverse-exponential distribution but that the intercept parameter was a function of both temperature and total water content; additionally it was noted that the distribution often deviated from this inverse exponential at small sizes. The Wilson and Ballard (1999) microphysics scheme currently operational in the Met Office Unified Model uses a distribution very similar to the distribution of Houze et al. (1979). Ryan (2000) collated a number of previous observations all of which showed an increase of the slope parameter

at colder temperatures suggesting a greater number of smaller particles. More recently Field et al. (2004) and Delanoë et al. (2005) have attempted to normalise the particle size distributions to find a universal distribution that can be used in numerical models to accurately represent the size distribution in a number of different conditions. This is important as the size distribution strongly influences the total growth rate and mean fall velocity of a collection of ice particles. This issue will be studied in more detail in the context of mixed-phase clouds later in this thesis.

1.2.4 Maintainence of mixed-phase clouds

Mixed-phase clouds have been observed to persist for many hours or longer (e.g. Shupe et al., 2006; Marsham et al., 2006); however, theoretical calculations suggest that in mixed-phase clouds with liquid water contents below 0.5 g m^{-3} and ice particle concentrations $N_i \sim 10^2$–10^3 L^{-1}, the liquid should glaciate within 20–40 minutes (Korolev and Issac, 2003). This glaciation is expected due to the Wegener-Bergeron-Findeisen process (Wegener, 1911; Bergeron, 1935; Findeisen, 1938) where ice grows at the expense of liquid water where the two phases coexist because of the difference in saturation vapour pressure over liquid and ice surfaces. Strictly this only applies when the air is supersaturated with respect to ice but subsaturated with respect to liquid and conditions can exist where both liquid and ice particles grow together (Korolev, 2007). However, ice grows faster than liquid at all temperatures below 0°C due to the difference in saturated vapour pressure and means that the presence of ice always acts to reduce the amount of liquid water present.

Despite the theoretical expectation that these clouds will become glaciated quickly, the numerous observations of long-lived mixed-phase clouds clearly require some other process to assist in their maintainence. Rauber and Tokay (1991) explained the existence of supercooled liquid water at the top of cold clouds due to an imbalance in the condensate supply rate and the bulk ice particle growth rate in regions of ascent. Liquid water can be produced in updrafts that are sufficiently deep so as to bring air to liquid saturation and sufficiently strong so as to achieve saturation before the ice growth has had time to reduce the vapour content of the parcel to below liquid saturation. The minimum requirements on updraft speed and depth increase with increasing ice particle concentrations and with decreasing temperature. Rauber and Tokay (1991) suggested that these conditions would not be difficult to meet at warmer temperatures (e.g. 0.1 m s^{-1} over

a depth of 100 metres at $-5°C$) but are more difficult to obtain at colder temperatures (e.g. 0.4 m s^{-1} over a depth of 600 metres at $-32°C$) and also become more difficult to achieve when the ice number concentration is larger. On the whole, observed mixed-phase clouds do not exist in the presence of a strong sustained updraft, with typical mean vertical velocities close to zero throughout the cloud layer (Shupe et al., 2008a). However, the cloud top is turbulent as a result of the radiative cooling at cloud top (described in section 1.2.2) and in the ascending part of the turbulent eddies the criteria for producing liquid may be satisfied. Rauber and Tokay (1991) suggested that updrafts could be caused by entrainment of air above the cloud top into the cloud or by vertical wind shear across the top of the cloud.

Possible mechanisms by which mixed-phase clouds are maintained were also studied by Korolev and Field (2008). Using a theoretical framework and then a simple modelling study they investigated how liquid water could be maintained in the presence of ice and whether uniform ascent, harmonic oscillations or turbulent fluctuations could provide the mechanism. Their con-

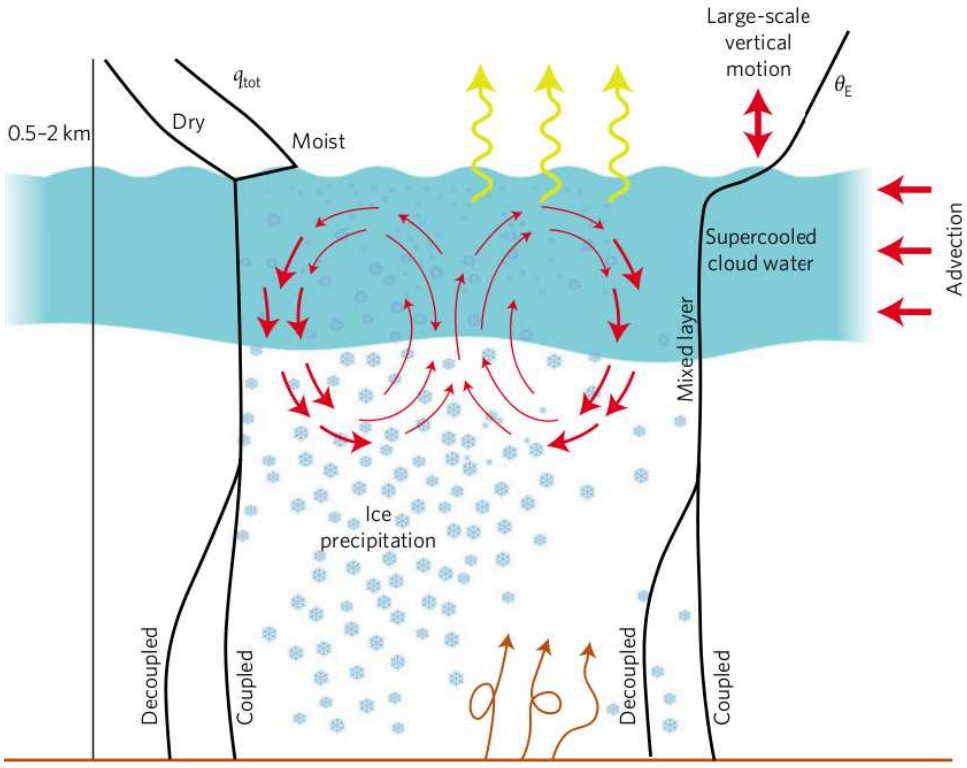

Figure 1.1 Schematic diagram of the primary processes and physical structure of Arctic mixed-phase clouds from Morrison et al. (2012)

clusions, similar to those of Rauber and Tokay (1991), were that vertical ascent that was both sufficiently strong and sufficiently deep is required to bring air to liquid saturation. This is true for all three scenarios presented, but long lived mixed-phase clouds similar to observations could only be maintained under harmonic vertical motion or turbulent fluctuations, with the former giving greater liquid water contents on average. Under harmonic oscillations it was possible for cycles of liquid activation to occur with each parcel only containing liquid for a short time.

Morrison et al. (2012), Smith et al. (2009) and Shupe et al. (2008a) have each published a schematic for the structure of mixed-phase clouds and how processes contribute to their maintainence. Figure 1.1 shows the schematic from Morrison et al. (2012) as the most complete of the three, although all three are broadly consistent. It should be noted that this schematic is for boundary layer clouds observed in the Arctic and whilst the structure of these clouds are similar to the altocumulus clouds studied in this thesis potential differences lie in the fact that the Arctic clouds can be coupled to the surface. The schematic shows the liquid water layer at cloud top and the radiative cooling associated with this layer. The radiative cooling requires only a small amount of liquid water and causes condensation to occur within the top of the cloud and also destabilises the cloud layer by cooling the air parcels at cloud top which become negatively buoyant. The destabilisation of parcels at the cloud top results in a turbulent mixed layer throughout the cloud where profiles of potential temperature and total water content are roughly constant with height. Ice nucleates within the liquid layer and grows rapidly due to the supersaturation with respect to ice present in the liquid cloud. These ice particles then begin to sediment out of the liquid layer and grow further or evaporate dependent of the ice supersaturation they experience once out of the layer. The turbulent eddies present as a result of the radiative cooling generally have strong narrow downdrafts and broad, weak ascent. This can give rise to vertical motions strong enough to bring the air to liquid saturation and the deviations from the mean velocity can be ± 2 m s^{-1} (Shupe et al., 2008a). There is also evidence that both liquid and ice water contents are higher in the cloud at times of upward air velocity and reduced ice and liquid contents during times of descent (Shupe et al., 2008a).

1.2.5 Numerical modelling

Surprisingly, given their important radiative and climatic importance, there are relatively few high-resolution numerical (e.g. cloud resolving or large eddy) simulations of mixed-phase clouds, particularly at mid-levels (Fleishauer et al., 2002). Much of the modelling that has been done pertains to Arctic mixed-phase stratocumulus or stratus, and although these clouds have a similar structure to mid-latitude mid-tropospheric mixed-phase clouds they can be coupled to the surface. The findings of these studies may still be relevant to mid-tropospheric clouds, but the possible influence of the surface needs to be remembered when comparing results.

Much of the modelling of mixed-phase clouds uses large eddy models (LEMs) or cloud resolving models (CRMs) at high resolution (e.g. Marsham et al., 2006; Fridlind et al., 2007, 2012; van Diedenhoven et al., 2009; Avramov et al., 2011). This is not surprising given the turbulent nature of the cloud top and enables focused experiments to be run at high resolution. Their small domain size and high resolution can be excellent for testing and improving microphysical parameterizations over a small number of cases. It is possible to use computationally expensive microphysics schemes (e.g. double-moment or bin resolved prognostic ice) in limited domain models and these high resolution simulations enable 3-dimensional turbulent or convective circulations to be resolved. In coarser resolution models, such as operational NWP models, the microphysics schemes are often simpler and the turbulent and convective processes are parameterized or neglected. It can therefore be difficult to understand deficiencies in coarse resolution models using CRM or LEM simulations due to the differences in grid-scale and resolved physics and the typical focus on a small number of cases.

In general, the microphysics schemes in current NWP and climate models tend to fall into well defined groups. The first of these groups contains models with a single prognostic variable for condensed water and uses a diagnostic split between the liquid and ice water content of clouds based on temperature alone. As will be shown later, these models tend to better predict the mean amount of liquid and ice than models with prognostic ice, but due to the temperature dependence are unable to model the correct structure of mixed-phase clouds with liquid at colder temperature at cloud top (Marsham et al., 2006) and therefore perform poorly when used for case studies. Secondly there are models with a prognostic ice water content that is separate from the liquid

water content, determined using a physically based parameterization of the ice particle growth rate by deposition of vapour (e.g. Wilson and Ballard, 1999) and an assumed inverse-exponential (or more complex) ice particle size distribution (e.g. Wilson and Ballard, 1999) or that each ice particle is the same size (e.g. Rotstayn et al., 2000). These models are able to model the correct structure of mixed-phase clouds, particularly in the Arctic (e.g. Jiang et al., 2000), but often find that the ice number concentration in the parameterizations is too large resulting in rapid glaciation of the clouds (Harrington et al., 1999; Jiang et al., 2000). A reduction of the ice number concentration allows a more realistic, persistent cloud to be maintained (Jiang et al., 2000). Thirdly, more complex models containing prognostic ice nuclei and parameterized ice nucleation have been used (Morrison et al., 2005; Fridlind et al., 2007). These models can struggle to produce enough ice when compared to observations (Fridlind et al., 2007), but are able to sustain a liquid layer at the top of ice clouds, primarily due to the depletion of ice nuclei from the liquid layer and therefore also removing the sink of vapour and liquid water (Morrison et al., 2005). The inclusion of additional nucleating pathways, for example the freezing of supercooled droplets, improved the ice water contents in these models. However, these pathways are currently only hypothetical.

Three dimensional large-eddy simulations (LES) of mid-level mixed-phase clouds performed by Smith et al. (2009) have helped to quantify how much each of the processes contribute to the maintainence of mixed-phase clouds. By simulating three cases and assessing the relative contributions to changes in the liquid and ice water contents within the cloud they concluded that the most important terms for determining the lifetime of the cloud were the large scale ascent/descent, depositional growth of snow and radiative heating and cooling. Of the three cases studies, both cases where the liquid layer persisted longer than 3 hours did so in the presence of large scale ascent while the other case had large scale descent. It may therefore be the case that these delicately balanced cloud systems are largely controlled by the large scale motions of the atmosphere, although this can not be conclusively stated from 3 case studies.

Adequate simulations of mixed-phase clouds are possible in simpler single-column models too and are comparable in terms of liquid and ice water contents to cloud resolving models (Klein et al., 2009). Previous studies have harnessed the relative simplicity of single-column models (relative to 2 or 3 dimensional simulations) to study the effect of different ice nucleation mechanisms (Morrison et al., 2005) and new microphysical parameterizations on the simulation of

mixed-phase clouds (Yuan et al., 2006). Underestimates of the liquid water content by a factor of 2–3 were found across 17 SCMs and 9 CRMs by Klein et al. (2009).

1.2.6 Weather impact of mixed-phase clouds

Mixed-phase clouds are important to understand and model correctly for the sake of both weather and climate predictions. For weather forecasting they impact on forecasts for the public, aviation and the military whilst their radiative impact is particularly important in climate simulations.

As already discussed, the existence and radiative importance of mixed-phase clouds prevents some solar radiation reaching the surface whilst acting as a source of ice and increasing the amount of trapped terrestrial long-wave radiation. Depending on the time of day this will warm or cool the surface air temperature and possibly affect later atmospheric dynamics (e.g. triggering of convection, boundary layer depth) as a result.

This was particularly notable in experiments using two versions of the ECMWF model, one with a single prognostic for condensed cloud water and the other with separate prognostic variables for both cloud ice and liquid (Richard Forbes, personal communication). The single prognostic scheme prescribed the ratio of liquid and ice water content within the a grid-box as a function of temperature, with no liquid permitted at temperatures colder than -23°C, whereas the scheme with two prognostic variables used physically based growth rates and fall velocities to determine the ice water content. In the simulation with two prognostic variables the amount of supercooled liquid in the simulations is substantially reduced. This simulation also exhibited surface temperature errors of up to 10 $^{\circ}$C colder than observed where supercooled liquid was absent from the simulations over Scandinavia. By reintroducing the supercooled liquid (through reducing the ice growth rate at the top of clouds), the temperature errors were largely removed. This clearly highlights the importance of realistic simulations of mixed-phase clouds for weather forecasting as well as for climate.

Mixed-phase clouds are also important for aviation as the presence of supercooled liquid water contents greater than 0.01 g m^{-3} are related to aircraft icing conditions (Brown et al., 1997). Icing can be a significant hazard to aircraft where the droplets freeze on to the cold aerofoil surfaces of the aircraft reducing the aerodynamic lift and increasing the weight, making it more difficult to

keep the plane in the air.

On slightly longer timescales mixed-phase clouds are important in the Arctic too. Despite forming primarily in the boundary layer, Arctic mixed-phase clouds are of a very similar structure to those observed in the mid-troposphere but may also be influenced by surface processes. Their presence again has a large radiative impact and can influence the date of transition into and out of winter where the ocean melts or freezes over (Curry and Ebert, 1992; Jiang et al., 2000).

The importance of clouds in climate and climate change are undeniable, but also uncertain. The role of clouds in our changing climate is still poorly understood and cloud feedbacks remain the most uncertain part of our current understanding of the climate system (Dufresne and Bony, 2008; Bony et al., 2006) and intermodel differences in cloud feedback constitute by far the most primary source of spread of both equilibrium and transient climate responses simulated by GCMs (Dufresne and Bony, 2008; Andrews et al., 2012) and is approximately three times larger spread than the water vapour, ocean uptake or radiative forcing feedbacks . In fact the magnitude and even the sign of the cloud feedback is highly uncertain in climate models and monthly comparisons of the cloud feedback suggested that it is likely positive, and contributes an extra 0.54 ± 0.74 W m^{-2} per degree of warming (Dessler, 2010). In reality month-by-month comparisons are too short to draw conclusions, however, reliable longer term data are unavailable and hence there is still a large uncertainty in cloud feedback.

As mixed-phase clouds have a cooling effect on the Earth (Hogan et al., 2003a) then an increase in the amount of cloud in the mid-latitudes at mid-levels and lower level polar clouds as predicted by some climate models (Tsushima et al., 2006) would constitute a negative climate feedback (Senior and Mitchell, 1993).

1.2.7 Representation in NWP and climate models

Given the large radiative impact of all clouds, it is important that they are represented accurately in numerical models if their radiative transfer calculations and future climate states are to be believed. Mixed-phase clouds are an important part of the global radiation budget and their accurate representation is key because models are particularly sensitive to their specification (e.g. Mitchell et al., 1989; Senior and Mitchell, 1993).

Previous studies have compared many models with observations both over a long time period and from case studies. The Cloudnet project (Illingworth et al., 2007) observed cloud with ground based remote sensors at sites across Europe and assessed model predictions of cloud over the same sites. This analysis found an absence of mid-level clouds in 6 of the 7 models, some missing as much as one-third of all mid-level cloud fraction. The liquid water content of the models was typically too large relative to the observations in some cases by a factor of 2 to 3. The exception came from the Met Office Unified Model which was largely within the range of observations for the global model and underestimated in the mesoscale model. The range in liquid water content at a given altitude between the model with the lowest and the model with the highest value was approximately an order of magnitude in the lowest 6 km of the atmosphere. This was similar in magnitude to that of the condensed cloud water path of climate models (Stephens et al., 2002). The ice water content was found to be better predicted than liquid by many of the models, in agreement with the findings of Vaillancourt et al. (2003), and was largely within or close to the observed range but again the inter-model spread was approximately an order of magnitude at the warmer temperatures.

In a comparison of 10 climate models with observations from ISCCP and CERES (Zhang et al., 2005) show a similar low bias in the mid-level cloud amount. The multi-model mean of cloud fraction in the 10 climate models only 30–40% of the satellite derived cloud amount and 9 of the 10 models underestimated the mid-level cloud amount. Models also failed to predict enough thin cloud and this meant a substantial underestimate of optically thin and intermediate mid-level cloud as shown in figure 1.2. In many models this was compensated for by upper or lower level cloud amounts greater than observed. These errors in cloud amount lead to problems with the radiative balance of the model and only half of the models analysed simulated the radiative impact of clouds within the observed range, with the other half having too large an effect.

Hogan et al. (2003a) outlined a few possible reasons why models might struggle to represent stratiform mixed-phase clouds. As the supercooled liquid often forms in thin layers at cloud top and the liquid can be maintained by turbulent updrafts near cloud top the horizontal and vertical resolution of the model may be important. The coarseness of current NWP and climate models means that they cannot resolve the turbulent motions within the cloud and even the magnitude of the cloud scale vertical motions will be underestimated due to the large grid-box sizes. Also,

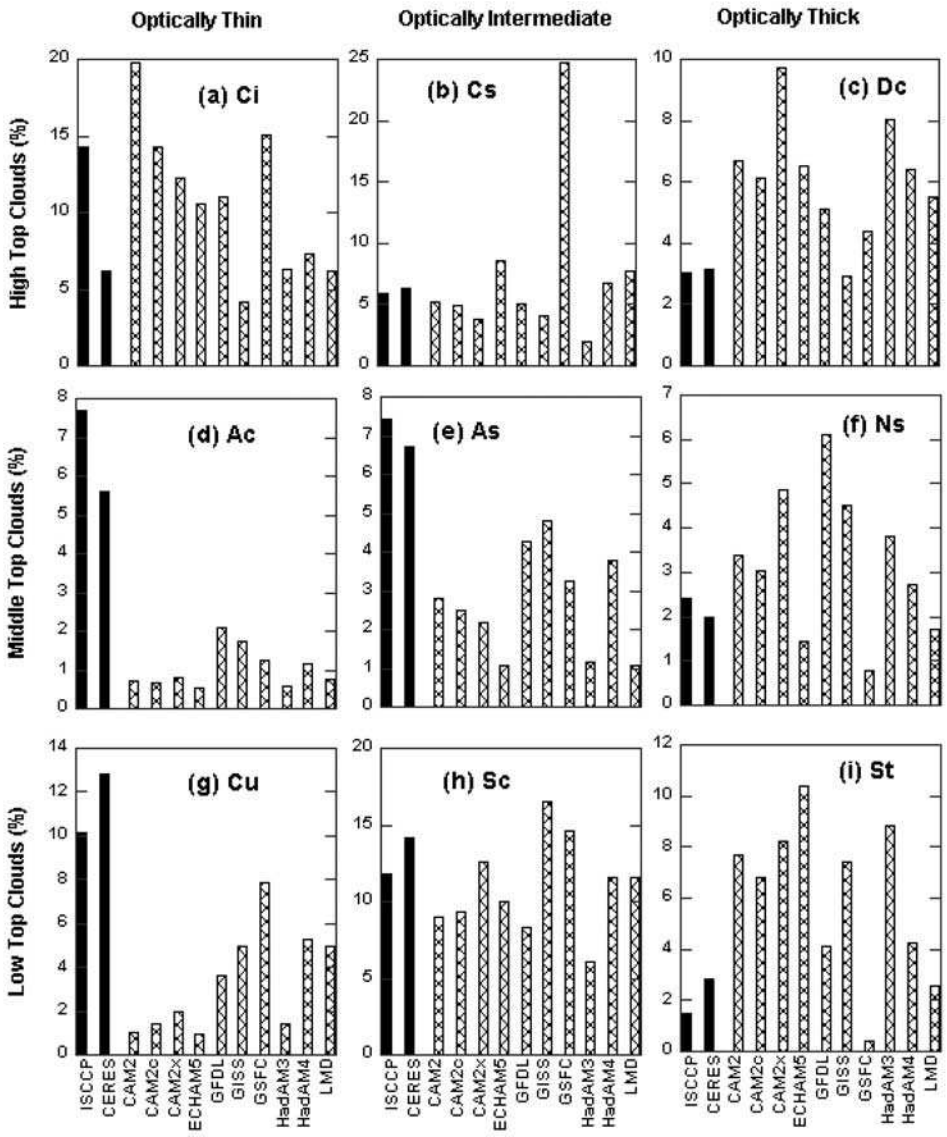

Figure 1.2 Cloud frequency averaged from 60°N to 60°S in the DJF season for the nine ISCCP cloud types in satellite measurements and in a number of climate models (from Zhang et al., 2005). Note particularly the low frequency with which clouds in panels d and e are modelled, the thin mid-level clouds.

the coarse vertical resolution may prevent a liquid layer being diagnosed using the grid-box mean quantities. Additionally some of the numerical models set a minimum temperature at which liquid can exist (e.g. -23 °C in the ECMWF model (ECMWF, 2010)) and warmer values of -15 °C (Smith, 1990) and -9 °C (Moss and Johnson, 1994) have been suggested. Clearly these are inconsistent with observations of supercooled liquid existing at temperatures down to -40 °C.

1.3 Observing clouds

1.3.1 Methods of observing clouds

There are many ways of observing clouds, the simplest method involves a human observer looking up. Because of this simplicity the cloud type, amount and altitude are commonly reported in SYNOP reports from around the planet. These have been compiled to obtain statistics of observed cloud amount and type (Warren et al., 1986a,b), but to enable a more quantitative analysis of cloud structure and microphysics data from instrumented aircraft, ground based remote sensors and satellite measurements can be used to give high resolution information of, for example, the liquid water content and liquid droplet sizes and indeed many other properties.

Aircraft observations allow a small portion of the cloud to be directly sampled by numerous instruments mounted on the aircraft but the data becomes much more useful when used in conjunction with data from other instruments, for example a ground based remote sensing site comprising at least a radar, but may also include a lidar, broadband radiometer, wind profiler, further radars and radiosonde launches. This allows, for the period of the field campaign, a great deal of data about the clouds to be gathered and analysed and allows the aircraft data to be interpreted within the larger scale context of the whole cloud system.

In some instances the remote sensing equipment may be permanently installed (e.g. Cloudnet (Illingworth et al., 2007) and Atmospheric Radiation Measurement (ARM, Stokes and Schwartz, 1994)), allowing for a prolonged period of observation of clouds that pass over the site. This gives enough information to start compiling a local climatology of clouds but unfortunately these sites are rare, with approximately 15–20 in the world, largely due to the expense of setting up and maintaining these sites. Therefore it is difficult to understand the global coverage using only ground-based measurements.

In order to get larger spatial coverage, remote sensing instruments have been placed on satellites. These instruments fall into two categories, active and passive. Active sensors (e.g. TRMM (Simpson et al., 1996), CloudSat (Stephens et al., 2002), CALIPSO (Winker et al., 2002)) both transmit and receive radiation and can retrieve detailed information from within clouds and about their vertical structure. Passive sensors only receive radiation either emitted or reflected from

the clouds or Earth's surface at a number of wavelengths and are therefore only able to retrieve vertically integrated cloud properties or information about the cloud near the cloud top. Because passive sensors are not able to resolve the vertical structure of clouds they are often placed in geostationary orbits and are able to sample a much larger area of the planet as a result, but even polar orbiting passive sensors have a larger sample size because they do not need to both transmit and receive signal.

1.3.2 Remote sensing theory

As mentioned, a number of sites and satellites have remote sensing instrumentation. In this section the theory of retrieving cloud properties from these observations is discussed with a focus on instruments based at Chilbolton, UK as these form the basis of much of the observations of mixed-phase clouds used in this thesis. Much of these data have been collected and processed as part of the Cloudnet project (Illingworth et al., 2007). The suite of ground-based remote sensing instrumentation at Chilbolton observes clouds using a combination of cloud radars, lidars and microwave radiometer from which it is possible to retrieve both the cloud boundaries and the liquid and ice properties of the cloud.

Cloud radar observations

The 35 GHz cloud radar at Chilbolton points vertically and runs near continuously. The radar transmits pulses of microwave radiation, with power P_T, that travel through the atmosphere. Some of this microwave radiation is reflected or scattered by objects in the atmosphere back towards the radar and detected by the receiver. This means that the radar detects some returned power (P_R) from liquid and ice cloud condensate, as well as birds, insects and aircraft. Using the time delay from pulse transmission to returned signal the distance of the target from the radar can be calculated. The meteorological form of the radar equation, neglecting attenuation due to atmospheric gases, is (following Probert-Jones, 1962):

$$P_R(r) = \frac{C_{\text{rad}}}{V}\frac{P_T}{r^2}\sum_V \sigma, \tag{1.2}$$

where C_{rad} is a constant that depends on the radar hardware, r is the mean distance of the targets from the radar in metres, σ is the backscatter cross section of each target which is summed over the volume V. The backscatter cross section of a single small spherical scatterer is related to its

diameter D, assuming the Rayleigh approximation, by (Rogers and Yau, 1988):

$$\sigma = \frac{\pi^5}{\lambda^4}|K|^2 D^6, \tag{1.3}$$

where λ is the wavelength of the transmitted pulse, $K = (m^2-1)/(m^2+2)$ is the dielectric factor and m is the complex refractive index. Using this (1.2) can be rewritten as

$$P_R(r) = \frac{\hat{C}_{\text{rad}}}{V}\frac{|K|^2}{r^2}\sum_{\Delta V} D^6, \tag{1.4}$$

with $\hat{C}_{\text{rad}}$ now including further radar specific constants. $|K|^2$ is assumed constant for all particles in the volume V, but it is different for liquid (≈ 0.93) and ice (≈ 0.21) and also as a function of temperature and radar wavelength (Rogers and Yau, 1988). The returned power can therefore give information about both the size and number of targets within a volume, although it is ambiguous whether a few large targets or many small targets have been detected. To enable comparisons between different radar equipment, the radar reflectivity Z is defined only as

$$Z = \frac{1}{V}\sum_{V} D^6, \tag{1.5}$$

in units of mm^6 m^{-3} and is often expressed in dB$Z = 10\log_{10}(Z)$.

Lidar observations

The 905 nm wavelength lidar at Chilbolton also points near vertically (5° off vertical to avoid specular reflection from horizontally oriented ice crystals) and can be used to help identify layers of liquid water in mixed-phase clouds. The lidar works in a similar way to the radar, transmitting a pulse of radiation and waiting for returned signal from targets in the atmosphere. As the frequency of radiation used is in the near-infrared region and therefore the wavelength is much shorter than the size of cloud particles, the amount of power returned from targets follows Mie and geometric optics approximations. The lidar equation in its most common form and in the single-scattering limit is (Wandinger, 2005):

$$P_R(r,\lambda) = P_T\frac{C_{\text{lid}}}{r^2}\beta(r,\lambda)\exp\left[-2\int_0^r \alpha(r,\lambda)dr\right], \tag{1.6}$$

where P_R is the power returned to the instrument, P_T the amount of power transmitted, C_{lid} a constant dependent on the lidar hardware, r the range from the instrument in metres, λ the lidar wavelength. The exponential term deals with the transmission losses (extinction) of the transmitted power to a range, r, quantified by the extinction coefficient, α, defined as

$$\alpha(r,\lambda) = \frac{1}{V}\sum_{V}\sigma_{ext}(r,\lambda), \tag{1.7}$$

where σ_{ext} is the extinction cross section per unit volume of air. As described in the section above for radar, a value of the measured returned power independent of the instrument hardware is defined. For lidar this is β', the lidar attenuated backscatter in units of sr^{-1} m^{-1}. This is expressed as

$$\beta'(r,\lambda) = \beta(r,\lambda)\exp\left[-2\eta\int_0^r \alpha(r,\lambda)dr\right], \tag{1.8}$$

where, following Platt (1973) an additional term, η, has been included to account for multiple scattering of the lidar beam. The maximum multiple scattering is included when this value is 0.5 reducing to no multiple scattering for a value of 1. The value appropriate for the 905 nm lidar at Chilbolton is 0.7 (O'Connor et al., 2004). In addition, an extinction-to-backscatter ratio, $s = \alpha/\beta$, is included such that (1.8) can be written in terms of α.

$$\beta'(r,\lambda) = \frac{\alpha(r,\lambda)}{s}\exp\left[-2\eta\int_0^r \alpha(r,\lambda)dr\right], \tag{1.9}$$

A typical value of s for liquid water drops measured by the 905 nm lidar is 18.8 ± 0.8 sr (O'Connor et al., 2004) but for cirrus a much larger range has been observed (5–150 sr, Lynch et al., 2002).

Microwave radiometer

At Chilbolton, the vertical integral of the liquid water content, known as the liquid water path, is derived from two brightness temperatures measured at frequencies close to 23.8 and 36.5 GHz. The approach for deriving an improved liquid water path from microwave radiometer is described by Gaussiat et al. (2007) with the addition of a co-located lidar. At times when the lidar indicates there is no liquid cloud present the radiometer brightness temperatures are effectively recalibrated which avoids the need for manual recalibration to correct for drift in the brightness temperatures. The stated error of liquid water path retrieved using this method is $\pm$10–15 g m^{-2} (Gaussiat et al., 2007).

1.4 Thesis outline

In this thesis we aim to bridge the gap between NWP and climate models, high resolution large eddy models and observations of mixed-phase clouds. To do this a new single column model is created, EMPIRE (Evaluate Mixed-Phase Importance in Radiative Exchange), designed to be similar to the cloud microphysical schemes in current NWP models and following the same con-

straints on computer resources. As EMPIRE is similar in nature to the NWP models, the results obtained from running it should be transferable to NWP models and ultimately lead to improved simulation of mixed-phase clouds in these models. The relative simplicity of EMPIRE can be utilised and it can be run many times with changed parameterizations to explore the parameter space and identify which processes are important in the maintainence of mixed-phase clouds.

By carefully analysing remote sensing observations of mixed-phase clouds from a number of days, statistics about mixed-phase clouds and their representation in both existing NWP models and EMPIRE have been produced and model parameterizations tested. Throughout the research, where indications that current parameterizations can be improved then work has been undertaken to suggest an improvement.

Throughout the thesis improvements are suggested to the ice cloud fraction parameterization and ice particle size distribution parameterization with both showing significant improvements in the model simulations of mixed-phase clouds. Additionally the issue of the model vertical resolution has been addressed, where models with a coarse vertical resolution struggle to simulate mixed-phase clouds. A new parameterization is introduced to allow mixed-phase clouds to be simulated correctly in coarse vertical resolution models such as operational NWP models.

The thesis is structured with chapter 2 describing EMPIRE, the new single column model. Chapter 3 compiles the observations made by ground based remote sensors at Chilbolton to generate statistics on the nature of mixed-phase clouds and then extracts comparable quantities from a number of NWP models. Additionally this chapter contains an evaluation of the ice cloud fraction parameterization and an investigation into the importance of correctly simulating the structure of mixed-phase clouds for radiation calculations. Chapter 4 uses the same observed statistics and compares with EMPIRE and then looks in greater detail at the mechanisms that maintain liquid water in the EMPIRE simulations to identify which processes are most important to model correctly. Additionally this chapter includes a number of suggested improvements to parameterizations, identifies what the correct parameterization should achieve and compares the improved parameterization with the original by using EMPIRE. In particular this is done to justify a proposed change to the ice particle size distribution parameterization. Chapter 5 then addresses the problem with low resolution models not correctly predicting mixed-phase clouds, which itself is identified in chapter 4. The reason for this problem is analysed and a parameterization to allow

coarse resolution models to simulated mixed-phase clouds is designed, implemented and tested. Chapter 6 summarises the key findings of the thesis together with suggested future directions of research on mixed-phase clouds.

CHAPTER 2:
EMPIRE: A SINGLE COLUMN MODEL FOR STUDYING MIXED-PHASE CLOUDS

2.1 Motivation

As outlined in chapter 1, current numerical forecast models do not represent clouds well, specifically mixed-phase clouds. In order to understand the reason for their misrepresentation in forecast models, the forecast models themselves need to be understood first. These models are, by necessity, large and complicated and therefore take a long time to run. Also, their 3D advection and dynamics makes interpreting changes in cloud fields difficult and attributing the cause of changes in model clouds equally difficult. One cannot say, for instance, whether changing a parameterization has directly caused a cloud to form that would not otherwise have done, or whether the parameterization has caused a change in the dynamics of the weather system which in turn results in a change in the clouds within that weather system.

To be able to sensibly assess the consequence of changing a particular model parameterization or process, a simpler model is required to assess the effect of cloud physics in isolation from the dynamics. One type of model that can be used for this type of study are single column models (SCMs) and a number of studies have used SCMs to model mixed-phase clouds (e.g. Morrison et al., 2005; Yuan et al., 2006; Liu et al., 2007). A SCM is similar to a 3D model, but only has grid boxes in the vertical. Horizontal transports of model variables (e.g. temperature and moisture) as well as vertical wind are prescribed, usually from a larger 3D model, or as is standard throughout this thesis ERA-Interim re-analyses (Dee et al., 2011). This model contains all the relevant cloud, turbulence and radiation physics of a 3D model, but with the added advantage

that it can run quickly and parameterizations can be easily modified and new ones introduced. Despite SCMs already existing, a new 1D model has been created from scratch so that changes in model output can be fully and rapidly understood and the changes in simulated clouds explained. Additionally this flexibility allows parameterizations to be added and removed more easily that would be possible with an existing model. The model has been built specifically to Evaluate Mixed-Phase Importance in Radiative Exchange and is therefore given the name EMPIRE.

In this chapter the construction of the model and the parameterizations used within it are summarised. The prognostic equations are described as are each of the parameterizations in turn, the numerics used to solve the equations and methods of forward modelling radar and lidar from model output to compare with observations.

2.2 Specification

The EMPIRE model is designed as a quick to run and easy to change version of a GCM. Designing EMPIRE in this way means that the model is simpler than a full GCM but the results will by applicable to GCMs. With this in mind we are restricted as to how complicated and computationally expensive the model is to run. Some features that are not currently in GCMs are also implemented so as to see their effect on the simulation of mixed-phase clouds. Possible shortcomings of GCMs include their poor vertical resolution and lack of non-local turbulent mixing scheme above the boundary layer. Both of these are addressed in EMPIRE as the vertical resolution is increased to 50 m where typical GCM resolutions would be 500–1000 m, and a non-local mixing scheme based on Lock et al. (2000) is included. GCMs also represent ice microphysics in a crude way, in some cases (such as the ECMWF model) the fraction of cloud condensate in liquid and ice phase is a function of temperature only. Almost all GCMs also use a bulk parameterization for ice growth, assuming all ice crystals are the same size or spread over an assumed particle size distribution. This is not ideal, but the use of more complex schemes such as dual-moment or bin-resolved microphysics in a GCM is more computationally expensive and allows extra degrees of freedom that is not currently constrained by observations. It has been shown in previous work that mixed-phase clouds can only be simulated correctly with a reduction of the ice number concentration (e.g. Harrington et al., 1999; Jiang et al., 2000) or the ice nucleation rate (e.g. Marsham

et al., 2006). Either of these may result from the depletion of ice nuclei within the cloud of all types of ice nuclei or a particular type such as deposition or condensation freezing nuclei (Morrison et al., 2005). For this reason prognostic ice nuclei have been included in some simulations of Arctic mixed-phase clouds (Morrison et al., 2005) where initial ice nuclei concentrations were parameterized. For prognostic ice nuclei to be included in a global model it is first required that their concentrations be known and their sources and sinks but these are currently not known and provides an extra degree of freedom in the models which is hard to constrain. Whilst the inclusion of prognostic ice nuclei is possible in small models such as cloud resolving models (CRMs) over a limited domain where ice nuclei concentrations are measured, it is currently not practical for GCMs. Therefore, EMPIRE is restricted to using a single-moment bulk microphysics scheme so that a direct comparison can be made between the results and GCMs and any improvement of mixed-phase cloud representation can be directly applied to GCMs.

As EMPIRE is a single column model and only represents a single vertical profile of the atmosphere it is not completely able to simulate all processes that cause changes to the conditions within the model. The most obvious situation is where the atmosphere is not horizontally homogeneous and horizontal advection therefore causes changes to the prognostic variables. EMPIRE uses advective forcing derived from the ERA-Interim (Dee et al., 2011) reanalyses in all situations. This dataset gives changes due to horizontal advection of potential temperature, humidity mixing ratio, and the zonal and meridional components of the horizontal wind. These values are specific to Chilbolton having been extracted from the full ERA-Interim dataset and having had the effect of local processes (e.g. radiation, microphysics) removed as these will be simulated by EMPIRE. Values from this ERA-Interim dataset are also used to initialise the model values of potential temperature, humidity and pressure and to prescribe the vertical velocities and surface fluxes of heat and moisture.

2.3 Model equations

2.3.1 Basic assumptions

EMPIRE is designed to be only as complex as is required for the task of modelling mixed-phase clouds. As it is a single column model there are some assumptions that must be made. The first such assumption is that large scale temperature and moisture variables are horizontally homogeneous, enabling the use of a single column model, and that the horizontal derivitaves, $\frac{d}{dx} = \frac{d}{dy} = 0$.

As the mixed-phase clouds being modelled are at mid-levels in the troposphere it is also assumed that they are not related to surface processes. Therefore there is no surface scheme in included in EMPIRE although there are some elements of a boundary layer scheme. This may lead to some biases near the surface, but these are expected to be unimportant in our representation of mixed-phase clouds. Any ice that falls to the melting level is assumed to turn to rain and fall to the surface instantly.

Model variables

The two most important prognostic variables in a cloud model are those that control cloud formation, namely the temperature and moisture variables. In EMPIRE, θ_l, the liquid-water potential temperature and q_t, the total water mixing ratio are used. These are chosen as they are both conserved within reversible moist adiabatic processes (Betts, 1973). θ_l is the potential temperature air would have if all the liquid water present were to be evaporated. If there is no liquid water present then θ_l just becomes the potential temperature θ. The liquid-water potential temperature is defined as

$$\theta_l = \theta - \frac{L\theta}{c_p T} q_l, \tag{2.1}$$

where L is the latent heat of condensation, c_p is the specific heat of air at constant pressure and q_l is the liquid water mixing ratio. The weak temperature dependence of L is neglected; EMPIRE uses a constant value of $L = 2.5 \times 10^6$ J kg^{-1}. The total water mixing ratio, q_t, is the sum of the water vapour mixing ratio and the liquid water mixing ratio

$$q_t = q_v + q_l. \tag{2.2}$$

It is assumed that liquid water evaporates and condenses rapidly when present in comparison to

the model timestep and therefore can treat the liquid water as a diagnostic variable. Ice sublimes more slowly than liquid and therefore a prognostic variable to account for the growth of ice is required. In the simplest scenario, q_l is calculated from the value of q_t in excess of the saturation mixing ratio, q_s. In practice, the calculation of q_s requires the air temperature, however, as only θ_l is known, this in turn requires prior knowledge of q_l. q_l can be written as

$$q_l = \begin{cases} q_t - q_s & \text{if } q_t > q_s \\ 0 & \text{otherwise} \end{cases} \tag{2.3}$$

These prognostic variables were first introduced by Betts (1973) and the validity of their use was discussed in Tripoli and Cotton (1981). The method of solving for T, q_v and q_l is detailed in section 2.3.5. The EMPIRE model has 3 other prognostic variables. These are the zonal and meridional horizontal windspeed (u, v) and ice-water mixing ratio (q_i).

2.3.2 Time evolution of u and v

It may appear odd to have prognostic horizontal wind speeds in a single column model. The horizontal winds are not required for advection calculations as they would be in 2D or 3D model as advection is governed by the model forcing. However, they are required to calculate the dynamic stability of air (through the Richardson number, see section 2.4.1.1) and correctly implement vertical mixing parameterizations.

Using prognostic equations for u and v allows well-mixed layers to develop in terms of momentum as well as temperature and humidity. This allows shear layers to be present at the edges of the mixed layers and these shear layers may be important in the evolution of mixed-phase clouds.

The prognostic equations

The horizontal momentum equations are written as:

$$\frac{\partial u}{\partial t} + \mathbf{u}.\nabla u = -\frac{1}{\rho}\frac{\partial p}{\partial x} + fv - \frac{1}{\rho}\frac{\partial}{\partial z}(\rho\overline{u'w'}), \tag{2.4}$$

$$\frac{\partial v}{\partial t} + \mathbf{u}.\nabla v = -\frac{1}{\rho}\frac{\partial p}{\partial y} - fu - \frac{1}{\rho}\frac{\partial}{\partial z}(\rho\overline{v'w'}), \tag{2.5}$$

where $f = 2\Omega\sin\phi$ is the coriolis parameter with ϕ being the degrees latitude and Ω the earth's rotation rate, p is the air pressure and ρ is the air density. In frictionless conditions and assuming a steady state then these equations become the geostrophic wind equations:

$$fv_g = \frac{1}{\rho}\frac{\partial p}{\partial x}, \tag{2.6}$$

$$fu_g = -\frac{1}{\rho}\frac{\partial p}{\partial y}. \tag{2.7}$$

Substituting these back into the original equations gives

$$\frac{Du}{Dt} = -f(v_g - v) - \frac{1}{\rho}\frac{\partial}{\partial z}(\rho\overline{u'w'}), \tag{2.8}$$

$$\frac{Dv}{Dt} = f(u_g - u) - \frac{1}{\rho}\frac{\partial}{\partial z}(\rho\overline{v'w'}). \tag{2.9}$$

These equations show that the change in windspeed at a given time is determined by the difference of the current wind speed from geostrophic and a flux divergence related to turbulence. The flux divergence term can be approximated using "flux gradient" or K-theory, which states

$$\overline{q'w'} = -K_q\frac{\partial q}{\partial z}, \tag{2.10}$$

where q can be any variable and K_q is the eddy diffusivity pertinent to that variable in $m^2\ s^{-1}$. So our final prognostic equations become

$$\frac{Du}{Dt} = -f(v_g - v) + \frac{1}{\rho}\frac{\partial}{\partial z}\left(\rho K_m\frac{\partial u}{\partial z}\right), \tag{2.11}$$

$$\frac{Dv}{Dt} = f(u_g - u) + \frac{1}{\rho}\frac{\partial}{\partial z}\left(\rho K_m\frac{\partial v}{\partial z}\right), \tag{2.12}$$

where K_m is the eddy diffusivity for momentum. Details of how K_m is parameterized are given in section 2.4.1.

2.3.3 Prognostic equations for advection and diffusion

The standard advection equation for any variable, q, is defined as:

$$\frac{\partial}{\partial t}(\rho q) + \frac{\partial}{\partial x}(\rho qu) + \frac{\partial}{\partial y}(\rho qv) + \frac{\partial}{\partial z}(\rho qw) = S_q, \tag{2.13}$$

where S_q is the source term of the variable, q. By setting $q = 1$ and $S_q = 0$ this gives the continuity equation:

$$\frac{\partial \rho}{\partial t} + \frac{\partial}{\partial x}(\rho u) + \frac{\partial}{\partial y}(\rho v) + \frac{\partial}{\partial z}(\rho w) = 0. \tag{2.14}$$

If it is assumed that the variation of density with time is negligible $\left(\frac{\partial \rho}{\partial t} = 0\right)$ then the equation becomes

$$\frac{\partial \rho}{\partial t} = \frac{\partial}{\partial x}(\rho u) + \frac{\partial}{\partial y}(\rho v) + \frac{\partial}{\partial z}(\rho w) = 0. \tag{2.15}$$

Using Reynolds averaging to break w and q into means and variations about the mean gives

$$wq = \bar{w}\bar{q} + \overline{w'q'} \tag{2.16}$$

and applying this to (2.13), expanding the terms and making the common assumption that ρ' is negligible gives

$$\rho\frac{\partial q}{\partial t} + q\frac{\partial \rho}{\partial t} + \frac{\partial}{\partial x}(\rho\left(\bar{q}\bar{u} + \overline{q'u'}\right)) + \frac{\partial}{\partial y}(\rho\left(\bar{q}\bar{v} + \overline{q'v'}\right)) + \frac{\partial}{\partial z}(\rho\left(\bar{q}\bar{w} + \overline{q'w'}\right)) = S_q \tag{2.17}$$

As already discussed, $\frac{\partial \rho}{\partial t} = 0$, so removing this term and rearranging the others yields:

$$\rho\frac{\partial q}{\partial t} + \frac{\partial}{\partial x}(\rho\bar{q}\bar{u}) + \frac{\partial}{\partial x}(\rho\overline{q'u'}) + \frac{\partial}{\partial y}(\rho\bar{q}\bar{v}) + \frac{\partial}{\partial y}(\rho\overline{q'v'}) + \frac{\partial}{\partial z}(\rho\bar{q}\bar{w}) + \frac{\partial}{\partial z}(\rho\overline{q'w'}) = S_q, \tag{2.18}$$

and by further expansion of terms

$$\begin{aligned}\rho\frac{\partial q}{\partial t} \quad + \quad \bar{q}\left(\frac{\partial}{\partial x}(\rho\bar{u}) + \frac{\partial}{\partial y}(\rho\bar{v}) + \frac{\partial}{\partial z}(\rho\bar{w})\right) + \rho\left(\bar{u}\frac{\partial \bar{q}}{\partial x} + \bar{v}\frac{\partial \bar{q}}{\partial y} + \bar{w}\frac{\partial \bar{q}}{\partial z}\right) \\ + \frac{\partial}{\partial x}(\rho\overline{q'u'}) + \frac{\partial}{\partial y}(\rho\overline{q'v'}) + \frac{\partial}{\partial z}(\rho\overline{q'w'}) = S_q.\end{aligned} \tag{2.19}$$

Here the whole of the second term is zero from the continuity equation (2.14), leaving us with

$$\rho\frac{\partial q}{\partial t} + \rho\left(\bar{u}\frac{\partial \bar{q}}{\partial x} + \bar{v}\frac{\partial \bar{q}}{\partial y} + \bar{w}\frac{\partial \bar{q}}{\partial z}\right) + \frac{\partial}{\partial x}(\rho\overline{q'u'}) + \frac{\partial}{\partial y}(\rho\overline{q'v'}) + \frac{\partial}{\partial z}(\rho\overline{q'w'}) = S_q, \tag{2.20}$$

but the horizontal advection and diffusion terms dealt with by ERA-Interim forcing (or assumed zero due to horizontal homogeneity otherwise) therefore these terms are included as part of the source term (S_q). Removing these terms and dividing by ρ yields:

$$\frac{\partial q}{\partial t} + \bar{w}\frac{\partial \bar{q}}{\partial z} + \frac{1}{\rho}\frac{\partial}{\partial z}(\rho\overline{q'w'}) = \frac{S_q}{\rho}. \tag{2.21}$$

The third term on the left hand side now refers to the small variations of q and w about their mean value and correlations between these variations. Applying K-theory (equation 2.10) to this introduces a diffusion term and gives our final prognostic equation:

$$\frac{\partial q}{\partial t} + \overline{w}\frac{\partial \overline{q}}{\partial z} - \frac{1}{\rho}\frac{\partial}{\partial z}\left(\rho K_q \frac{\partial q}{\partial z}\right) = \frac{S_q}{\rho}. \tag{2.22}$$

Equation 2.22 is used for the variables θ_l, q_t and q_i, although K_{q_i} is set to 0 so ice is not affected by turbulent mixing. The source terms can be summarised as

$$S_{\theta_l} = R + \frac{L_s}{c_p} S_{q_i}, \tag{2.23}$$

$$S_{q_t} = -S_{q_i}, \tag{2.24}$$

$$S_{q_i} = N + D. \tag{2.25}$$

where R is the layer averaged heating or cooling rate passed from the radiation scheme, N is the change in ice mass from nucleation and D is the net effect of depositional growth and evaporation of ice. Equation 2.22 can also be used for u and v if the source terms are written as

$$S_u = \rho f (v - v_g) \tag{2.26}$$

$$S_v = -\rho f (u - u_g) \tag{2.27}$$

2.3.4 Vertical transport of ice by diffusion

Throughout this thesis, the turbulent mixing scheme is not applied to the ice water content. This choice has been made as the choice of how to implement the turbulent mixing of ice is difficult and does not necessarily follow the same route as the turbulent mixing of the thermodynamic variables.

The largest value of eddy diffusivity (K) in the simulations in this thesis is around 100 $m^2\ s^{-1}$ and occurs around 200 m below the cloud top. The effect of the turbulent mixing in the top of the cloud layer to the ice water content can be thought of a vertical velocity (w), with an appropriate scaling ($w = K/z$, where z is the depth from cloud top in metres). This gives a maximum value of w of 0.5 m s^{-1}. At this depth from cloud top the grid-box mean ice fall velocity is around

0.8 m s^{-1}. From this we can see that the effect of turbulent mixing on the ice is always smaller than the effect of the gravitational pull on the ice particles and as such the inclusion of turbulent mixing on the ice only serves to slow the fall of ice from the cloud top, rather than increasing the ice water content there. In many cases the turbulent mixing is less strong than this and has a smaller effect. In addition there are two negative feedbacks that largely negate the effect of the reduced sedimentation rate and therefore larger ice water contents near cloud top - these are (a) increase in fall velocity due to increased mass of ice particles and (b) reduction in turbulent mixing strength due to less liquid water and hence less radiative cooling to destabilise the layer. These act to reduce the amount of ice near cloud top due to faster sedimentation. The resulting change is a movement in the equilibrium position of the cloud, but not a change to the structure or dynamics of the cloud itself.

The inclusion of a the turbulent mixing scheme for ice makes no difference to the conclusions of the thesis. Using the exact implementation as for the thermodynamic variables (which probably overestimates the effect) reduces the amount of supercooled liquid water in the control simulations by 40% and across the range of sensitivity tests reduces the mean by 35%. This is associated with a reduction in cloud duration of 5% in the control simulation and sensitivity test average. This is a similar magnitude as the sensitivity tests where the turbulent mixing scheme is modified, which is one of the smallest sensitivities of all those tested. The main conclusions regarding the importance of the ice growth processes and the sensitivity to vertical resolution are robust, whether or not ice mixing is included. Additionally, the vertical profiles of liquid water and ice - which are important when parameterizing the sub-grid profile in chapter 5 - do not change in shape. The vertical profile of ice water content in the top 400 m of the cloud layer remains a linear function of height, although with an increased value of ice water content throughout the depth of the layer and hence the parameterization still fixes the main deficiencies in the coarse resolution models.

2.3.5 Calculating T, q_v and q_l from θ_l and q_t

θ_l and q_t are good as prognostic variables because they are conserved in reversible moist adiabatic processes. However, the model usually requires the air temperature and liquid water mixing ratio for use in various parameterizations. Therefore a process to calculate these is required.

Equation 2.1 can be written equivalently using T_l, the liquid water temperature, instead of θ_l as

$$T_l = T - \frac{L}{c_p} q_l. \tag{2.28}$$

Assuming that any water vapour in excess of the saturation mixing ratio (q_s) is converted instantly to liquid then q_l can be calculated as

$$q_l = \begin{cases} q_t - q_s(T,P) & \text{if } q_t > q_s(T,P), \\ 0 & \text{otherwise,} \end{cases} \tag{2.29}$$

where $q_s(T,P)$ is calculated using the following approximation to the Clausius-Clapeyron equation:

$$q_s(T,P) = \frac{m_v}{m_d P} \times 611 \times \exp\left(17.269 \times \frac{T - 273.16}{T - 35.86}\right), \tag{2.30}$$

where m_v and m_d are molar masses of water vapour and dry air respectively, P is air pressure in Pascals and T is air temperature in Kelvin. Whilst P is known, T itself depends on q_s so T is approximated using T_l. For this a first-order Taylor series expansion of $q_s(T,P)$ about T_l is used:

$$q_s(T,P) \approx q_s(T_l,P) + \left.\frac{dq_s}{dT}\right|_{T_l} (T - T_l), \tag{2.31}$$

and whilst this assumes that the exponential function q_s is linear about T_l, the approximation gives good results for values of θ_l below 290 K. This approximation allows us to be reasonably accurate for the simulation of most supercooled mixed-phase cases. Using this Taylor series expansion allows us to solve for T, q_v and q_l using the following equations:

$$T = \frac{T_l + \frac{L}{c_p}\left[q_t - q_s(T_l,P) + \left.\frac{dq_s}{dT}\right|_{T_l} T_l\right]}{1 + \frac{L}{c_p}\left.\frac{dq_s}{dT}\right|_{T_l}}, \tag{2.32}$$

$$q_l = \max\left[q_t - q_s(T,P),\, 0\right], \tag{2.33}$$

$$q_v = q_t - q_l, \tag{2.34}$$

and to further increase the accuracy of these equations, they are solved in a four stage iterative process where our initial estimate of T from the first stage is used in place of T_l in the second iteration, and similarly for the third and fourth iterations.

2.4 Parameterizations used

There are many important atmospheric processes that require parameterizations to be incorporated into numerical models, either because they represent processes on scales smaller than the grid-scale (e.g. turbulence and cloud formation) or to represent the change of other prognostic variables with time (e.g. radiative transfer and ice growth processes).
In EMPIRE the processes that are parameterized are:

1. Vertical diffusion (local and non-local turbulent mixing)
2. Ice nucleation, growth and sedimentation
3. Radiative exchange
4. Partial cloudiness

2.4.1 Vertical diffusion

In equations (2.12) and (2.22) derived earlier, terms for turbulent vertical fluxes of variables calculated as the gradient of the variable in the vertical multiplied by an eddy diffusivity K_q. Described below are two methods for parameterizing K_q for use in these equations using schemes based on 'local' (Louis, 1979) and 'non-local' (Lock et al., 2000) mixing.

Which of these two schemes is used at a given time and location is determined from the Richardson number, defined as

$$Ri = \frac{N^2}{S^2} = \frac{\frac{g}{\theta}\frac{d\theta}{dz}}{\left|\frac{d\mathbf{u}}{dz}\right|^2} \tag{2.35}$$

where N^2 is the Brunt-Väisälä frequency and tells us about the static stability of the atmosphere and S is the vertical wind shear. Where the Richardson number is less than zero the atmosphere is statically unstable and the non-local scheme is used, and where it is positive the local scheme is used. If the local scheme gives larger values of K_q than the non-local scheme in unstable conditions then the larger value is used to ensure smoothness of the diffusivity profile.

2.4.1.1 Local mixing

The local vertical mixing scheme in EMPIRE is based on Louis (1979), and is very similar to the scheme used in the Met Office Unified Model, where the value of K_q is parameterized based on the local atmospheric stability and vertical wind shear. These two terms are combined through the Richardson number (2.35). K_q is parameterized as

$$K_q = l^2 \left| \frac{d\mathbf{u}}{dz} \right| F(Ri) \tag{2.36}$$

where $F(Ri)$ is given by

$$F = \begin{cases} (1-5Ri)^2 & 0 \leq Ri < 0.1, \\ (20Ri)^{-2} & 0.1 \leq Ri. \end{cases} \tag{2.37}$$

and l is the neutral mixing length, increasing in size with distance above the ground, z, and calculated using

$$l = \frac{0.4z}{1+\frac{z}{10}} \tag{2.38}$$

The function of F is taken from Met Office Documentation (Lock, 2007, pp. 15). In cases where $Ri < 0$ the value of K_q is calculated as if $Ri = 0$, but the non-local mixing scheme is also active. The value of K_q used is the larger of that parameterized by the local and non-local schemes.

2.4.1.2 Non-local mixing

In addition to the local mixing parameterization a non-local mixing parameterization is used to allow enhanced mixing in convectively unstable regions. Where the atmosphere is statically unstable, that is to say $Ri < 0$, then K_q is parameterized using an unstable parcel method. The method follows that described in Lock et al. (2000) but only the part of the scheme dealing with negatively buoyant parcels is used. This is because localised heating rarely occurs away from the Earth's surface, but localised radiative cooling occurs at the top of all clouds and can lead to destabilisation. As boundary layer dynamics are not of concern then neglecting the positively buoyant parcels should not result in erroneous simulations. K_q is parameterized using the following method:

1. Find unstable layer tops. This is done by identifying layers where $Ri < 0$ and finding the highest model level in each of these layers where the radiation scheme diagnoses cooling.

2. Modify θ_{vl} for an air parcel at the top of this layer to account for radiative cooling using

$$\theta_{vl}^{\mathrm{mod}} = \theta_{vl}^{\mathrm{top}} - tR \tag{2.39}$$

where R is the model level radiative cooling rate in K s^{-1} and t is the cloud-top residence timescale for mixed-layer eddies, taken to be 500 seconds as in Lock et al. (2000).

3. Find the equilibrium height where the negatively buoyant parcel will sink to by searching downwards from the layer top to find $\theta_{vl}(z) \leq \theta_{vl}^{mod}$ and take z to be the equilibrium height.

4. Use the mixed-layer depth to calculate entrainment rate between two model levels at the top of the mixed layer using

$$w_e = \frac{\frac{A_1 V_{sum}^3}{z_{ml}} + g\beta_T \alpha_t \Delta F}{\Delta b + c_T \frac{V_{sum}^2}{z_{ml}}} \tag{2.40}$$

from Lock et al. (2000), where $A_1 = 0.23$, z_{ml} in the mixed-layer depth in m, $\beta_T \approx T^{-1}$, $\alpha_t = 0.2$, ΔF is the radiative flux divergence in K m s^{-1}, Δb is the buoyancy jump across the inversion, $c_T = 1$ and $V_{sum}^3 = V_{rad}^3 + V_{br}^3$ which are the velocity scales for radiation and buoyancy reversal respectively, in (m s^{-1})^3, defined as:

$$V_{rad}^3 = \frac{g z_{ml} \Delta F}{T} \tag{2.41}$$

$$V_{br}^3 = A_{br} \chi_s^2 \max[0, -\delta b] \Delta b^{0.5} z_c^{1.5} C_{frac} \tag{2.42}$$

where $A_{br} = 0.24$, z_c is the cloud depth in m, C_{frac} is the cloud fraction and

$$\chi_s = -q_{l_{max}} \frac{1 + \frac{L}{c_p}\gamma_s}{\Delta q_t - \gamma_s \Delta \theta_l} \tag{2.43}$$

$$\delta b \approx g\left(\frac{\Delta \theta_l}{T} + 1.644 \Delta q_t\right) \tag{2.44}$$

$$\gamma_s = \frac{dq_s}{dT} \tag{2.45}$$

where $\Delta\theta_{vl}$ and Δq_t are the grid level changes of θ_{vl} and q_t across the inversion and $q_{l_{max}}$ is the cloud top liquid water mixing ratio.

5. Use the entrainment rate to improve the estimate of cloud top θ_{vl} using

$$\theta_{vl}^{mod} = \theta_{vl}^{top} + \frac{w_e \Delta \theta_{vl} - \Delta F}{V_{sum}}. \tag{2.46}$$

6. Re-calculate the equilibrium height as in step 3 using new θ_{vl}^{mod}.

7. Apply the following function for K_q throughout the mixed-layer:

$$K_q = 0.85\kappa V_{sum} \frac{z'^2}{z_{ml}} \left(1 - \frac{z'}{z_{ml}}\right)^{0.5} \tag{2.47}$$

as in Lock et al. (2000), where $\kappa = 0.4$ and z' is the distance from the bottom of the mixed layer, z_{ml}. Note that the exponent on the final term is set to 0.8 in the UM (Lock, 2007), unlike the value of 0.5 in Lock et al. (2000). The shape of the parameterized diffusivity profile can be seen in figure 2.1.

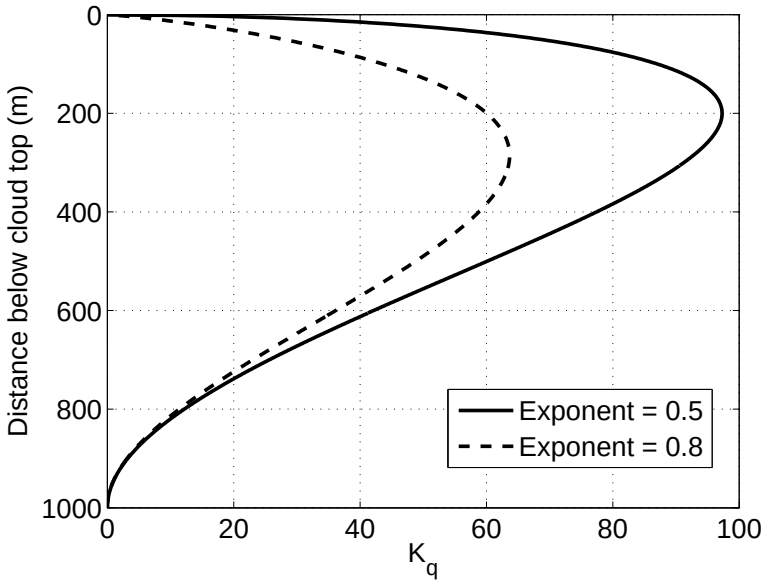

Figure 2.1 Vertical profile of eddy diffusivity for a mixed-layer depth of 1000 m and $V_{sum} = 1$ m/s as calculated from the non-local mixing scheme using equation 2.47, with an exponent of 0.5 and 0.8.

2.4.2 Ice production and sedimentation

Ice production in mixed-phase clouds is the main factor which determines the glaciation rate and therefore, together with sources of liquid such as radiative cooling and turbulence, determines how long the liquid persists for. There are three different factors which are important for defining how much ice is produced; these are: nucleation, depositional growth and sedimentation. Other microphysical processes, such as ice-rain interactions, rain production and Hallett-Mossop (Hallett and Mossop, 1974) ice multiplication are thought to be unimportant in stratiform mixed-phase

clouds and are therefore not included in EMPIRE. The ice scheme is consistent with Wilson and Ballard (1999) although with the implicit assumptions about ice crystal habit, terminal velocity and mass-diameter relation removed and can be changed freely. This in turn makes it similar to the Rotstayn et al. (2000) scheme with the difference being that the Rotstayn scheme assumes all ice crystals are the same size, whilst Wilson and Ballard (and EMPIRE) assume an exponential distribution of sizes based on temperature and ice water content.

Nucleation

Ice nucleation occurs through either homogenous or heterogenous nucleation. Homogenous nucleation is where ice is produced from the freezing of liquid without the need for an external mechanism for freezing. In contrast, heterogeneous nucleation occurs when liquid water is frozen with the aid of an ice nucleus. Homogenous nucleation only occurs at temperatures below $-40\,^{\circ}$C whereas heterogenous nucleation dominates at temperatures between $0\,^{\circ}$C and $-40\,^{\circ}$C, with an increasing number of available ice nuclei, and therefore increasing chance of a nucleation event, at colder temperatures (Rogers and Yau, 1988). Ice nuclei are not as abundant in the atmosphere as cloud condensation nuclei and therefore often limit the rate of production of ice particles; however, for simplicity it is assumed that there are always enough ice nuclei present in EMPIRE. Following Wilson and Ballard, ice is nucleated every time step within a grid-box when the following conditions are satisfied:

1. At temperatures colder than $-40\,^{\circ}$C, if liquid is present, then all liquid is converted instantly to ice.
2. Heterogenous nucleation occurs in a grid-box if there is liquid present and the temperature is colder than $-10\,^{\circ}$C.

The number of ice crystals nucleated follows the Fletcher (1962) relation, but limited to a maximum value, as used in Wilson and Ballard (1999):

$$n = \min\left(0.01\,\exp\left(-0.6T\right),\ 10^5\right) \tag{2.48}$$

where n is the number of ice crystals activated per cubic metre at temperature $T(^{\circ}C)$. Each ice crystal nucleated is given an initial mass of 1×10^{-12} kg. The size of the initial nucleated mass is not important in the model simulations as the depositional growth term dominates the ice particle growth once it has formed.

Depositional growth of ice particles

Growth by deposition is the primary way that small ice particles can grow. The growth of a single ice particle by vapour diffusion can be calculated following this equation from Rogers and Yau (1988)

$$\frac{dm}{dt} = \frac{4\,\pi\,CFSS_i}{\left(\frac{L_s}{R_vT} - 1\right)\frac{L_s}{KT} + \frac{R_vT}{e_i(T)D}} \tag{2.49}$$

where m is the mass of the ice crystal in kg, C is the capacitance of the ice particle in m, dependent on its size and shape, F is the ventilation coefficient, SS_i is the supersaturation of the air with respect to ice, L_s is the latent heat of sublimation, K is the thermal conductivity of air, D is the diffusivity of water vapour in air and e_i is the saturated vapour pressure over ice. The ventilation coefficient is computed as $F = 0.65 + 0.44Sc^{1/3}Re^{1/2}$ (Pruppacher and Klett, 1978) with the Schmidt number ($Sc = 0.6$) and the Reynolds number ($Re = v(D)\rho D/\mu$) where $v(D)$ is the fall-speed of the ice particle and μ is the dynamic viscosity of air. The temperature dependence of L_s, K and D are neglected; EMPIRE uses values suitable for 0 °C, which are $L = 2.83 \times 10^6$ J kg^{-1}, $K = 2.40 \times 10^{-2}$ J m^{-1} s^{-1} K^{-1} and $D = 2.21P^{-1}$ m^2 s^{-1}, where P is the air pressure in Pascals. The total growth rate of ice in a grid-box is calculated by applying equation (2.49) to each ice particle. This involves integrating over an assumed distribution of ice particle sizes:

$$\left.\frac{dq_i}{dt}\right|_{\text{deposition}} = \frac{1}{\rho}\int \frac{dm}{dt} N_{\text{ice}}(D)\, dD \tag{2.50}$$

where $N_{\text{ice}}(D)$ is the number of ice particles of diameter, D, in metres given by the Wilson and Ballard size distribution as:

$$N_{\text{ice}}(D) = N_{0\text{ice}}\exp\left(-0.1222T\right)\exp\left(-\Lambda_{\text{ice}}D\right) \tag{2.51}$$

where $N_{0\text{ice}} = 2.0 \times 10^6$ m^{-4} and T is the temperature in degrees Celsius. Λ_{ice} is defined as

$$\Lambda_{\text{ice}} = \left(\frac{\text{IWC}}{aN_{0ice}\Gamma(b+1)\exp(-0.1222T)}\right)^{\frac{-1}{b+1}} \tag{2.52}$$

where IWC is the ice water content in kg m^{-3}, Γ is the gamma function and a and b are the coefficient and exponent in the mass-diameter relation (equation 2.53).

The mass (kg) of an ice crystal is commonly related to its diameter (m) through the following relationship

$$m = aD^b \tag{2.53}$$

where a and b are constants with values for different particle habits given in Table 2.1. In many ice schemes the ice particles are assumed to be spherical, which is unphysical as almost all ice crystals are not spherical and results in both the growth rate and terminal fall velocity of the ice particles being calculated incorrectly. However, by assuming spheres and that the capacitance, $C = D/2$, then the diffusional growth equation (2.49) reduces to that of spherical droplets but with supersaturations and latent heat terms relevant for ice. In reality the shape (habit) of the ice crystals is variable and the primary mode of growth depends on both temperature and supersaturation of the air (Rogers and Yau, 1988). The capacitance is dependent on the habit of the ice crystal but is not a well defined function. Numerical simulations by Westbrook et al. (2008) found that the capacitance of aggregates is around half that of spheres, implying that models assuming spherical ice particles may overestimate their growth rate by a factor of 2. Table 2.1 shows values from experimental data and model parameterizations for different habits, which are included in EMPIRE as alternative habits.

Table 2.1 Summary of different crystal habits used in EMPIRE with values for a, b, c, d for use in equations 2.53 and 2.54 and how the capacitance, C, is assumed to vary with diameter D.

Habit	a	b	C	c	d	Reference
Spheres	0.069	2.00	D/2	25.2	0.527	Wilson and Ballard (1999)
Spheres	366.519	3.00	D/2	-	-	Rotstayn et al. (2000)
Spheres	0.0185	1.90	-	-	-	Brown and Francis (1995)
Hexagonal Plates	0.00376	2.00	D/π	-	-	Rotstayn et al. (2000)
Hexagonal Plates	-	-	-	17.9	0.62	Heymsfield and Kajikawa (1987)
Dendrites	0.2423	2.53	D/π	3.29	0.33	Avramov and Harrington (2010)

Ice sedimentation

Ice crystals are assumed to fall at their terminal velocity, which is assumed to be related to the diameter in a similar way to the mass by

$$V = cD^d. \tag{2.54}$$

values for c and d are given in table 2.1 for diameters in m and fall velocities in m s^{-1}. The transfer of ice from grid level to grid level is calculated using the mass weighted fall speed, defined as

$$V_m = \frac{\int V(D)m(D)N_{\text{ice}}(D)\,dD}{\int m(D)N_{\text{ice}}(D)\,dD}. \tag{2.55}$$

and uses the same assumed size distribution as for the ice growth. Ice is not permitted to fall more than one grid level in a timestep. To improve the accuracy of ice sedimentation a Total Variation Diminishing (TVD) advection scheme is used; this helps to preserve gradients of ice water content. The TVD scheme is described in section 2.6

2.4.3 Radiative transfer

The radiative transfer in EMPIRE is calculated using the Edwards-Slingo radiation code (Edwards and Slingo, 1996). A radiation scheme is required to accurately model the atmospheric temperature changes due to the emission and absorption of radiation. In mixed-phase clouds, this happens most notably at the cloud top where a layer of liquid water emits longwave radiation. Other radiative impacts, such as the absorption and reflection of solar radiation by clouds, will need to be modelled accurately to correctly simulate the evolution of mixed-phase clouds.

The Edwards-Slingo radiation code is a two-stream model which calculates the longwave and shortwave fluxes through layers of the atmosphere and infers heating and cooling rates from the radiative flux convergence/divergence. The effective radius of liquid droplets is set to 10 μm and the effective radius for ice crystals is set to 50 μm. The radiation scheme also includes the effects of water vapour, ozone, carbon dioxide, methane, oxygen, nitrous oxide and CFCs.

By default the radiation scheme is called every 15 minutes throughout the simulation so that the model is able to react quickly if cloud forms. GCMs typically call the radiation scheme less frequently than this, typically about every 3 hours for climate models, and this could be one reason why GCMs do not represent mixed-phase clouds well. Mixed-phase clouds are thought to be largely driven by the radiative cooling from cloud top and as such a good representation of the radiative exchange is important.

2.4.4 Partial cloudiness

Most atmospheric variables vary on spatial scales much smaller than typical grid-box sizes. Most models, however, only store information about the grid-box mean values. In some cases, such as for pressure and temperature this is reasonable, but for other variables this does not give the model

sufficient information to achieve realistic simulations. One such example is for cloud formation; clouds form when the humidity of the air reaches or exceeds saturation. However, cloud does not usually form uniformly across scales of many kilometres. Clouds can form even when the large-scale mean humidity is below saturation due to local anomalies of moisture and/or temperature. By assuming some variation of humidity within the grid box the formation of cloud as the grid-box mean humidity approaches saturation can be parameterized. One can assume many things about the sub-grid scale variability of moisture and temperature. In EMPIRE this variability is parameterized following Smith (1990) where a triangular distribution of total water mixing ratio within the grid box is assumed and the fraction of the grid-box in which cloud exists and the liquid water mixing ratio of the cloud that is present is calculated from this distribution.

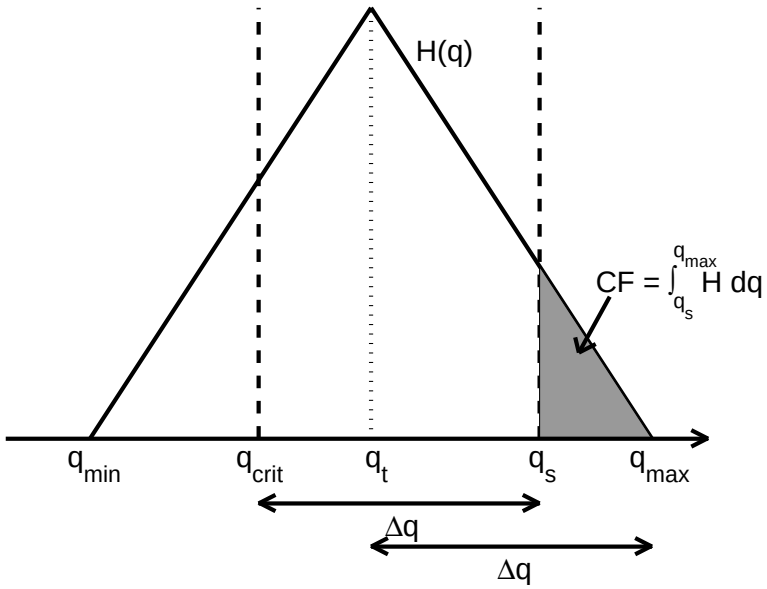

Figure 2.2 Illustration of a typical sub-grid distribution of total water mixing ratio as parameterized by the Smith (1990) scheme. The mean of the distribution is greater than q_{crit} so part of the grid-box is assumed to be cloudy. The fraction of the grid-box which is cloudy is represented by the grey shaded area relative to the whole area under the distribution.

Figure 2.2 illustrates the triangular moisture distribution from Smith (1990). If the temperature and pressure are known, q_s can be calculated, so the only further thing needed to calculate the cloud fraction and the liquid water mixing ratio of the cloud is the width of the triangle. The width of the triangle is the measure of moisture variance within the grid-box. In the Met Office model the width of the distribution is described by RH_{crit}, the critical relative humidity at which

cloud starts to form. The grid-box mean q_t at which cloud begins to form is therefore:

$$q_{\text{crit}} = \text{RH}_{\text{crit}} q_s, \tag{2.56}$$

so it then follows that the width of the distribution (from the mean value to either extreme) is

$$\Delta q = q_s - q_{\text{crit}} = (1 - \text{RH}_{\text{crit}}) q_s. \tag{2.57}$$

The maximum and minimum values of the distribution can also be defined for later use as

$$q_{max} = q_t + \Delta q; \qquad q_{min} = q_t - \Delta q. \tag{2.58}$$

There are three options for defining RH_{crit}:

- a fixed constant value which may vary with height (e.g. Met Office model)
- a prognostic variable which is modified by various physical processes (e.g. Tompkins, 2002)
- a value diagnosed from other model fields using similarity theory from turbulent boundary layers

EMPIRE uses a fixed value of $\text{RH}_{\text{crit}} = 0.85$ for all model levels, this is in the range of values used by the Met Office Unified Model, which decreases from 0.91 at the surface to 0.83 in the 4km resolution model in the free troposphere and to 0.80 in the global model (Humphrey Lean, personal communication). If the shape of the triangular distribution, $H(q)$, is defined such that $\int_{q_{min}}^{q_{max}} H \, \mathrm{d}q = 1$, then the cloud fraction, CF, and liquid water mixing ratio, q_l, can be calculated as

$$\text{CF} = \int_{q_s}^{q_{max}} H \, \mathrm{d}q \tag{2.59}$$

$$q_l = \int_{q_s}^{q_{max}} (q - q_s) H \, \mathrm{d}q \tag{2.60}$$

This gives a one to one relationship between the liquid water content of the grid-box and the cloud fraction for given temperature, pressure and RH_{crit}. The ice cloud fraction is calculated in a similar way using the ice water content of the grid-box to calculate the cloud fraction using the same equation but with a saturation mixing ratio relative to ice. Although there is no physical basis to relate the ice mixing ratio to ice cloud fraction in the same way as is done with liquid

cloud this is the method used by the Met Office model and is used in EMPIRE for consistency. When both liquid and ice exist within a grid-box they are assumed to be minimally overlapped (again following the Unified model) meaning that the model does not produce truly mixed-phase cloud until the grid-box cloud fraction reaches 100%.

2.5 Model initialization and forcing

As a single column model, EMPIRE knows nothing about the atmosphere outside of the single column. To be able to deal with the time varying nature of the atmosphere, a way of forcing the model such that it evolves in time in a suitable way is required. There are two methodologies for forcing a single column model, these are a) using a relaxation to some known state or b) incrementing the prognostic variables based on advection into or out of the model column. Each method has its advantages and disadvantages; the relaxation method will not allow the simulation to drift too far from the forced state and will significantly change the variables in EMPIRE if the forced state is very different to the modelled state. Conversely, using increments only from advection allows EMPIRE to maintain an entirely different state from the forcing data but this means that large drifts from the forced state are not preventable.

Adding terms for relaxation and advective forcing to our prognostic equation, (2.22), gives

$$\frac{\partial q}{\partial t} + w\frac{\partial q}{\partial z} - \frac{1}{\rho}\frac{\partial}{\partial z}\left(\rho K_q \frac{\partial q}{\partial z}\right) = \frac{S_q}{\rho} + \left.\frac{\partial q}{\partial t}\right|_{\text{forcing}} - \frac{q - q_{\text{truth}}}{\tau_{\text{relax}}}. \tag{2.61}$$

where $\left.\frac{\partial q}{\partial t}\right|_{\text{forcing}}$ is the advective forcing term, q_{truth} is the observed state that the model is being relaxed towards and τ_{relax} is the relaxation timescale, typically 3 hours where used in EMPIRE.

We are fortunate to have access to an advective forcing dataset based on ERA-Interim. This advective forcing dataset gives 3-hourly increments of temperature, moisture, and horizontal wind speeds due to horizontal advection. These are calculated from ERA-Interim 3-hourly changes, but with the changes due to physical parameterizations such as microphysics and radiation removed.

The ERA-Interim reanalysis forcing data is used in EMPIRE for almost all cases. This is used alone and without any relaxation to an observed state. The parameterized model physics is expected to be the dominant part of any observed change in temperature and humidity and

therefore EMPIRE would not drift too far from ERA-Interim; this assumption was tested and found to be acceptable with temperature differences between EMPIRE and ERA-Interim typically less than 1 K after 24 hours. As all models and ERA-Interim underestimate q_l (shown later) the relaxation term is not used in EMPIRE as this would force the model towards a state that is potentially to dry. Small errors in the thermodynamic profiles due to leaving out the relaxation term are more acceptable than forcing cloud formed in EMPIRE to dissipate in cases where the forcing data may well be incorrect.

The EMPIRE model is set up in such a way that it can be run from initial conditions from a variety of sources. This flexibility allows the model to be initialize using profiles from other models, atmospheric radiosonde ascents, ERA-interim reanalysis or idealised profiles.

2.6 Model numerics

The prognostic equations derived earlier are solved using a fully implicit scheme for the time derivative and a centred scheme for spatial derivatives for both the advection and diffusion terms. A tridiagonal solver is used to solve all grid-levels simultaneously. The only exception to this is the ice sedimentation scheme which is solved using a Total Variation Diminishing (TVD, e.g. Sweby, 1984) advection scheme. A TVD scheme is used to give an accurate representation of the ice sedimentation which preserves gradients and has minimal numerical diffusion. This cannot be achieved with conventional advection schemes. This is particularly important as it is expected that the formation and sedimentation of ice is a large factor in the depletion of liquid water from mixed-phase clouds.

The TVD scheme works to prevent numerical instabilities and oscillations whilst maintaining gradients in the ice water content field. To do this it requires a flux limiter, that is a means of limiting the flux from one grid-box to the next to a sensible value such that spurious extrema and negative values and spurious amplification of existing extrema are avoided (Thuburn, 1997). This is done by calculating the gradient of the field around each grid-point and defining a ratio, r, of the gradients on each side of the point

$$r_i = \frac{q_i - q_{i-1}}{q_{i+1} - q_i} \tag{2.62}$$

where subscripts i, $i-1$, $i+1$ refer to the grid-point index. The flux from one grid box to the next can be approximated in many ways. The TVD scheme required both a high-order and a low-order scheme to work. High-order schemes are generally more accurate and better represent gradients in the advected field but can introduce oscillations, whilst low-order schemes are stable but are artifically diffusive and are generally less accurate. An example of a high-order and low-order scheme would be a 2nd order, centred-in-space scheme and an upwind advection scheme respectively. These are the two schemes used in EMPIRE's TVD scheme.

Fluxes calculated from the high- and low-order schemes are then weighted at each point based on the gradient of the quantity at that point, r. Many different functions exist for the weighting of the high- and low-order fluxes and EMPIRE uses the van Leer (1974) function:

$$\phi = \frac{r+|r|}{1+|r|} \quad \text{if } r > 0 \quad \text{or} \quad \phi = 0 \quad \text{otherwise}, \tag{2.63}$$

and the flux is calculated at each point using

$$F = F_L - \phi \times (F_L - F_H) \tag{2.64}$$

where F is the total flux, F_L is the low-order flux, F_H is the high-order flux. By requiring that the flux leaving one grid-box enters the next grid-box the scheme is perfectly conservative. An improved representation of the time varying nature of the sedimentation is captured by the addition of a fourth order Runge-Kutta scheme.

2.7 Radar and Lidar forward models

Many of our observations of mixed-phase clouds come from instrumented sites where surface based radar, lidar and microwave radiometers give information about cloud structure. These instruments do not provide perfect information about the clouds present due to the way that they work. For instance, the lidar signal can be fully attenuated by liquid water and therefore any clouds above that height cannot be sampled by the lidar. In addition, the radar sensitivity decreases with distance from the instrument and thus cirrus clouds with low reflectivity, high in the troposphere are not detected. To allow reasonable comparison between these observations and EMPIRE simulations, radar and lidar forward models are applied to the EMPIRE output. This

means taking the model output and sampling the cloud fields (ice and liquid water content) as if it were seen by a radar and lidar. By doing this any potential biases of unsampled clouds are removed and this also allows us to directly compare model output with radar and lidar observations for case studies.

Radar Forward Model

The radar forward model is constructed using an expression from Hogan et al. (2006). This provides ice water content as a function of radar reflectivity factor Z (dBZ) and temperature T (°C). The relationship has been derived by comparing radar measurements with in-cloud observations using aircraft-based sensors across many mid-latitude case studies. The appropriate relationship for ice water content, IWC (g/kg), from radar reflectivity at 35GHz frequency is

$$\log_{10}(\mathrm{IWC}) = 2.42 \times 10^{-4} ZT + 0.0699Z - 0.0186T - 1.63 \tag{2.65}$$

which can be inverted to give radar reflectivity factor (in dBZ) in terms of IWC and temperature

$$Z = \frac{\log_{10}(\mathrm{IWC}) + 1.63 + 0.0186T}{2.42 \times 10^{-4} T + 0.0699} \tag{2.66}$$

The minimum detectable signal for a radar decreases as the square of the distance from the antenna. This is because the amount of power returned from targets at a greater distance decreases following the inverse square law. For the 35 GHz radar at Chilbolton the minimum detectable signal (in dBZ) is given by

$$Z_{min} = -105 + 20\log_{10} r \tag{2.67}$$

where r is the radial distance from the radar antenna in metres. The same constraint on the minimum detectable signal is also applied to the forward model so that low reflectivity clouds that could not be observed in reality are not included.

The reflectivity in the forward model is only calculated using the model ice water content field and does not include liquid water. This is because it is assumed that the liquid water observed in these supercooled clouds has a small size and as the radar return is proportional to D^6 these small droplets will likely not influence the radar reflectivity predicted from the forward model. The return from rain is not included, as rain is not a variable in EMPIRE and the effects of attenuation in the radar forward model is neglected because the liquid and ice water contents are

low in mixed-phase clouds and therefore the sensitivity will likely have a much larger effect than attenuation.

Lidar Forward Model

The lidar forward model predicts the attenuated backscatter coefficient, β' that would be detected by the instrument. This is done following Marsham et al. (2006) and briefly described below. The extinction coefficient, α_i is assumed to be

$$\alpha_j = 1.5 \times \frac{\mathrm{WC}_j}{\rho_j r_{ej}} \tag{2.68}$$

where the subscript j refers to the phase of the hydrometeor (liquid or ice), WC is the water content in kg m^{-3}, ρ is the density of liquid or ice and r_e is the effective radius. The effective radius for liquid is held at a constant value of 10 μm to be consistent with the radiation scheme, whilst the ice effective radius is calculated from the mean ice particle mass assuming they are spheres with a density of 700 kg m^{-3} following Rotstayn et al. (2000).

The backscatter coefficient, β, can be calculated from the extinction coefficient if the lidar ratio, S, is known. A value of $S = 18.5$ sr is assumed for both liquid and ice as in Marsham et al. (2006)

$$\beta_j = \frac{\alpha_j}{S_j}. \tag{2.69}$$

β is summed across both liquid and ice species and then the attenuated backscatter coefficient is calculated using

$$\beta' = \beta \exp\left(-2\,\eta\,\tau\right) \frac{1 - \exp(-2\,\eta\,\alpha\,\Delta z)}{2\,\eta\,\alpha\,\Delta z}, \tag{2.70}$$

where τ is the optical depth of hydrometeors between the lidar and the base of the model level being calculated, defined as

$$\tau = \int_0^z \alpha \; \mathrm{d}z, \tag{2.71}$$

and η accounts for multiple scattering of the lidar beam (Platt, 1973) which takes a value of 0.7 for the Chilbolton lidar (O'Connor et al., 2004) where 0.5 would give the maximum multiple scattering and 1 gives no multiple scattering. The fraction on the right hand side of (2.70) accurately deals with the attenuation within the layer being calculated (Hogan, 2006) where Δz is the depth of the model layer.

CHAPTER 3:

EVALUATING NUMERICAL MODEL PREDICTIONS OF MIXED-PHASE CLOUDS

Clouds are one of the biggest factors that influence radiative exchange and surface temperatures on daily, seasonal and longer timescales. It is therefore important to evaluate the skill of models in predicting clouds and their radiative impact. As such, previous studies have evaluated model cloud forecasts and attempted to understand deficiencies in the model that lead to erroneous cloud forecasts (e.g. Hogan et al., 2001; Tselioudis and Jakob, 2002; Illingworth et al., 2007; Bouniol et al., 2010; Delanoë et al., 2011). In this chapter the focus is specifically on mixed-phase clouds. Ground based radar and lidar observations of clouds are used to identify mixed-phase clouds and estimate the liquid and ice water contents of these clouds. Using these data, a number of days for which good observations of persistent mixed-phase clouds exist are selected and the observed clouds from these days are collated. The observed cloud properties are then compared with a number of numerical model predictions of cloud at the same time, in terms of their mean liquid and ice water contents, cloud fraction, structure and radiative impact. Much of the analysis follows the approach of Illingworth et al. (2007) by averaging the high resolution observations on to the model-grid of each model analysed. However, by selecting only days where mixed-phase clouds are present, comparing the cloud properties with observations as a function of temperature rather than height and evaluating the liquid and ice cloud fractions separately detailed information specifically about mixed-phase clouds can be extracted.

3.1 Remote sensing data and processing

The data for the observations of mixed-phase clouds used in this thesis come from ground based remote sensing instrumentation based at Chilbolton, UK which forms part of the Cloudnet research project (Illingworth et al., 2007). Much of the raw data from the instruments has been combined and processed as part of the Cloudnet project. This includes quality control of the data, conversion of reflectivity, backscatter and brightness temperatures to liquid and ice water contents and cloud fractions, averaging of the high resolution data to model grid scales and incorporation of model forecasts of temperature and pressure. An example of the process to combine these observations is shown in figure 3.1 for an observed mixed-phase cloud on 2 April 2005 and a description of this process follows.

The radar reflectivity (panel 3.1a) and lidar backscatter (panel 3.1b) are used together with the radar Doppler velocity (not shown) to determine the nature of the target (target classification, panel 3.1c). Because the lidar is sensitive to the numerous small liquid droplets and the radar is most sensitive to the larger ice particles it is possible to determine the phase of the target; this is aided by the radar Doppler velocity which highlights falling ice particles.

Where ice particles are observed, the ice water content within each pixel is determined using the empirical relationship from Hogan et al. (2006). This empirical relationship was derived from aircraft observations of clouds made during EUCREX; whilst this relationship was formulated on mid-latitude clouds which were not specifically mixed-phase clouds it is anticipated that the ice falling from mixed-phase clouds will follow a similar relationship between ice water content (IWC in g m^{-3}) and radar reflectivity (Z in dBZ) to that derived by Hogan et al. (2006). The relationships used are

$$\log_{10}(\mathrm{IWC}) = 0.000242ZT + 0.0699Z - 0.0186T - 1.63 \qquad \text{for 35GHz radar and} \qquad (3.1)$$

$$\log_{10}(\mathrm{IWC}) = 0.000580ZT + 0.0923Z - 0.00706T - 0.992 \qquad \text{for 94GHz radar,} \qquad (3.2)$$

where T is the temperature in °C.

The liquid water content values are obtained through the use of all three instruments. The Cloudnet retrieval algorithm uses the lidar to identify the base of a liquid cloud layer, but due to the attenuation of the lidar beam by liquid water it is unable to detect the cloud top reliably, so

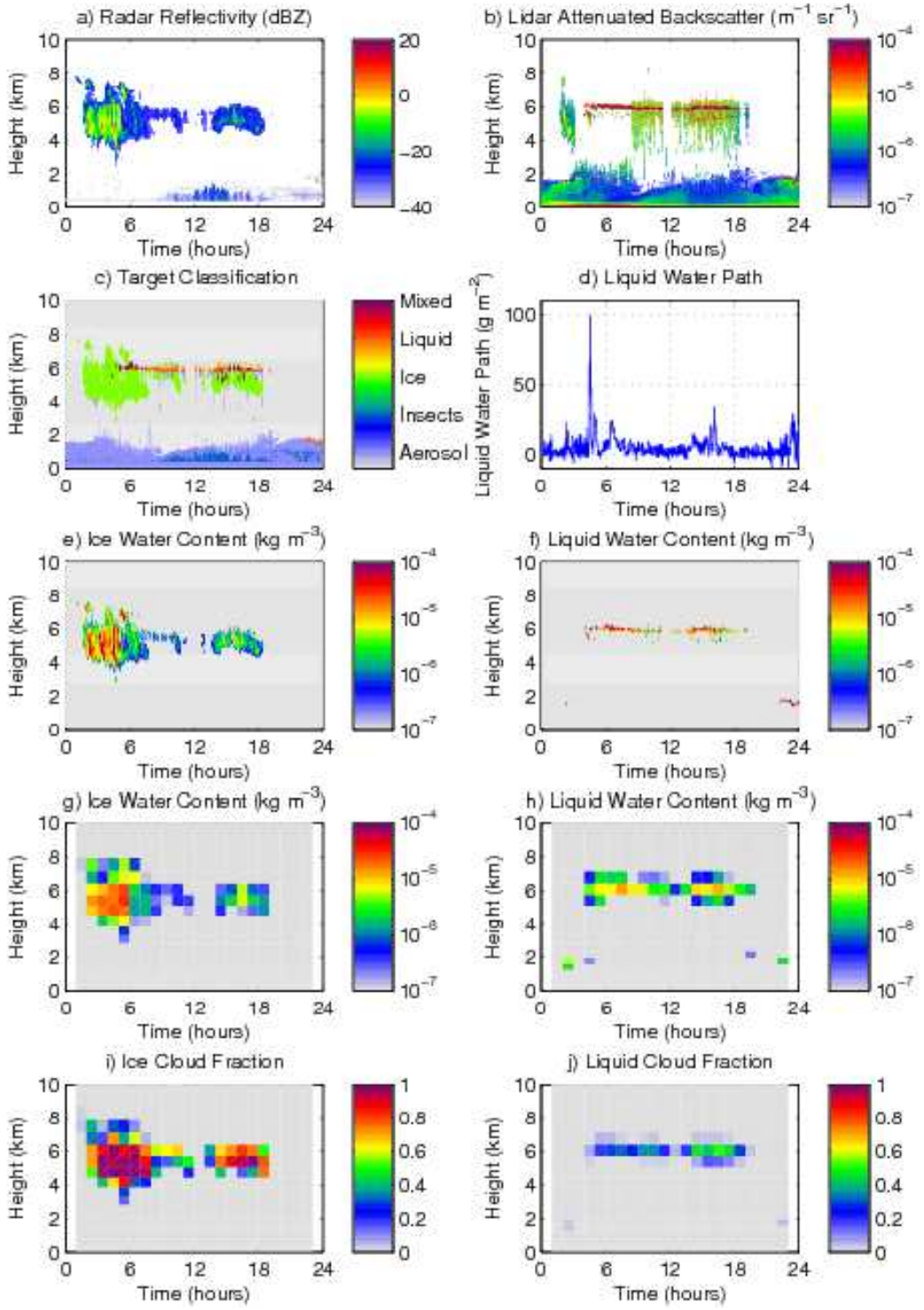

Figure 3.1 Illustration of the a) radar and b) lidar observations from 2 April 2005 used together in c) to determine the nature of the target. The liquid water path measured by the microwave radiometer is shown in d) and the derived ice and liquid water contents in e) and f). These are then averaged to the Met Office Mesoscale model grid scale for water contents and clouds fraction of liquid and ice (g-j).

instead the cloud top height derived from the radar is used. Using the cloud top and base height and model temperature and pressure, the liquid water content profile is calculated assuming that the cloud is adiabatic from cloud base to cloud top. The liquid water path (the integral of the liquid water content) measured by the microwave radiometer (panel 3.1d) is then used to scale the in-cloud liquid water content profile such that both liquid water paths agree. There are a number of complications with this method, primarily caused by the presence of multiple layers of cloud. With multiple layers the attenuation of the lidar beam means higher layers may not be detected at all and if they are then the liquid water path of each layer is uncertain as there exists only a single retrieval of liquid water path for the atmospheric column. As a result of this only single-layer mid-level mixed-phase clouds have been selected for analysis and only at times when there are no low level clouds; this restriction significantly reduces the number of days and times suitable for analysis.

Once the liquid and ice water contents have been calculated on the high-resolution data (panels 3.1e,f), it is then averaged to the model grid scale. This involves averaging over height ranges consistent with the spacing of the model vertical levels and over sufficient time to represent the horizontal grid spacing of the model (calculated using the models horizontal wind speed). This is done separately for each model and therefore results in a number of different 'observations'. The liquid and ice water contents (panels 3.1g,h) are the observed mean in the vertical and horizontal (time) space corresponding to the model grid-box whilst the cloud fraction is the number of pixels where the liquid or ice water content in larger than zero. The cloud fraction is not split by phase in the Cloudnet data so the total cloud fraction is assumed to be ice and the liquid cloud fraction has been calculated using the same code used to generate the total cloud fraction but using the liquid water content values.

3.2 Details of numerical models

A number of numerical weather prediction (NWP) and regional climate models (RCMs) will be compared later and their ability to predict mixed-phase clouds analysed. In this section an outline of each of the models used in this comparison is given and the key differences in the models are highlighted, particularly that may explain their varying ability to predict mixed-phase clouds.

Table 3.1 Details of the numerical models and their cloud schemes used in later comparisons. Modified from Illingworth et al. (2007).

	UKMO--Meso	UKMO--Global	ECMWF	Météo-France	RACMO	ERA-Interim
Horizontal Resolution (km)	12	60	40 (25)	23.4	18	79
Number of Vertical Levels	38	38	60 (91)	41 (60)	40	60
Grid-box depth at 5 km (m)	615	636	551 (397)	491	523	548
Minimum Liquid Temperature (°C)	-40	-40	-23	$-40(-23)$	-23	-23
Prognostic Cloud Variables[1]	q_t, q_i	q_t, q_i	q_c, A	q_c	q_c, A	q_c, A

[1] Prognostic cloud variables are q_t – total water mixing ratio, q_c – cloud (liquid + ice) water mixing ratio, q_i – ice water mixing ratio and A – cloud fraction.

Table 3.1 shows details of the model resolution, which ranges between 12 and 79 km in the horizontal and 397 and 636 metres in the vertical at 5 km altitude. Our dataset spans 7 years from 2003 to 2009 and as these models are being compared over a long period, where the model settings have changed, the initial value is given and the most recent value is given in brackets. The table also gives details about the cloud scheme used in each model, the prognostic variables used and the coldest temperature at which liquid water is permitted to exist.

Only two of the models have a cloud scheme where cloud ice is a prognostic variable separate from liquid (UKMO-Meso and UKMO-Global). The other models have a single prognostic variable for total condensed water in the cloud and the ratio of liquid and ice in any grid-box is a diagnostic function of temperature. This simplification does not allow the models with diagnostic ice to capture the structure of mixed-phase clouds that are observed (Marsham et al., 2006).

3.3 Definition of diagnostics

To be able to compare the model output with the observations of mixed-phase clouds diagnostics need to carefully chosen so that they can be equivalently calculated from both modelling and observational datasets. Three diagnostics are chosen that will serve as the method of comparison; each of these are mean quantities over the whole dataset (described below) and are divided up into temperature ranges each spanning 5 °C. The data is averaged over particular temperature ranges as it is expected that microphysical processes such as ice nucleation, deposition growth rate and ice particle habit are the important processes in controlling the structure of mixed-phase clouds

and these processes are themselves dependent on temperature.

Mean liquid water content

The mean liquid water content is our primary chosen diagnostic. This is the mean liquid water content observed from the whole dataset, including times when no cloud is observed. This is an important diagnostic because it is a physical quantity directly comparable to the model liquid water content and because it is an important factor in calculations of radiative exchange, particularly for solar radiation. It also has the advantage that, as a dataset mean, it is not sensitive to the resolution of the data and is not dependent on making any other assumptions to make the model data comparable with observations. The drawback with this diagnostic is that it requires a minimum of two instruments to locate and quantify the amount liquid and is therefore liable to large errors.

Mean liquid cloud fraction

The mean liquid cloud fraction is calculated from all times whether or not a cloud is observed. Like the mean liquid water content this quantity is not sensitive to the resolution of the data used; however, it is not as easy to ensure that like values from observations and models have the same physical interpretation. Models typically only have a single cloud fraction quantity which applies to both liquid and ice cloud. In some models (e.g. the Met Office Unified Model) the liquid and ice cloud fractions are calculated separately and then combined to create a single value. The Met Office model uses a minimum overlap assumption for liquid and ice clouds which means that the liquid and ice clouds are assumed to fill different parts of the grid-box whilst the total cloud fraction is less than 1. Therefore the liquid and ice cloud fractions are added together to obtain the total cloud fraction, assuming this gives a value not greater than 1. The liquid and ice cloud fractions can therefore be calculated separately using the model water contents and these values are used in the comparisons. Other models calculate a single cloud fraction from the total condensed water content regardless of phase and determine the ratio of liquid to ice water content later. In these cases it is not possible to determine how much of the cloud fraction comes from liquid and ice or whether it is all mixed-phase. It is therefore assumed that the liquid and ice are maximally overlapped and uniformly mixed throughout the cloudy part of the grid-box and this allows us to use the cloud fraction value output from the model for both the liquid and ice cloud fractions in our comparisons. Another difficulty is that the cloud fractions output from the model do not have a strong physical basis. Model cloud fractions are diagnosed largely for the

radiation scheme calculations and have little impact of the model evolution in any other way. The parameterization of ice cloud fraction is particularly challenging as there is no theoretical reason why a higher mean ice water content should mean a higher ice cloud fraction and indeed some studies have shown this assumption to be false (Bodas-Salcedo et al., 2008). For liquid water it might be expected that a grid-box that has a higher fraction saturated with respect to water to also have a larger liquid water content as is suggested by Smith (1990). However, the relationship between liquid water content and liquid cloud fraction is the subject of ongoing research (e.g. Wood and Field, 2000).

The observed liquid cloud fraction is calculated using the fraction of lidar measurements detecting liquid water. Points where the lidar was unable to detect anything due to attenuation by lower altitude clouds are not included but additional points are added at the top of liquid-layers where the lidar has been attenuated within the liquid-layer but the radar observations indicate the cloud extends higher than this and is likely to contain liquid. As a result of this the colder temperatures have fewer data points than the warmer temperatures due to the lidar being attenuated. It is expected that the omission of these points where the lidar signal was attenuated will artifically increase the cloud fraction at these colder temperatures, but that the overall effect of this will be small because the selected cases have only single-layer clouds.

Mean in-cloud liquid water content

The mean in-cloud liquid water content is simply the mean of in-cloud liquid water content calculated by dividing the mean liquid water content in each grid-box by the liquid cloud fraction. This enables us to determine whether modelled clouds are predicting the correct ratio of liquid water and cloud fraction. This quantity is the most sensitive to the resolution chosen as, for instance, a single small cloud passing over the observation site will have a high mean liquid water content when present, but when averaged to the scale of a model grid-box has a cloud fraction below 1 and a lower grid-box mean liquid water mixing ratio. Dividing these quantities for a single cloud will give the same result regardless of resolution; however, this scenario becomes more complicated if a second cloud occurs within the same grid-box but with different properties.

Ice cloud quantities

The three equivalent quantities are calculated for ice clouds as well as liquid clouds. They are calculated using the same methodology, however, the quantity of ice detected is calculated from

the radar reflectivity on a point-by-point basis using the empirical relationships from Hogan et al. (2006) described earlier before being averaged to the model grid.

3.4 Model evaluation

3.4.1 Selection of days for analysis

Many previous studies of clouds have chosen to compare observations of clouds with models using a case study methodology. This methodology allows a direct comparison to be made between observed cloud variables and those from the model, but case studies can be unrepresentative and therefore an analysis of many cases is sought to allow a robust comparison.

Although a study of the full climatology of mixed-phase clouds would be ideal, obtaining reliable information about their structure from surface based remote sensors is difficult. To detect the liquid layer in mid-level clouds requires that the lidar signal is not attenuated by low-level clouds. The nature of low-level clouds is that they are usually liquid-phase and typically have an optical depth large enough to completely attenuate the lidar signal. In addition, to obtain the liquid water content within the cloud a measure of the liquid water path is needed. This is obtained from microwave radiometer measurements but when multiple cloud layers are present it is not possible to reliably determine the relative contribution to the liquid water path from each layer.

Therefore a number of days are selected where reliable observations of mid-level mixed-phase clouds have been made. Days are chosen if they contain long-lived liquid layer clouds and at the times when this cloud is present, there is no low level cloud and ideally no cirrus. Times where multiple layers of liquid or mixed-phase cloud are present are also excluded as the liquid water content in each layer can not be retrieved. Unfortunately this significantly reduces the number suitable days for analysis relative to the number of days on which mixed-phase clouds occur. Days that are suitable for part of the day are included, but only the parts of the day that fit the above criteria are included in the analysis.

This situation gives us more useful information than a case study would, but is not as satisfactory as a full climatology. It is also possible that by selecting days where mixed-phase clouds

are observed, but without using any information from the models, that the model data may be biased from that of a true climatology. The full data set contains around 7 years of data, however, after selecting suitable days and restricting times in these suitable days to those with no low-level clouds the data set contains 312 hours of data from 21 suitable days.

3.4.2 Cloud statistics

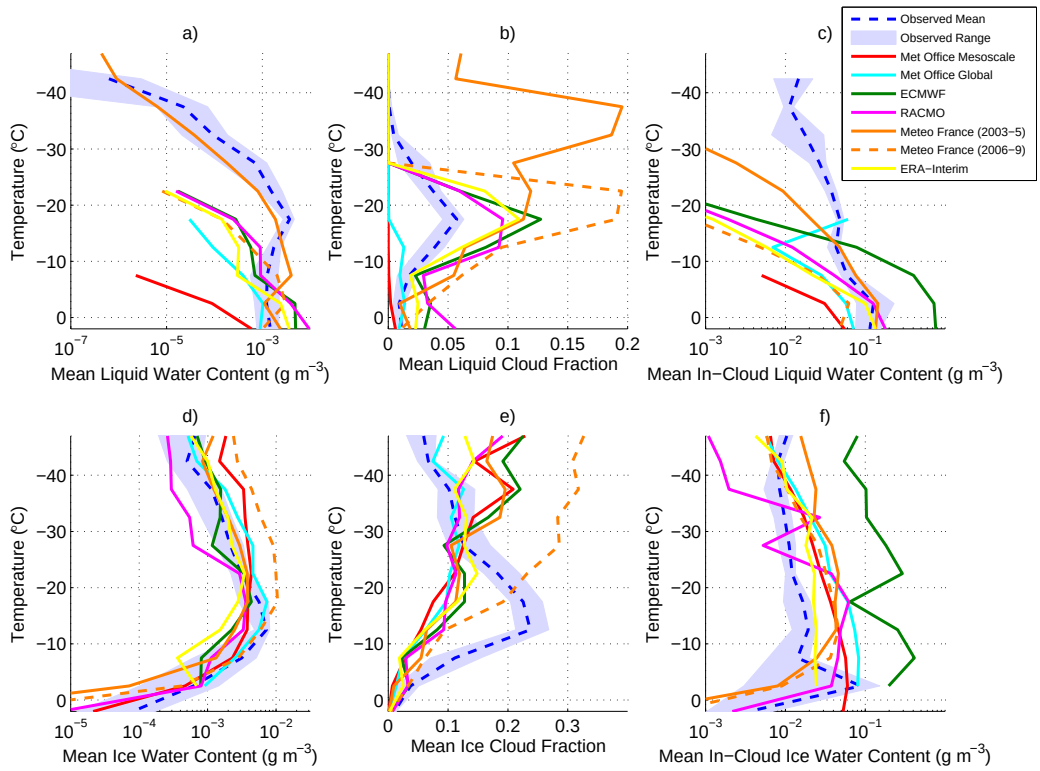

Figure 3.2 Mean liquid and ice cloud properties from radar and lidar observations and also from a number of NWP forecast models, regional climate models and ERA-Interim reanalyses. Shown are: a) mean liquid water content, b) mean liquid cloud fraction and c) mean in-cloud liquid water content, each as defined in section 3.3. Panels d-f) show the same quantities but for ice. These data are for the selected 21 days where mixed-phase clouds or clear skies are observed, each plotted as a function of temperature.

Figure 3.2 shows the three cloud quantities described above for both the liquid and the ice phase from observed cloud derived from radar and lidar observations and also from a number of NWP forecast models, regional climate models and the ERA-Interim reanalyses. Each of these are plotted as a function of temperature, with the observed quantities being the mean of the observations averaged on to the numerous model grids and the shaded area representing the range

of these observations at that temperature.

The observations of mixed-phase clouds shown by this analysis are interesting. On average, for the 21 days analysed, the mean liquid water content for temperatures between 0 and -20 °C is roughly constant with temperature with a value between 1.6–2.1 $\times 10^{-3}$ g m^{-3} depending on the model grid chosen. For temperatures colder than -20 °C the mean liquid water content decreases exponentially until at -40 °C there is virtually no liquid water. The observed liquid cloud fraction shows a peak at around -18 °C with a maximum cloud fraction of 5.7% whilst the in-cloud liquid water content decreases steadily with decreasing temperature from a value of 0.11 g m^{-3} at 0 °C to 0.011 g m^{-3} at -40 °C.

The observations of the ice phase show a maximum in mean ice water content (7.4×10^{-3} g m^{-3}) and a peak in the ice cloud fraction (23.7%) at -12 °C. This peak in the ice water content is around 5 °C warmer than the peak in the liquid cloud fraction as might be expected given the typical structure of mixed-phase clouds with thin liquid layers atop a thicker ice layer. The mean in-cloud ice water content is fairly constant with changing temperature at temperatures colder than -5 °C at around 0.02 g m^{-3}.

In terms of the liquid water clouds this analysis shows a number of differences between observed clouds and those simulated by the models. All models studied here underestimate the mean supercooled liquid water content at temperatures below -15 °C. The worst performing model is the Met Office Mesoscale model which has no liquid at temperatures colder than -10 °C. The Meteo France (2003-5) model is the best performer and lies within the range of observations for temperatures between -15 °C and -40 °C, albeit on the extreme low side of this range and has a mean liquid water content too low by a factor of 2 between -10 °C and -30 °C. This model, like most models, uses a diagnostic scheme to determine the ratio of liquid and ice cloud condensate based on the temperature, but is the only diagnostic scheme that allows liquid to exist at temperatures as cold as -40 °C. Other diagnostic schemes have a different temperature limit beyond which liquid is not able to exist; in this sample all other models with a diagnostic ratio of liquid and ice do not permit liquid at temperatures below -23 °C.

The Meteo France (2003–5) model has a much higher mean liquid cloud fraction than the observations, particularly at the colder temperatures, the worst example being a predicted liquid

cloud fraction of 19.5% at -37°C where the maximum of the observations at this temperature is only 0.02%. From 2006 onwards the model changed and the minimum temperature at which liquid can exist changed to -23°C. This brought the model in line with other diagnostic models and improved the prediction of liquid cloud fraction, but this also reduced the total liquid water content and now shows a similar underestimate as other models.

The Met Office mesoscale and global models are particularly interesting as they are the only models in which ice water content is a prognostic variable separate from liquid. At temperatures warmer than -10°C the predicted liquid water content is just 4.5% (mesoscale) and 62.7% (global) of that observed whilst most other models overestimate the liquid water content at these temperatures. Model performance is worse at colder temperatures with no liquid at temperature colder than -10°C in the mesoscale model and -20°C in the global model. These are the two models with the least amount of liquid water and the lowest mean liquid cloud fraction. This is an important point; the Wilson and Ballard (1999) microphysics scheme used in the Met Office Unified Model is a collection physically-based parameterizations of the microphysical process rates. The fact that this parameterization scheme results in an severe underestimation of the supercooled liquid water highlights the fact that either these parameterizations are not accurate in the case of mixed-phase clouds or that other processes not included in the model must be involved in the maintainence of mixed-phase clouds. The poorer performance of this physically-based parameterization compared to the temperature-dependent split of liquid and ice used by other models motivates much of the work throughout this thesis.

The model predictions of the ice phase are somewhat better than for liquid with the models spanning the range of observations throughout the temperature range analysed. The ice cloud fraction, however, is too large for all models at temperatures colder than -30°C by as much as 0.1, doubling the observed value. At warmer temperatures all models underpredict the ice cloud fraction and at -12°C the mean observed cloud fraction is 23.4% but the multi-model mean is only 7.3% and the largest model value is only 9.5%. The cluster of model predicted ice cloud fractions is remarkably tight given how different they are from the observations.

There are two possible explanations for this absence of ice cloud at -15°C, one being that the models fail to predict ice cloud at this temperature often enough and the other being that the model predicts too little cloud fraction when it does predict cloud. This implies that either the

clouds are not forming often enough, or that when they do form they are dissipating too rapidly. This issue with ice cloud fraction is addressed further below.

3.4.3 Ice cloud fraction

In this section the large difference present between the observed ice cloud fraction and that predicted by all of the models is investigated. At temperatures warmer than -30 °C the mean ice cloud fraction predicted by the models is similar across all models between 5 and 10%, but the observations show a peak at -12 °C of 23.4%. Throughout the same temperature range the mean ice water content observed and modelled agrees very well, and certainly does not indicate that 60% of ice clouds are not predicted as the cloud fraction suggests.

Of the models used in the comparison above, there are three different methods for the calculation of the cloud fraction. The Met Office Unified Model separately calculates cloud fraction for liquid and ice using the Smith (1990) scheme. For liquid, the cloud fraction can be calculated by the fraction of the grid-box where the water vapour exceeds saturation. This gives a monotonic relationship for how cloud fraction changes with liquid water mixing ratio, and this relationship is used in a slightly modified form to calculate the ice cloud fraction from the ice water content.

In the ECMWF model a prognostic equation is used to calculate the total cloud fraction within the grid-box based on advection of cloud and sources from stratiform and convective clouds and sinks from evaporation (ECMWF, 2010). There is no separate cloud fraction for the liquid and ice phases. RACMO is based on the ECMWF model and therefore uses the same scheme. The Meteo France model also uses the Smith (1990) scheme, but uses the total (liquid plus ice) condensed water mixing ratio to determine the cloud fraction (Lopez, 2002). Therefore, the Unified Model is the only model to attempt to calculate the ice cloud fraction explicitly. It is surprising, given the differences in approach, that the mean predicted ice cloud fraction is so similar across all models.

Figure 3.3 shows a scatterplot of the grid-box mean ice water content and ice cloud fraction from the Met Office Mesoscale model and observations averaged to the same model grid for the times analysed above. Each point represents a single grid-box and the lines in panel d show the mean cloud fraction for a given ice water content in separate temperature intervals. Notably, the observed data points are shifted up and left on this figure relative to the model points, indicating

that the observed ice cloud fraction is larger for a given ice water content than is predicted by models. Whilst not shown, this result is consistent across all models.

Figure 3.3d shows the mean ice cloud fraction for a given ice water content for different temperature intervals. The Met Office model has a fixed relationship between ice water content and cloud fraction which varies as a function of temperature, and therefore there is a very clear temperature dependence of this quantity in figure 3.3b and d. In contrast to this there is very little temperature variation in the observations, and the small temperature dependence shown is of the opposite nature to that suggested by the model parameterization.

This large difference in behaviour between models and observed clouds is addressed further by expanding the dataset to many more days and looking at times where clouds other than mixed-

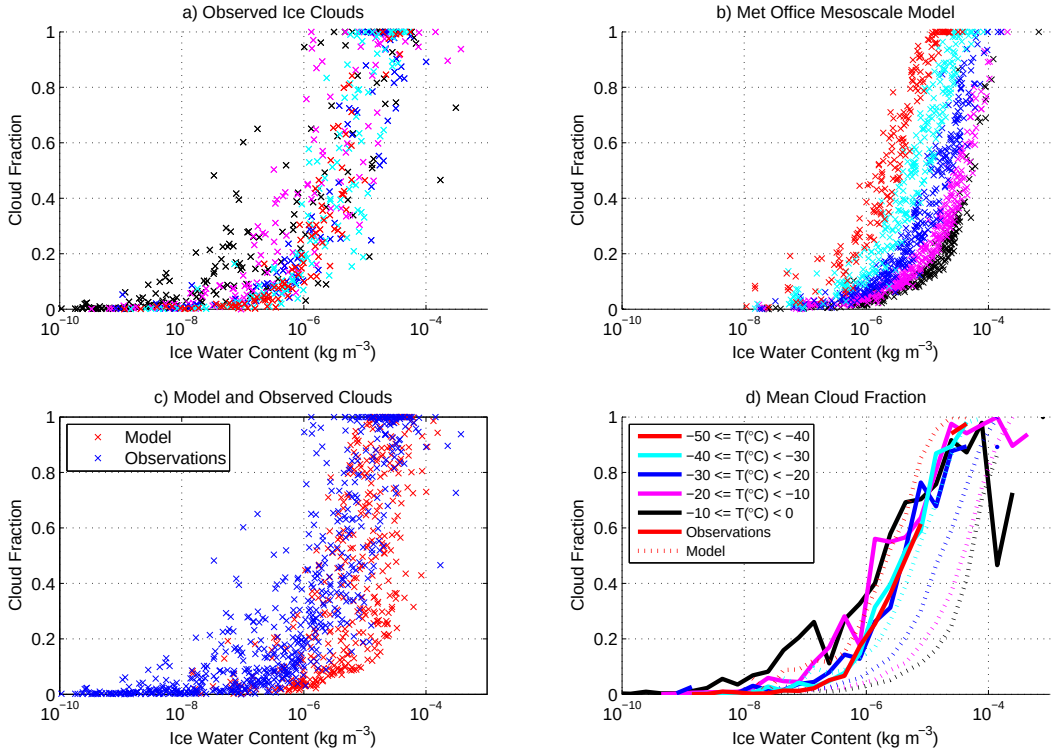

Figure 3.3 Ice cloud fraction plotted as a function of ice water content using data from the 21 days selected for comparison. The panels show: a) observed clouds at Chilbolton using radar derived values b) the UKMO-Mesoscale model for the same period. Panel c) shows the data from panels a) and b) overlayed and d) shows the mean cloud fraction for data binned by ice water content and temperature. The colours in panels a, b and d relate to temperature as shown by the key in panel d).

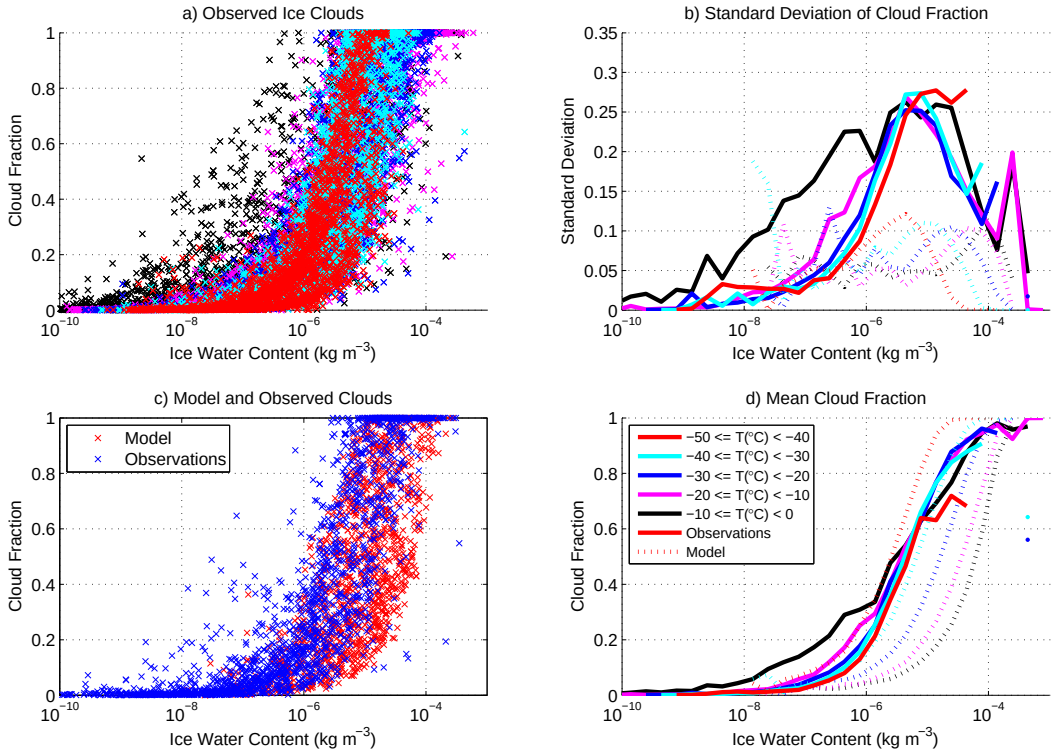

Figure 3.4 Panels a, c and d are as figure 3.3 but for 2 full years of data (2003-4). Panel b also shows 2 years of data but shows the standard deviation of cloud fraction within each ice water content-temperature bin for comparison with the mean values in panel d.)

phase clouds are observed. From figure 3.4, which shows the same quantities as figures 3.3 in panels a,c and d but for two years of observations over Chilbolton; the relationship between ice water content and cloud fraction is found to be robust and not specific to mixed-phase clouds. Again, there is little evidence of a temperature dependence, with all except the warmest temperature bin showing the same relationship. It is possible that the warmest temperature bin is affected by significant contamination of liquid water which is being detected by the radar and therefore cloud fraction is being calculated from both liquid and ice. For colder temperatures, as discussed above, where liquid water contents and physical droplet sizes are small, the radar return is small and does not contribute significantly to the calculated cloud fraction, especially in the presence of falling ice particles.

Despite the considerable spread in the data in each ice water content bin, the mean cloud fraction in each bin is similar for all temperature ranges shown. This suggests a robust distribution independent of temperature and allows us to calculate the cloud fraction as a function of ice water

content only. Doing this will give a significant improvement over the current assumptions made by the models.

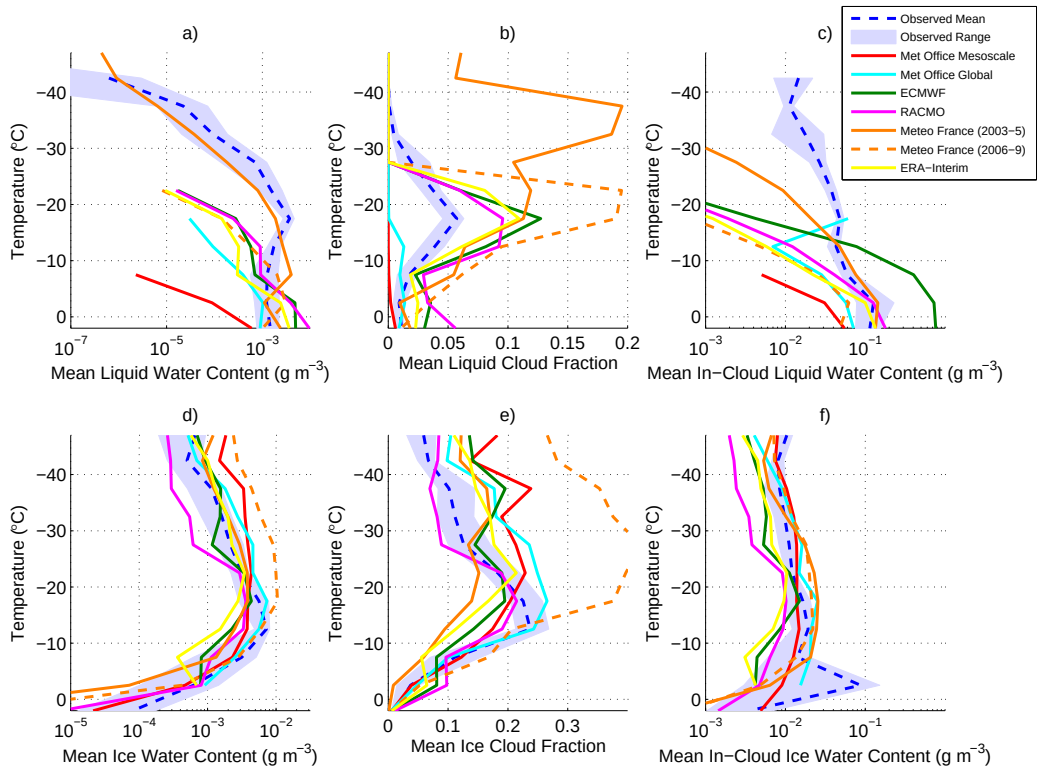

Figure 3.5 As 3.2, but the ice cloud fraction values from the models have been adjusted using the mean relationship from observations in figure 3.4d).

The mean ice cloud fraction is calculated in a number of ice water content ranges, each spanning one quarter of an order of magnitude. Using this calculated mean, and adjusting each model cloud fraction to the observed mean in the equivalent ice water content range results in a substantial reduction in the predicted ice cloud fraction bias (figure 3.5). The ice cloud fraction increases significantly, particularly at the warmer temperatures, and fits the observations much more closely whilst still slightly underestimating the peak. At colder temperatures there is also an increase in the cloud fraction, but it is smaller and the modified mean ice cloud fraction still matches the observations quite well. It is also notable how the mean in-cloud ice water content reduces as the cloud fraction increases and that the modified cloud fraction now gives a very good fit of the mean in-cloud ice water content.

Obviously this change to the model output does not allow the model to interact with the changed cloud fraction in any way. It might be expected that the radiation scheme calculations

would be significantly affected by an increased cloud fraction and reduced in-cloud ice water content, as indeed may precipitation and microphysical processes where the fraction of a grid-box that contains ice is important (e.g. calculating water vapour contents in cloudy and clear air) or where vertical overlap of cloud is important (e.g. falling precipitation). These changes can not be evaluated without re-running the full models and therefore are unable to answer this question. However, experiments described in the next chapter using EMPIRE will look at the effect of changing the ice cloud fraction parameterization.

This change in ice cloud fraction relationship to ice water content increases the cloud fraction at mid-levels, a region that has been identified before (Illingworth et al., 2007; Bodas-Salcedo et al., 2008) as an area commonly missing cloud in NWP models. Therefore, it is possible that changing the parameterized ice cloud fraction in the models will result in an improved mean cloud fraction when compared to observations.

These observations show a clear relationship between ice water content and cloud fraction. However, given the large spread of the cloud fraction around the mean (standard deviation of 0.25) the ice water content is clearly not the only controlling factor. This is in agreement with Bodas-Salcedo et al. (2008) and Delanoë et al. (2011) who also find that ice cloud fraction cannot be parameterized as a monotonic function of the grid box mean ice water content if it is to be consistent with observations. Both studies were conducted with CloudSat observations and compared forward modelled radar reflectivity to the CloudSat measured reflectivity and found that in some regions the comparison was good, but the modelled cloud fraction in the same regions was too low.

The reason for the large spread of cloud fractions with the same ice water content is unclear and definitely warrants further exploration but it seems likely that the difference may in part be due to differing cloud regimes. For instance, the mixed-phase clouds studied here often have a low ice water content, but due to their persistent nature and because the source of ice is a long lived liquid layer cloud, these clouds often have a large cloud fraction when observed by radar, even if their optical depth is small. In contrast, convective clouds may have large ice water contents, particularly in the updraft region, but may only fill part of a grid-box. It may therefore be the case that the ice cloud fraction also varies as a function of vertical velocity or perhaps is related to the variance of ice water content within the grid-box. However, further exploration of ice

cloud fraction is beyond the scope of this thesis but certainly in need of additional analysis. The relationship used here, based on the mean cloud fraction for a given ice water content removes the significant bias from the model, however, does not represent in any way the observed variability.

3.4.4 Mixed-phase cloud structure

The vertical structure of mixed-phase clouds is derived from radar and lidar observations. The liquid and ice water contents are calculated at 60 metre vertical resolution and are then averaged across all observed mixed-phase clouds during our selected 21 days. Figure 3.6 shows that the mean liquid water content decreases rapidly down from cloud top through the top 300 metres with a peak value of 0.083 g m^{-3} and then decreases more slowly as distance from cloud top increases further. In contrast, the ice water content increases approximately linearly down from cloud top through the top 500 metres of the cloud where it reaches its maximum value. Further from the cloud top the ice water content slowly decreases.

This structure helps us to understand the processes in these clouds. The liquid layer at the cloud top is commonly near-adiabatic in structure, particularly in turbulent updrafts, but the depth of the layer can vary. Figure 3.7 shows a histogram of liquid layer depths and whilst the mean depth is 380 $\pm$ 38 m (95% confidence), some much deeper layers do exist. Averaging this adi-

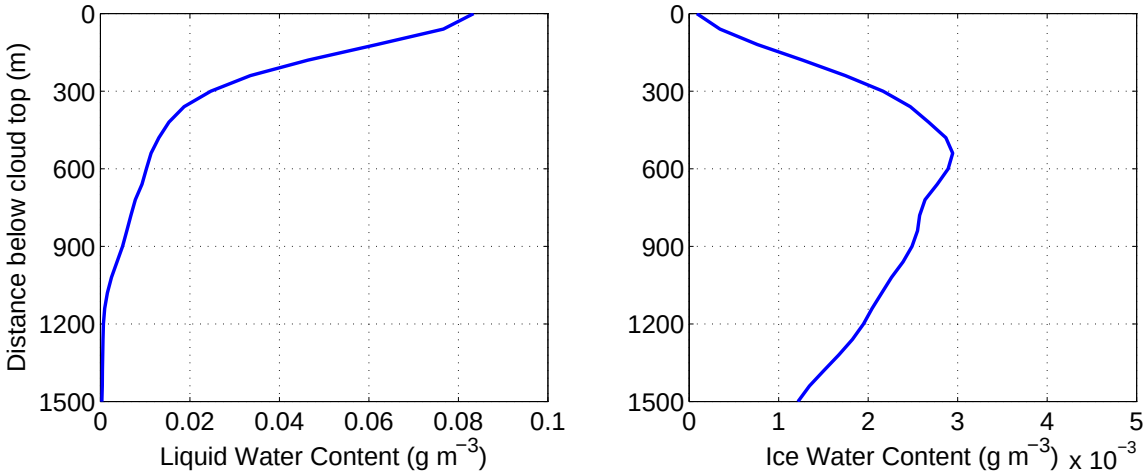

Figure 3.6 Observed mean liquid and ice water contents averaged by depth beneath cloud top. Values are derived from radar, lidar and microwave radiometer observations for the 21 days analysed.

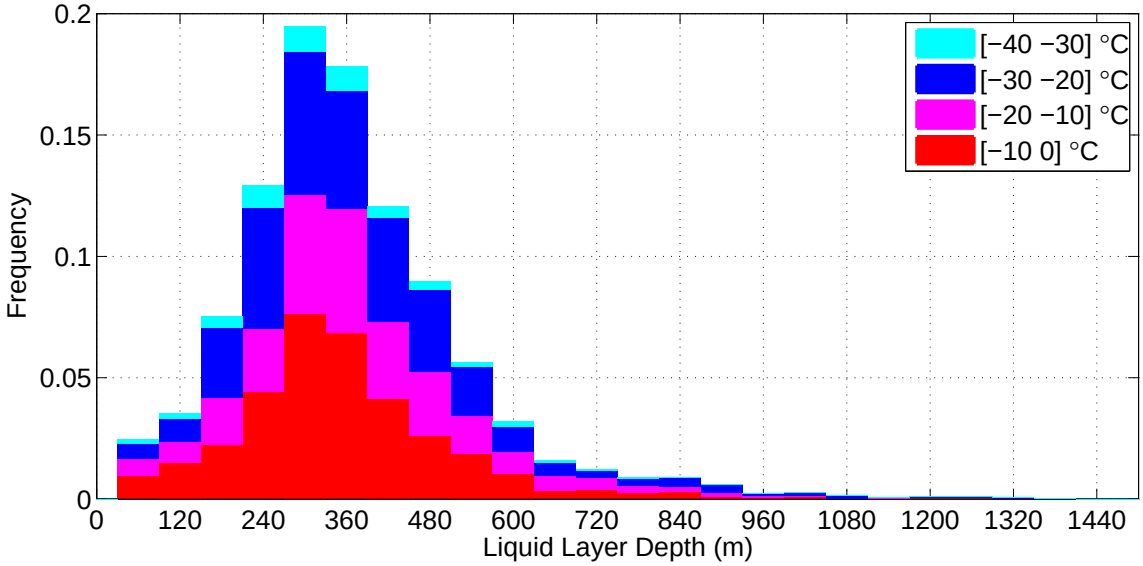

Figure 3.7 Histogram of cloud liquid layer depths, derived using a combination of radar and lidar observations at Chilbolton for the 21 days analysed. In each depth bin the relative contribution of clouds in 10 °C intervals is shown by the colours. The sum of frequencies over all depth bins is 1.

abatic profile of differing depths will lead to larger values of liquid water content at cloud top where liquid is always present and a reduced value lower in the cloud where liquid is not always present. The ice particles initially form and grow within the liquid layer, so low values of ice water content near the cloud top are expected. They grow rapidly whilst in the liquid layer, leading to a peak in ice water content just below the mean depth of the liquid layer and then evaporate when they fall in to air unsaturated with respect to ice lower in the cloud. The mean depth of the liquid water layer is 380 $\pm$ 38 m and is independent of temperature as shown in figure 3.7 where all temperature ranges have a peak in observed frequency around 300 metres.

The structure of mixed-phase clouds as predicted by models is also analysed. For this analysis the same 21 days are used, selecting only clouds that have both ice and liquid in the top cloudy model level and no condensed cloud water in the layer above this. The averaging is similar to that of the observations but first the model data is interpolated to a 60 metre grid centred on the middle of the upper-most grid-box. The model liquid and ice profiles shown in figure 3.8 are quite different to those observed, with the exception of the Met Office models. The mean liquid and ice water contents are roughly constant with height throughout the model clouds. The mean model liquid water contents are typically less than 0.01 g m^{-3}, nearly an order of magnitude less than

the peak in the observations, whilst the peak ice water contents are also underestimated by at least a factor of 2. Generally the liquid water content increases whilst the ice water content decreases lower in the cloud which results from the temperature dependent liquid and ice split in the models. The exceptions are the two Met Office models, which both have roughly the same mean structure as the observations but underestimate the peak in both by a factor of 3. In addition, as has already been seen, these models with prognostic ice water content do not produce mixed-phase clouds or indeed supercooled liquid nearly often enough when compared with observations and hence the underestimate of liquid water content values is enhanced.

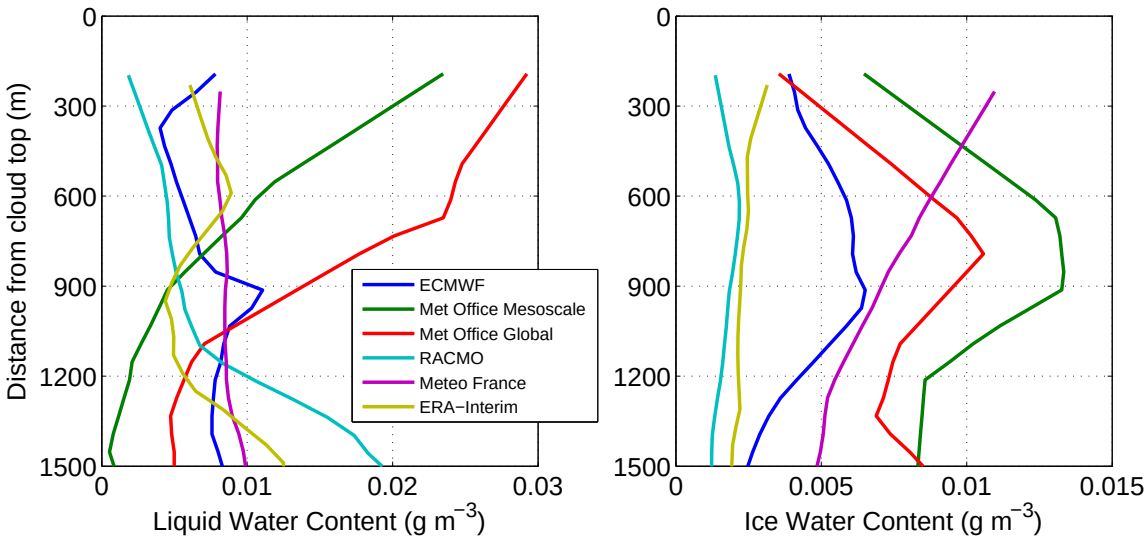

Figure 3.8 Mean liquid and ice water contents averaged by depth beneath cloud top from models. The distance offset from zero at cloud top represents half the mean grid-box depth of the uppermost cloudy grid-level.

3.5 Radiative impact of mixed-phase cloud structure

Correctly predicting the phase of the cloud condensate is very important for calculating the radiative impact of mixed-phase clouds. This is the reason for the large sensitivity to mixed-phase cloud specification in GCMs (e.g. Mitchell et al., 1989; Senior and Mitchell, 1993; Sun and Shine, 1994; Gregory and Morris, 1996). Calculations of the radiative impact of mixed-phase clouds by Hogan et al. (2003a) showed that the supercooled liquid water layer at cloud top dominated the

overall radiative impact of the cloud, strongly increasing the amount of reflected short wave radiation and only slightly decreasing the total outgoing long wave radiation. The net result is a reduction in the amount of radiation absorbed by the atmosphere of between 63.7–133.9 W m^{-2}. Clearly the presence of supercooled liquid in mixed-phase clouds is having a large (cooling) effect on the planet, but Hogan et al. (2003a) did not assess the importance of the liquid-over-ice structure of mixed-phase clouds. Sun and Shine (1994) calculated the radiative impact of three different cloud structures of liquid and ice (uniformly mixed, horizontally stratified and horizontally adjacent), concluding that the impact of a uniformly mixed cloud was largest, but the horizontally stratified cloud was ice over liquid, opposite to what is observed in mixed-phase clouds studied in this thesis. As has been seen in this chapter, models generally are not able to simulate both the quantity of supercooled liquid water and the structure of mixed-phase clouds, and in some cases models struggle to get either correct. In this section the importance of correctly predicting the structure of mixed-phase clouds for radiative transfer calculations will be assessed.

Taking the Edwards and Slingo (1996) radiation scheme used in EMPIRE (see section 2.4.3), five experiments are performed and the long wave (LW) and short wave (SW) cloud radiative forcing (CRF) is calculated at both the top of atmosphere (TOA) and the surface (sfc) in each case. The CRF is defined as

$$\mathrm{CRF}_{\mathrm{TOA}} = F^{\mathrm{up}}_{\mathrm{clear,\ TOA}} - F^{\mathrm{up}}_{\mathrm{cloudy,\ TOA}} \tag{3.3}$$

$$\mathrm{CRF}_{\mathrm{sfc}} = F^{\mathrm{up}}_{\mathrm{clear,\ sfc}} - F^{\mathrm{down}}_{\mathrm{clear,\ sfc}} - F^{\mathrm{up}}_{\mathrm{cloudy,\ sfc}} + F^{\mathrm{down}}_{\mathrm{cloudy,\ sfc}}, \tag{3.4}$$

where F is the up- or down-welling flux of either short or long wave radiation in W m^{-2}. F_{clear} was calculated by setting all liquid and ice water contents and cloud fractions to zero whilst F_{cloudy} was calculated under various assumptions about the vertical distribution of liquid and ice outlined below. The results of these experiments are summarised in table 3.2. The vertical distribution of the liquid and ice in the five experiments are:

(A) All Cloud - F_{cloudy} is calculated using the observed liquid and ice water contents in all clouds observed during the 21 day sample.

(B) No liquid - as (A) but any supercooled liquid is removed and added to the ice water content.

(C) No mixed-phase - as (A) but with liquid and ice at temperatures between 0 and -40°C removed.

(D) Mean structure - as (A) but where cloud exists between 0 and -40°C the in-cloud liquid

water content is set equal to the mean in-cloud liquid water content in that temperature range at the time of observation. The ice water content is changed similarly and ensures the liquid water path and ice water path are unchanged.

(E) Temperature dependence - as (A) but the liquid and ice contents in each grid-box are summed and then split following to the ECMWF scheme (ECMWF, 2010). The function of this diagnostic split is

$$\frac{q_l}{q_l + q_i} = \left(\frac{T - T_{\text{ice}}}{T_0 - T_{\text{ice}}} \right)^2 \qquad \text{for } T_{ice} \leq T(K) \leq T_0, \tag{3.5}$$

where $\frac{q_l}{q_l+q_i}$ is the fraction of condensate that is in liquid phase, $T_{ice} = 250.16$ K is the temperature below which all condensate is ice and $T_0 = 273.16$ K is the temperature above which all condensate is liquid.

The data in table 3.2 demonstrated that cloud structure is important, even if the liquid and ice water paths are themselves correct. In experiment D the liquid and ice optical depths are, on average, unchanged from experiment A and in experiment E the optical depths change only by -7.5% and 6.8% for liquid and ice respectively. However, the CRFs change significantly, particularly in experiment E where the SW TOA CRF becomes less negative by 15.01 W m^{-2}, reducing by more than half the short wave effect of all mixed-phase clouds (relative to experiment C which has no clouds between 0 and -40 °C). Experiment D modifies all clouds such that the ice and liquid water content are constant with height, and this reduces the CRF for both SW and LW at the surface by 1.29 W m^{-2} and at the top of atmosphere by 5.43 W m^{-2} and therefore reduces the cooling effect of mixed-phase clouds. The same results are found for experiment E but the magnitude of all the changes are greater with a surface decrease of 9.86 W m^{-2} and top of atmosphere decrease of 9.93 W m^{-2}. The changes in experiment E are more complex, however, as there are two changes occurring together. By forcing the cloud condensate to follow the parameterized fraction of liquid and ice there is a redistribution of the liquid and ice within the cloud but for temperatures below 250 K the liquid is being converted to ice and thus decreasing the liquid water path and optical depth.

To understand the changes in experiment E, further experiments are run for A and E, but separating times where the liquid cloud top temperature (CTT) is colder than 250 K from times where it is warmer. For the experiments (A2, E2) where CTT is between 250 and 273 K the liquid and ice optical depths are almost unchanged. This is coincidence (or a sign that the liquid fraction

Table 3.2 Summary of cloud radiative forcings calculated for different experiments in both short wave (SW) and (LW) at the surface (sfc) and top of the atmosphere (TOA). Also included are the mean liquid and ice optical depths.

	Mean Cloud Radiative Forcing (W m^{-2})				Mean Optical Depth	
Experiment	$\mathbf{LW_{TOA}}$	$\mathbf{SW_{TOA}}$	$\mathbf{LW_{sfc}}$	$\mathbf{SW_{sfc}}$	$\tau_{\mathbf{liq}}$	$\tau_{\mathbf{ice}}$
A) **All cloud**	24.30	−48.58	26.61	−52.16	2.39	2.49
B) **No liquid**	14.40	−28.12	17.70	−34.23	1.15	3.72
C) **No mixed-phase**	4.35	−20.49	8.67	−22.46	1.15	0.13
D) **Mean structure**	23.83	−42.68	20.32	−44.58	2.39	2.49
E) **Temperature dependence**	19.22	−33.57	22.97	−38.66	2.21	2.66
(E - C) / (A - C)	75%	47%	80%	55%	85%	107%
A1) **CTT** $<$ **250 K**	40.08	−45.92	33.93	−45.45	1.62	2.22
A2) **250 K** $<$ **CTT** $<$ **273 K**	30.61	−72.12	37.02	−79.80	4.00	4.71
A3) **CTT** $<$ **273 K**	34.77	−60.62	35.66	−64.72	2.96	3.62
E1) **CTT** $<$ **250 K**	23.59	−22.13	22.99	−26.04	0.99	2.86
E2) **250 K** $<$ **CTT** $<$ **273 K**	29.47	−52.86	36.05	−62.54	3.94	4.77
E3) **CTT** $<$ **273 K**	26.89	−39.93	30.31	−46.51	2.64	3.93

parameterization has been tuned to give this result) as the liquid and ice contents in each grid-box are assigned using the local temperature only and no constraint is made on the total water path of either phase. In contrast, the experiments (A1, E1) where CTT is colder than 250 K the liquid optical depth is reduced on average by 39% and the ice optical depth is increased by 29%, largely because liquid water at these colder temperatures is removed and replaced with ice, whilst the compensating conversion of ice to liquid at warmer temperatures only occurs if these clouds are very deep or multi-layered, which is rare. Experiment A3 combines times used for A1 and A2 (and likewise for E3) as a comparison with the earlier experiment A. However, A3 does not include times where liquid is present only at temperatures warmer than 273 K, or where no liquid is present at any height and the values for CRF are increased as a result of using times only when cloud is present.

Where liquid clouds are observed at temperatures colder than 250 K a large decrease in the magnitude of CRF is found, for both long wave and short wave, if the condensate is split according to temperature. This is expected as this is largely converting liquid to ice and therefore reducing the total optical depth of the clouds. The net CRF of this change is +7.30 W m^{-2} at TOA and +8.47 W m^{-2} at the surface. Where the liquid cloud tops are restricted to between 250 and 273 K, the change in optical depth for both liquid and ice is small, so the observed change in the CRF

is a result of the cloud structure rather than a mean change in the amounts of liquid and ice. The changes in LW CRF are small at both the surface (-0.97 W m^{-2}) and TOA (-1.14 W m^{-2}); however, the change in SW CRF is of much greater magnitude (surface: -17.26 W m^{-2}; TOA: -19.74 W m^{-2}). This results in an overall large reduction in the cooling effect of the clouds of 38% (16.29 W m^{-2}) at the surface and 44% (18.12 W m^{-2}) at the TOA.

By combining these results the changes observed earlier in experiment E can be explained more fully. The CRF changes between E3 and A3 are caused by two factors, a removal of liquid from temperatures colder than 250 K and the restructuring of clouds warmer than 250 K, moving the liquid towards the bottom of the cloud and the ice towards the top. The removal of liquid from cold temperatures reduces the total optical depth by 39% and therefore also reduces the CRF for both LW (TOA by 41%; surface by 32%) and SW (TOA by 52%; surface by 43%) whilst the restructuring affects the SW much more strongly than the LW, particularly at the top of atmosphere where the SW is reduced by 27% and the LW by only 4%. The combination of these two effects is a decrease in magnitude of LW CRF but a larger decrease in the SW CRF, therefore using this temperature based split of liquid and ice results in a reduction of the cooling impact of mixed-phase clouds.

In comparison, experiment B, has even less of a radiative impact from mixed-phase clouds. This experiment has no supercooled liquid water, instead where it was observed it has been converted to ice. This gives an indication of how the models with prognostic ice might perform currently, if they were able to model the cloud perfectly aside from the phase of the condensate. All the CRF values decrease in magnitude, even compared to the diagnostic split experiment (E). Therefore the presence of liquid water in these clouds is shown to be exteremly important in capturing the radiative impact and models that simulate liquid in the incorrect vertical location relative to the ice are better simulating the cloud radiative effect than the models with prognostic ice that have almost no supercooled liquid present.

3.6 Conclusions

In this chapter, numerical model simulations of mixed-phase clouds have been compared with those observed through a combination of ground-based remote-sensing instrumentation. The

comparisons required careful processing of the data to ensure like with like comparisons are made, particularly in terms of temporal and spatial resolution of the data and by using forward models of the radar and lidar to ensure the model clouds are observable.

The comparisons highlighted the fact that models generally do not predict mixed-phase clouds well. All models underpredict the liquid water content between -10 and -30 °C by a factor of 2 or more and the low bias gets worse as the temperature decreases. They seem able to simulate the ice water contents better than those for liquid; however, most showed problems in predicting liquid or ice cloud fraction as large as observed.

Of the two approaches for predicting cloud ice in the numerical models, fully prognostic or a diagnostic fraction of the total water content, neither is sufficient to produce adequate simulations of mixed-phase clouds. Whilst the models employing a temperature-dependent diagnostic split of liquid and ice are clearly more able to produce and sustain supercooled liquid water, the structure of the simulated clouds is not the same as the observed structure. The liquid is in larger concentrations near the base of the cloud where the temperature is warmer and the ice is distributed fairly evenly throughout the depth of the cloud. This error in cloud structure is shown to be significant when calculating the radiative influence of the clouds and the cloud radiative forcing is less negative by 18.60 W m^{-2} at TOA for mixed-phase clouds when the liquid and ice is partitioned as a function of temperature in this way.

Models with prognostic ice schemes are better able to reproduce the observed cloud structure; however, they have the largest underestimate of the amount of supercooled liquid water present in the simulations as a whole and therefore also fail to capture the important radiative impact of these mixed-phase clouds. The radiative effect of clouds that are completely glaciated is much smaller than clouds that have an incorrect structure. The fact that these schemes, with physically based microphysical parameterizations and a separate prognostic variable for ice, are unable to reproduce the long-lived mixed-phase clouds means that the radiative impact of these clouds is not represented correctly in these models. The reasons for the underestimate of supercooled liquid water content in these models is not clear and motivates the use of the simpler, but similar, model EMPIRE in the rest of the thesis.

Our analysis also highlighted a large difference in the observed ice cloud fraction and that

produced by the model. Further investigation, using two years of data, led to the discovery that ice cloud fraction is a function of ice water content, as parameterized in the models, but that there is no evidence of the parameterized temperature dependence. The mean cloud fraction as a function of ice water content slightly increases at warmer temperatures, which is in direct contrast with the modelling assumptions that it decreases. By correcting the relationship between ice water content and cloud fraction and applying this retrospectively to the model output data, a much better simulation of the mean ice cloud fraction for all models is found. The observed peak of ice cloud fraction at -12 °C is captured better by all models with cloud fraction at this temperature increasing by 50–117% for the models where a diagnostic split of liquid and ice is used and by 219–288% for the versions of the Unified Model with prognostic ice water content. The total ice cloud fraction improved from 5.9% at -12 °C to 20.9% in the Unified Model, comparing much better with the observed value of 23.4% and the global model was within the range of observations. This correction could very easily be applied in weather and climate models and may, at least partially, remove the underestimates in mid-level cloud fraction observed by Illingworth et al. (2007).

Numerical models for weather prediction are not currently able to predict mixed-phase clouds sufficiently well and either have too little liquid water on average or have the cloud vertical structure incorrect. For accurate weather and climate predictions models are required to perform better than they currently do and simulate mixed-phase clouds with both the correct frequency of occurrence and a correct vertical structure such that their radiative importance is accurately captured. To achieve this there is a need for a better understanding of the reasons why mixed-phase clouds are able to persist for long periods of time and what is missing or incorrect in the models with fully prognostic microphysics schemes that prevents their existence in models.

CHAPTER 4:

IMPORTANT PHYSICAL PROCESSES IN MAINTAINING MIXED-PHASE CLOUDS

In this chapter, a number of different approaches are used to determine which of the physical processes parameterized in EMPIRE are most important in the maintainence of mixed-phase clouds. As EMPIRE is constructed to be very similar in structure to a GCM the results about the important processes in EMPIRE can be used to infer the likely important processes in GCM simulations. Because EMPIRE is able to run much more quickly than a GCM would be able to, it is possible to perform many experiments to determine the relative importance of various physical processes on modelling mixed-phase clouds.

First, the ability of EMPIRE to simulate mixed-phase clouds is assessed using observations and is compared to other numerical models analysed in the previous chapter. The processes in the simulations important in allowing mixed-phase clouds to exist are also determined, by assessing the change in liquid water content caused by each process. The most important processes to be included in numerical models to allow successful simulation of mixed-phase clouds is also assessed. This is done by performing a number of experiments with EMPIRE, modifying the settings of the parameterizations and adding and removing numerous physical processes which may contribute to the long lived nature of mixed-phase clouds.

The results of these changed physics experiments are divided into sections based on the physical nature of the change. The first such section addresses changes to the turbulent mixing specification in EMPIRE and determines the importance of the vertical transport of moisture and temperature for maintainence of supercooled liquid. The next section assesses the impact of decreasing the frequency of calling the radiation scheme and changing the parameterized effective radius of the liquid droplets. Thirdly, many changes to the ice microphysics scheme are assessed including changes to the ice particle fall speed, growth rate, habit and number concentration. Sec-

tions four and five describes the impact of changing RH_{crit} in the liquid cloud fraction scheme and changing the vertical resolution respectively. The impact of all these changes are compared in terms of the liquid and ice water contents and the radiative properties of the simulated clouds in section six.

Based on the findings of these experiments, a number of possible improvements to the current physical parameterizations that are most important or show significant sensitivity are identified. For this reason the parameterizations of ice cloud fraction and the ice particle size distribution used in numerical models are modified. These improvements are described, justified and implemented in EMPIRE to quantify the possible improvements in simulations of mixed phase clouds in GCMs.

4.1 Comparison of EMPIRE with observations and GCMs

As described in chapter 2, EMPIRE is a single column model based on the Met Office Unified Model. The model is designed to be similar in structure to a GCM, but has higher vertical resolution (50 m by default) to capture the thin mixed-phase clouds and also has improved physics including non-local turbulent mixing in unstable conditions anywhere in the troposphere and frequent radiation updates. This should allow EMPIRE to capture mixed-phase clouds in a physical way that GCMs are currently unable to do.

The same framework is used to analyse EMPIRE as was used in the previous chapter for the GCMs. The results of this analysis are shown in figure 4.1. The mean liquid water content in EMPIRE is greater than all GCMs analysed except the earliest version of the Meteo France model, but is still not as large as the observed mean liquid water content at temperatures colder than -15 °C. In terms of cloud fraction, EMPIRE has significantly more liquid cloud fraction than either of the two models with prognostic ice water content (both versions of the Unified Model) but is still much less than the observations and is also much less than predicted by the models with diagnostic ice water content.

The ice water contents simulated by EMPIRE are similar to those predicted by GCMs and also similar to observations throughout the range of temperatures analysed, although there is too much

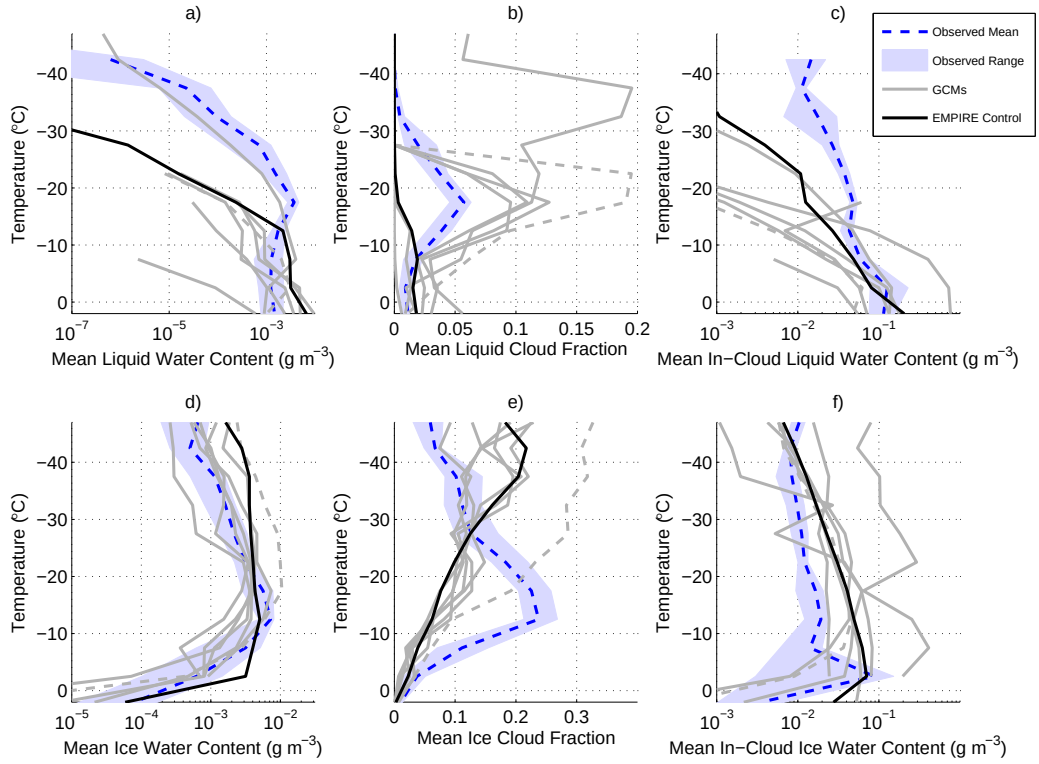

Figure 4.1 Mean liquid and ice cloud properties from EMPIRE simulations (black), from observations (blue) and also from a number of NWP forecast models, regional climate models and ERA-Interim reanalyses (grey; as shown in figure 3.2). Shown are: a) mean liquid water content, b) mean liquid cloud fraction and c) mean in-cloud liquid water content, each as defined in section 3.3. Panels d-f) show the same quantities but for ice. These data are for the selected 21 days where mixed-phase clouds or clear skies are observed, each plotted as a function of temperature.

ice at temperatures below −25 °C. The ice cloud fraction is very similar to the GCM predicted cloud fraction and shows the same biases as the GCMs, notably having too little cloud fraction at warm temperatures and particularly not capturing the peak at around −12 °C. There is a stronger indication of the excess ice at cold temperatures in the cloud fraction comparison than in the ice water content. This excess ice is as a result of cirrus clouds often forming as persistent layers in EMPIRE; this is partly as a result of the single column approach being unable to simulate the horizontal variability observed in reality. In addition the non-local turbulent mixing scheme allows continual glaciation at the cloud top in some conditions whereas, in reality, sporadic glaciation events might be expected leading to a well defined fall streak.

Overall EMPIRE performs better in terms of liquid water content than most of the GCMs and

better than the models with prognostic ice in terms of liquid cloud fraction. However, in both instances the quantities are less than the observed values for temperatures below -15 °C. The ice water contents are similar to both observations and GCMs and the cloud fraction similar to GCMs but dissimilar to the observations, due to the reasons described in the previous chapters pertaining to model ice cloud fraction parameterization errors. The mean ice water content is too large at cold temperatures in EMPIRE, peaking at around a factor of 5 larger at -40 °C.

4.2 Process rates

In this section the dominant processes in generating and depleting liquid water from mixed-phase clouds are identified. To do this, an idealised simulation is run with no vertical velocity but otherwise the model contains all the standard physics described in Chapter 2. The vertical resolution for the idealised experiment is improved from 50 to 25 metres. The model is initialised from a radiosonde sounding from Larkhill at 0600 UTC on 05 September 2003 and then run for 60 minutes to allow the cloud to reach equilibrium. During the following 60 minutes the change to the liquid water content is calculated from each process at each vertical level during each timestep. The average tendency from this 60 minute period is shown as a function of height in figure 4.2 together with the profile of liquid water content after 31 minutes, denoted by the red dashed line. The black line represents the average total tendency over the 60 minute period, a sum of all the tendencies.

During the simulation the radiative cooling at cloud top contributes most to the production of liquid water (+0.45 g kg^{-1} h^{-1}) whilst turbulent mixing near the cloud top reduces the liquid water content significantly (-0.40 g kg^{-1} h^{-1}) by mixing the radiatively cooled air with warmer air lower in the cloud. Lower in the cloud the turbulent mixing acts as a source of liquid water, by enhancing the upward transport of water vapour and the downward transport of radiatively cooled air which increases the total water mixing ratio and reduces the saturation mixing ratio. The radiative impact on the cloud at this level is a weak warming as the absorption by the ice particles is larger than the cooling, resulting in a negative tendency for liquid water. Ice growth by deposition increases with depth from the cloud top with the growth rate related to the ice water content. The net result of all of these processes is a slight reduction (-0.03 g kg^{-1} h^{-1}) in

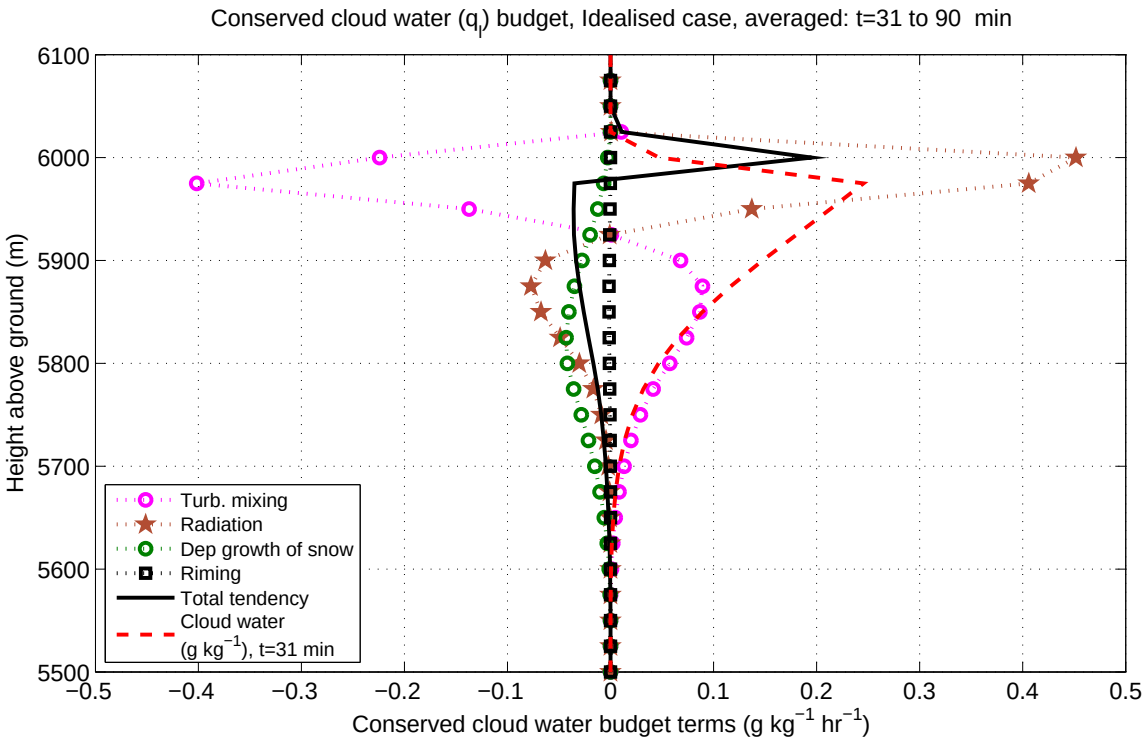

Figure 4.2 The sources and sinks of cloud condensed liquid water seperated by each process type for an EMPIRE simulation of mixed-phase cloud. The values are averaged between 31 and 90 minutes from the start of the simulation. The red dashed line shows the liquid cloud water content at the beginning of this time period in units of g kg^{-1}.

the amount of liquid water throughout the depth of the cloud, largely related to the depositional growth of ice particles. However, at the cloud top, at and above the height of maximum liquid water content there is an increase in the amount of liquid water (+0.20 g kg^{-1} h^{-1}), caused by radiative cooling but unlike lower in the cloud the cooled air is not mixed with warmer air lower in the cloud by turbulent mixing. This results in the increasing tendency at the cloud top and as the simulation evolves this leads to an increase of cloud top height with time.

These findings agree well with those of Smith et al. (2009) shown in figure 4.3 who used large-eddy simulations to assess the process rates in mixed-phase clouds. The process rates are, by coincidence, of roughly equal magnitudes to the process rates from EMPIRE, but the main difference is that the increasing liquid water content at cloud top is largely a result of large scale ascent whereas in this EMPIRE simulation there is no large scale ascent and the increasing tendency is caused by an offset in the location of the maximum cooling and peak in the turbulent

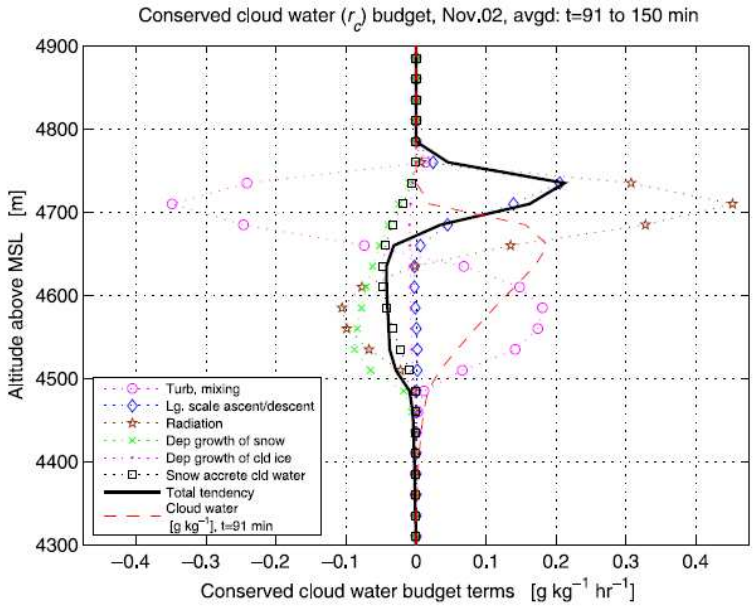

Figure 4.3 The sources and sinks of cloud condensed liquid water seperated by each process type for an LES simulation of mixed-phase cloud from Smith et al. (2009), comparable with figure 4.2.

mixing. The other significant difference between these two process rates analysed is the inclusion of the riming term in Smith et al. (2009), which is similar in magnitude to the rate from depositional growth in the top of the liquid layer, whilst in EMPIRE riming has an almost negligible contribution. The difference is due to the assumed density and habit of the ice particles in Smith et al. (2009); the particles are much less dense resulting in a particle of larger diameter for the same ice mass. For a given mass, particles have a larger size and therefore "sweep out" a larger volume. For low values of ice water content (as found in mixed phase clouds; $< 10^{-3}$ g m^{-3}) and air density the difference in riming from EMPIRE can be an order of magnitude or more as a result of the ice particle density and habit differences. As the ice water content or density increases this difference reduces.

4.3 Process types

In the coming sections the importance of changes to the physics in EMPIRE is assessed. The changes are split into sections according to the type of change made to the model. Changes to the model liquid and ice water contents are assessed, together with the cloud fraction of each phase

and the mean in-cloud water contents. In the coming figures (4.4 – 4.9) the EMPIRE control simulation is shown in black, the range of observations is shown in blue, the values from the NWP models are shown in grey and the results of simulations containing changes to the physics are shown in colours. Differences in liquid and ice water content between simulations are quoted as changes to the mean at temperatures between −10 °C and −30 °C. At temperatures colder than −30 °C the liquid water content is negligibly small and the ice water content is too large relative to observations, whereas at temperatures warmer than −10 °C the cloud scheme can cause some falling ice to effectively melt and become liquid, artificially increasing the liquid water content at these temperatures and is therefore not included in the mean values stated.

4.3.1 Turbulent mixing

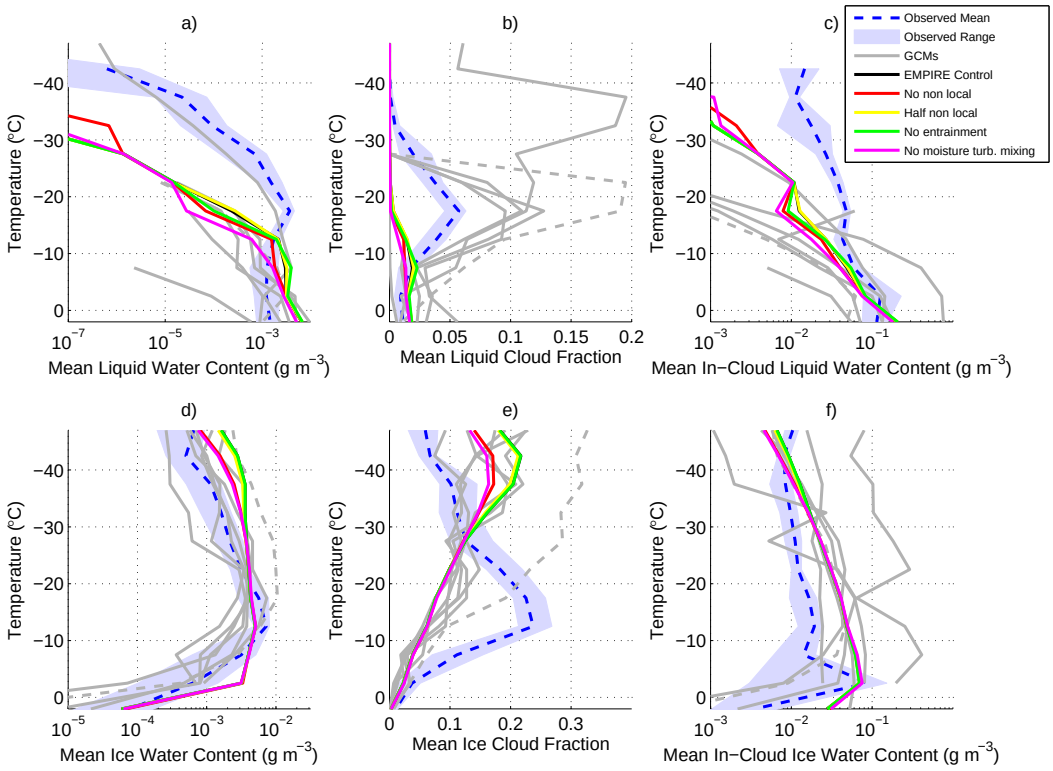

Figure 4.4 As figure 4.1, showing liquid and ice water contents and cloud fractions from EMPIRE experiments where the turbulent mixing specifications have been changed. The experiments are: (red) non local turbulent mixing not included, (yellow) eddy diffusivity from non local scheme halved in model, (green) cloud top entrainment set to 0 and (magenta) non local turbulent mixing of q_t not included.

Figure 4.4 shows the liquid and ice quantities defined in Chapter 3 but for changes in the

specification of turbulent mixing in the model. The grey lines represent the GCMs which were discussed in Chapter 3. The specification of turbulent mixing is found to have a small effect in the EMPIRE simulations of mixed-phase clouds and changes to the turbulent mixing specification change the amount of liquid water in the model simulations (figure 4.4a). Turbulent mixing, of which the non-local mixing is the major contributor, is an important process affecting the amount of liquid water in both EMPIRE (figure 4.2) and LES simulations (figure 4.3). These parameterizations represent the turbulent overturning at the top of the cloud caused by the radiative cooling of the liquid water layer and reduces the amount of liquid water at cloud top but also supplies additional water vapour to the cloud top. The importance of the turbulent mixing is not surprising as the radar observations of mixed-phase cloud layers indicates an area of strong turbulence at the cloud top. Experiments with the non-local mixing included have more liquid water than experiments that do not have this scheme included, with the mean liquid water content 23% lower between $-10\,^{\circ}$C and $-30\,^{\circ}$C when the non-local scheme is absent. There are, however, two competing processes at work. The turbulent mixing scheme is able to remove the region of instability at cloud top which has been caused by the cloud top radiative cooling from the liquid layer. The cooling of this thin layer at rates of around 90 K day^{-1} results in a layer which is absolutely unstable and the turbulent mixing is required to represent the negatively buoyant air parcels sinking into the cloud and in effect spreading the cloud-top cooling over a deeper layer. At the same time the mixing will also increase the total water mixing ratio in the region of the cloud top by bringing up higher values from lower in the cloud. The result of the turbulent mixing is to warm the very top of the cloud layer by removing the cold, radiatively induced, anomaly and to increase the total water mixing ratio at the cloud top. The warming will reduce the amount of liquid water at the cloud top by increasing the saturation mixing ratio; however, the upward transport of water vapour counteracts this and results in more liquid water content on average in simulations with the non-local turbulent mixing scheme.

Current GCMs do not have a non-local turbulent mixing scheme outside of the boundary layer, and therefore they will not maintain liquid water clouds in this manner. If they do form liquid water clouds that are persistent and interact with the radiation scheme then the subsequent radiative cooling may be problematic for the model evolution. Without a turbulent mixing scheme the radiative cooling will likely feed back and further increase the liquid water mixing ratio of the cloud, enhancing the cooling. Eventually this will result in a layer that becomes unstable and

may result in the convection scheme being triggered. This could result in the stratiform cloud developing into a convective cloud in an unphysical way.

As EMPIRE does not have a convection scheme, model simulations that no not include the non-local turbulent mixing scheme evolve differently. At times where a liquid layer forms and induces radiative cooling in the cloud layer the cold anomaly that is produced remains at the cloud top. The liquid layer cools radiatively and produces further liquid water by reducing the saturation mixing ratio. This is clearly an unphysical situation as the resulting cloud layer can be many degrees colder at the top of the cloud than at a depth of a few hundred metres below cloud top. This situation requires the local mixing scheme to remove the cold anomaly from the cloud top but this is a slower process and the radiative cooling sustains the cold anomaly. Despite this, simulations that do not include non-local turbulent mixing contain 23% less liquid water on average than simulation that do include it.

To assess the importance of the non-local turbulent mixing on the lifetime of mixed-phase clouds an experiment was performed where the vertical transport of the total water mixing ratio variable (q_t) by turbulent mixing was turned off, whilst the turbulent mixing of the temperature field was maintained. As can be seen in figure 4.4 this resulted in significantly less liquid water clouds in the simulations at all temperatures, but particularly the colder temperatures with simulations containing only 27% of the liquid water of the control simulation at temperatures between $-10\,^{\circ}$C and $-30\,^{\circ}$C. This indicates that the turbulent mixing processes at cloud top are important in maintaining liquid water clouds in EMPIRE but the inclusion or absence of a non-local scheme does not affect the liquid water content sufficiently to bring EMPIRE close to observations. As we will see in the coming sections other changes have a much larger effect, so whilst turbulent mixing is important to include correctly to simulate the cloud structure it is certainly not the sole reason for the poor performance of models.

4.3.2 Radiation

The above section outlines the importance of the turbulent mixing on the maintainence of liquid water clouds. This turbulent mixing at the cloud top is initiated by radiative cooling of the liquid water layer at the top of the cloud that destabilises the air. To do this the radiation scheme must

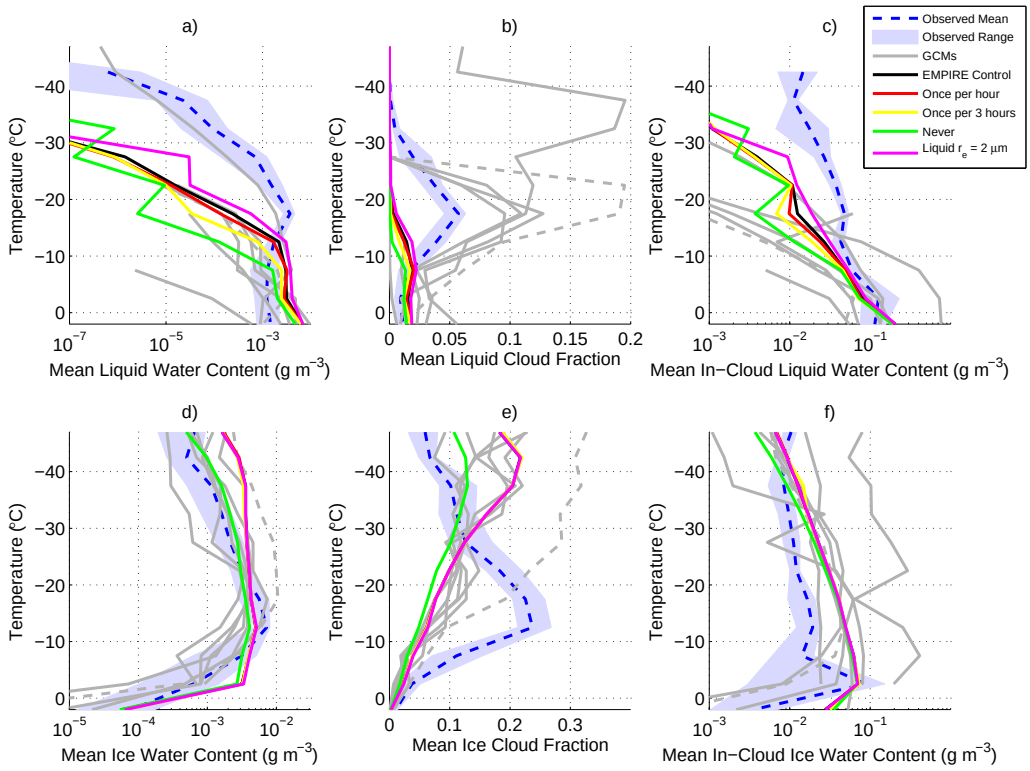

Figure 4.5 As figure 4.1, showing liquid and ice water contents and cloud fractions from EMPIRE experiments where the radiation scheme specifications have been changed. The experiments are: (red) radiation scheme only called once per hour, (yellow) once per 3 hours and (green) never. The magenta line is for the run where the effective radius of liquid drops is reduced from 10 to 2 microns. In the control simulation the radiation scheme is called every 15 minutes.

be called frequently enough that the scheme is able to 'see' the liquid water cloud before the cloud becomes completely glaciated. Liquid water at the cloud top significantly increases the rate of radiative cooling, and to some extent is self sustaining by cooling its surrounds and initiating turbulent mixing. Without the radiative cooling at this level the liquid will quickly be removed by the depositional growth of ice. Often GCMs call the radiation scheme too infrequently (e.g. every 3 hours) and this allows a large proportion of liquid in the newly formed cloud to become glaciated before it has any radiative effect. In this situation the model may never able to implement the cooling that would maintain the liquid water layer.

Figure 4.5 shows the effect of reducing the frequency of the radiation scheme, showing a reduction of 65% in the mean liquid water content between -10 °C and -30 °C when the frequency is reduced to once every 3 hours. Where the radiation scheme is only used once per hour the re-

duction in the same temperature range is only 23%. With no radiation at all the reduction in mean liquid water content is 94%. Long intervals between radiation calls in NWP models are required due to computational expense of running the scheme but this is contributing to the absence of liquid water in their simulations.

The radiative properties of the cloud particles is also important as identified here by changing the effective radius of the liquid droplets from 10 to 2 microns. Observations of mixed-phase clouds by Hogan et al. (2003a) found that the effective radius of liquid droplets was 2 microns. This has the effect of increasing the optical depth of the liquid layer by a factor of 5 and therefore increasing the radiative effect of the liquid phase. This resulted in an increase of 39% in the mean liquid water content between -10 °C and -30 °C whilst the mean ice water content remained almost unchanged.

4.3.3 Ice microphysics

The ice microphysics is of fundamental importance to the evolution of mixed-phase clouds as it is the conversion of liquid water to ice in the clouds that determines the length of time the liquid cloud remains. There are many factors that affect the rate of glaciation, these may be physical parameters such as the ice particle habit and the terminal fall velocity of the ice particles. It is also important to understand the size of ice particles in the cloud and how the ice particles exist in the cloud relative to the liquid water (i.e. the liquid and ice cloud overlap).

Our initial experiment completely turns off the ice production in EMPIRE, and the result of this is a large increase in liquid water cloud to values well above those observed (not shown). This demonstrates that the combination of the model and the ERA-Interim forcing used is able to produce an adequate amount of liquid water in the absence of any process which removes the liquid. It must therefore be concluded that models are able to produce enough liquid water, on average, but that the reason they do not is due to an ice production rate that is too quick.

Changing the relationship between the ice particle mass and the terminal fall velocity of that particle also has an effect on the model simulations. Increasing the fall speed by 50% results in a 75% increase in the amount of liquid water between -10 °C and -30 °C in the simulations. As the ice particles are falling faster, they fall through the cloud more quickly, spending less time

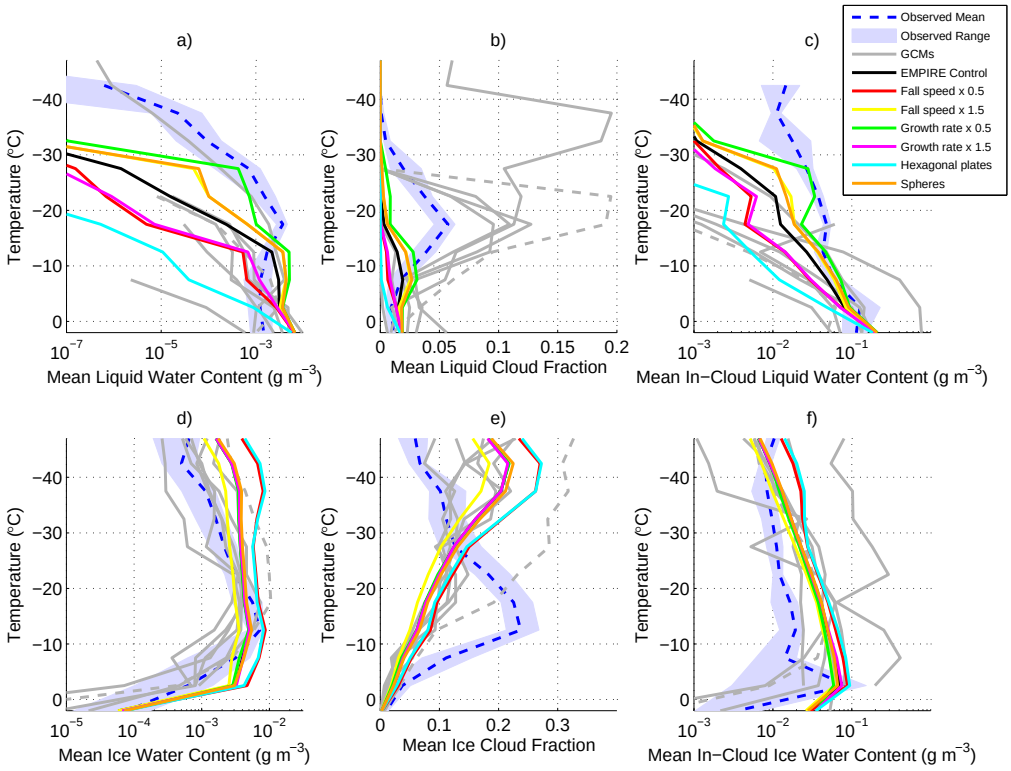

Figure 4.6 As figure 4.1, showing liquid and ice water contents and cloud fractions from EMPIRE experiments where the ice microphysics specifications have been changed. The experiments are: (red) ice particle fall speed reduced by 50%, (yellow) ice particle fall speed increased by 50%, (green) ice particle growth rate reduced by 50%, (magenta) ice particle growth rate increased by 50%, (cyan) ice particle habit changed to hexagonal plates and (orange) ice particle habit changed to spheres.

in the liquid-saturated layer at the cloud top. As the growth rate has not changed, the fact that they spend less time co-existing with the liquid results in less deposition on to the ice particles and therefore a greater fraction of the cloud condensate remains in liquid phase. The converse of this is also true, where halving the terminal fall velocity of ice particles reduces the liquid water between $-10\,^{\circ}$C and $-30\,^{\circ}$C by 76% as the ice and liquid co-exist for longer, growing by vapour deposition and removing a greater quantity of liquid water from the cloud. This means that for slower terminal velocities the liquid cloud lifetime is shorter due to more rapid glaciation by the ice particles. This in turn removes the source of ice particles from within the liquid layer and ultimately reduces the lifetime of the cloud overall. This is of particular interest as this result is of opposite sign to that for cirrus clouds where increasing the terminal fall velocity of the ice particles means they fall more quickly out of the supersaturated region and result in a shorter cloud lifetime. As a result of this, the ice particle fall velocity is one of the parameters within the

cloud scheme that are popular tuning parameters in climate models (Bender, 2008) as the cloud lifetime and therefore the radiation balance can be changed quite simply without influencing other processes too greatly. However, increasing the fall velocity of ice particles to decrease the amount of cirrus will increase the amount of mid-level liquid water cloud and decreasing the fall velocity to increase the cirrus cloud amount will decrease the amount of supercooled liquid water in the model simulations.

The model is also sensitive to changes in the specified ice particle growth rate. An increase in the ice particle growth rate of 50% results in a 70% decrease of the mean liquid water content for temperatures between -10 °C and -30 °C. However, unlike changing the fall velocity, this does not change the mean ice water content significantly, resulting in only a 1% increase. This suggests that the increased growth rate only glaciates the cloud more quickly and hence reducing the time the liquid is present for but does not produce any more ice overall. The opposite of this is also true, where a decreased growth rate by 50% results in a 156% increase in the amount of liquid water but only a 2% decrease of the ice water content.

Ice crystals form in different habits (shapes) at different temperatures and supersaturations (Rogers and Yau, 1988). The change in habit has two consequences for ice crystal growth. As the habit of the ice crystal changes so does its ability to grow by vapour deposition, this change is described though the capacitance, and shapes with extreme aspect ratios (much larger horizontal extent than vertical extent) have the largest capacitances. In figure 4.6 experiments are run with three different habits: aggregates (control), hexagonal plates and spheres. In the model, the habit is controlled by changing the description of the mass-diameter relationship, the terminal velocity and capacitance of the particles; these are summarised for each habit in table 4.1.

The capacitance for an ice particle of a particular mass is approximately doubled for hexagonal plates relative to the aggregates used by default but the capacitance of spheres is about 25% less than aggregates, although these ratios change with particle mass. The change in habit also

Table 4.1 Summary of the habits used in EMPIRE for particles of diameter, D, in metres.

Habit	Capacitance	Mass (kg)	Terminal velocity (m s^{-1})
Control (aggregates)	$D/2$	$0.0185D^{1.9}$	$25.2D^{0.527}$
Hexagonal Plates	D/π	$0.00376D^{2}$	$17.9D^{0.62}$
Spheres	$D/2$	$0.069D^{2}$	$25.2D^{0.527}$

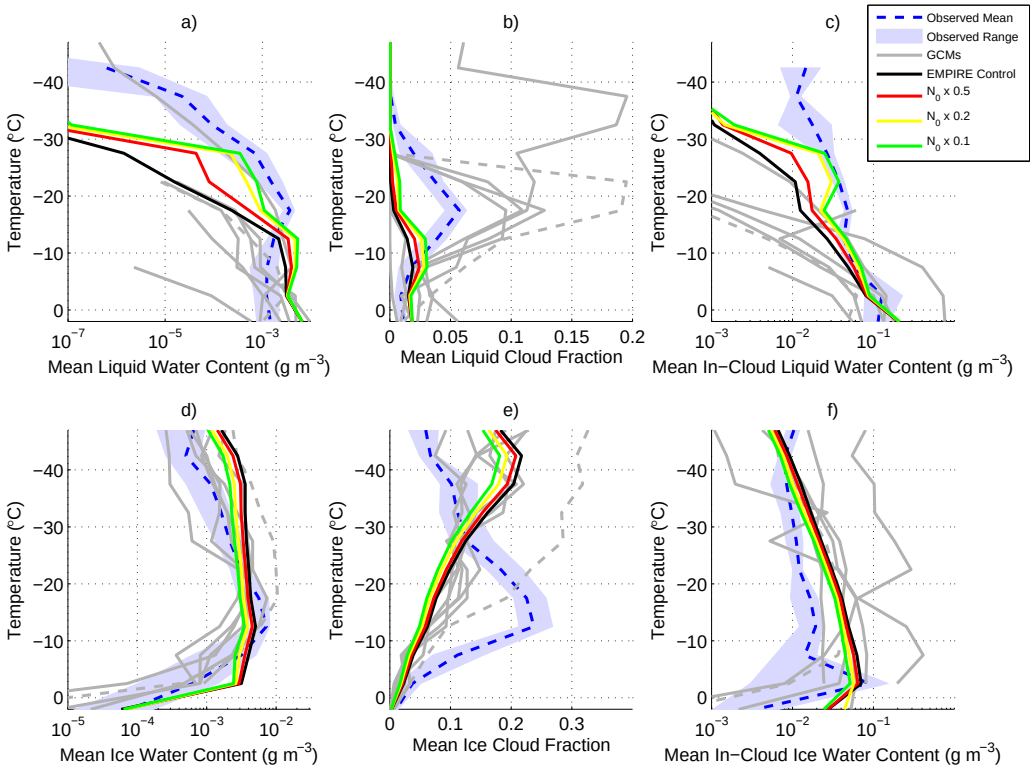

Figure 4.7 As figure 4.1, showing liquid and ice water contents and cloud fractions from EMPIRE experiments where the ice particle size distribution specifications have been changed. The experiments are: (red) N_0 in ice particle size distribution scaled by 0.5, (yellow) N_0 scaled by 0.2, (green) N_0 scaled by 0.1.

affects the terminal fall velocity of the ice particles, again with the extreme aspect ratio particles falling more slowly. In EMPIRE aggregates fall around 10–15% faster than spheres of the same mass and hexagonal plates fall speed is only 50–60% that of aggregates. The net result of this is that the particles which are plate- or dendrite-like (e.g. hexagonal plates) grow more quickly than spherical or aggregate ice particles commonly assumed in models and also fall more slowly. Both of these effects, as individually identified earlier in the chapter, result in a net increase in growth rate of ice particles and a net decrease in the amount of liquid water in model simulations. As a result of this, the ice crystal habit is one of the changes that EMPIRE is most sensitive to in terms of liquid water content.

A more subtle way of changing the mean ice particle growth rate and fall velocity within a grid-box is to change the ice particle size distribution. As the growth rate of a single ice particle is dependent on its size, or more exactly its capacitance which depends on both size and shape, then changing the relative contributions to the ice mass from the small and large particles can alter the

mean ice growth rate and similarly the fall velocity. Large ice particles grow by vapour deposition more quickly than small particles do, this is because they have a larger surface area on to which vapour can deposit. However, the smaller particles have less initial mass and therefore can increase in mass at a faster rate relative to their initial mass. The result of this is that a population of small ice particles will enable quicker growth than a smaller number of larger particles with the same total mass. It is common, at least in the simple single-moment microphysics schemes used in GCMs, for the ice particles size distribution to be represented by an inverse exponential function, similar to that of Wilson and Ballard (1999),

$$N(D) = N_0 \exp(-0.1222T) \exp(-\Gamma D), \tag{4.1}$$

where N_0 is the intercept parameter and Γ is the slope parameter. The integral of the product of this function and the mass-diameter relationship gives the total ice water content and therefore N_0 and Γ are inversely related such that an increase in N_0 causes an increase in the slope of the exponential function to keep the integral constant. Therefore a change in the size distribution of ice particles can be represented by changing the N_0 parameter. An increase in N_0 results in an increase in the number of small particles and a compensating decrease in the number of large particles, whilst a decrease in N_0 increases the mean ice particle diameter. The result of decreasing N_0 in EMPIRE is to increase the mean liquid water content, particularly at colder temperatures. A reduction of N_0 by a factor of ten increases the mean liquid water content approximately an order of magnitude at temperatures between -20 °C and -30 °C (figure 4.7). There is considerable variability and uncertainty in the ice particle size distributions measured in mixed-phase clouds, indeed in all clouds, due to a number of factors. Therefore it is not unreasonable for N_0 to be incorrect by a factor of 10. In fact, there may be fewer ice crystals in thin mixed-phase clouds where there is not an abundant source of ice nuclei. The uncertainty in N_0 is potentially a significant reason why mixed-phase clouds cannot currently be modelled and will be investigated further later in this chapter.

4.3.4 Liquid cloud fraction scheme

The cloud fraction scheme is a key part of the model in determining how much cloud cover exists and the in-cloud water contents. There are a number of different cloud schemes used in the GCMs, however, EMPIRE uses the Smith (1990) cloud scheme as this was the basis for the Met Office

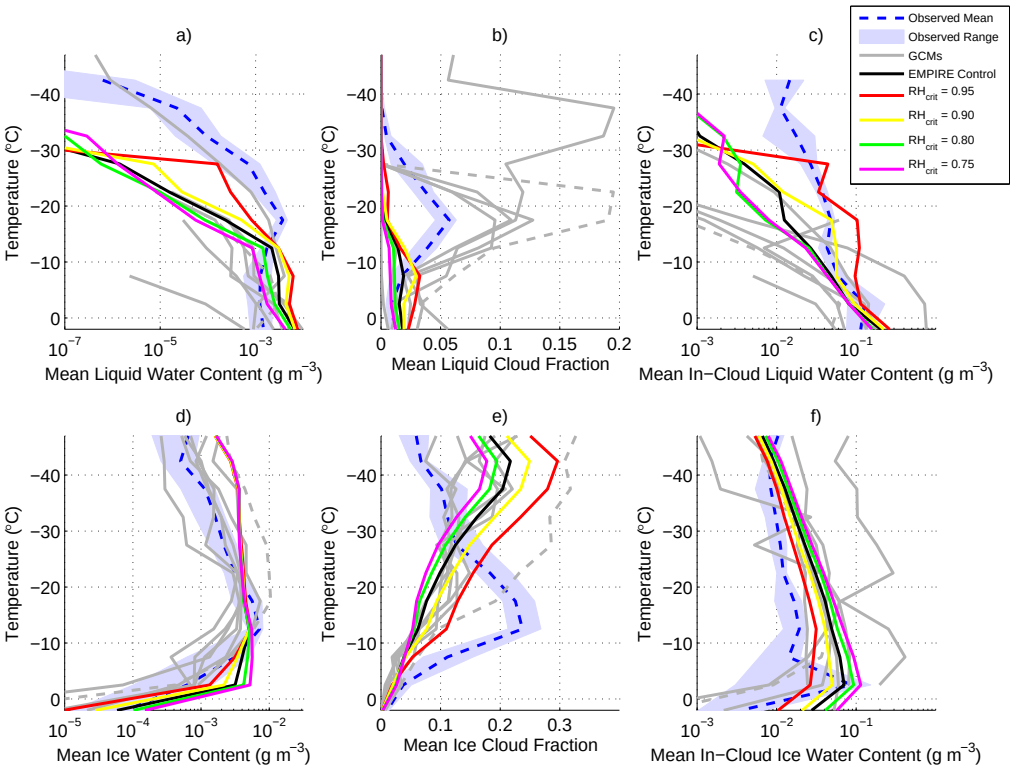

Figure 4.8 As figure 4.1, showing liquid and ice water contents and cloud fractions from EMPIRE experiments where the cloud fraction scheme specifications have been changed. The experiments change RH_{crit} in the cloud fraction scheme to : (black) Control (85%), (red) 95%, (yellow) 90%, (green) 80% and (magenta) 75%.

Unified Model. This scheme calculates the cloud cover and water contents using the grid-box mean total water mixing ratio and temperature. It assumes that there is a distribution of values of q_t within the grid-box and that once any part of that distribution exceeds the saturation mixing ratio then cloud exists in that part of the grid-box. This is formulated using RH_{crit}, the critical relative humidity that the grid-box mean total water mixing ratio must reach for cloud to begin to form. In the Met Office Unified Model this changes with both altitude and model resolution. Typically values are around 0.90-0.95 at the surface, with larger values for the finest horizontal resolution, reducing to 0.80 above the boundary layer for all horizontal resolutions (Humphrey Lean, personal communication). This means that above the boundary layer, once the grid-box mean relative humidity exceeds 80% cloud begins to form. As the model horizontal resolution increases it might be expected that the sub-grid variability of q_t to reduce, and as such the values for RH_{crit} are greater in the Unified Model with highest horizontal resolution. EMPIRE's default value is 0.85, but as can be seen from figure 4.8, changing the critical relative humidity in the

model can change the amount of liquid cloud that is predicted.

This in itself is not particularly surprising, as with a lower value for RH_{crit} it becomes easier for some part of the grid-box to reach saturation. Interestingly, increasing RH_{crit}, and therefore making it more difficult for the model to produce cloud and more likely to predict clear skies, the total amount of liquid water and liquid cloud fraction in the model actually increases. One explanation for this result is that for lower values of RH_{crit} the model produces cloud more readily, however, the cloud it produces only fills a small part of the grid-box and has a lower water content than would be found for an equal cloud fraction if RH_{crit} were higher. As there is less liquid this allows the cloud to glaciate more quickly, as this only requires a small amount of ice production within the cloud. For higher RH_{crit} values the cloud has a larger water content and therefore will take longer to glaciate.

4.3.5 Vertical resolution

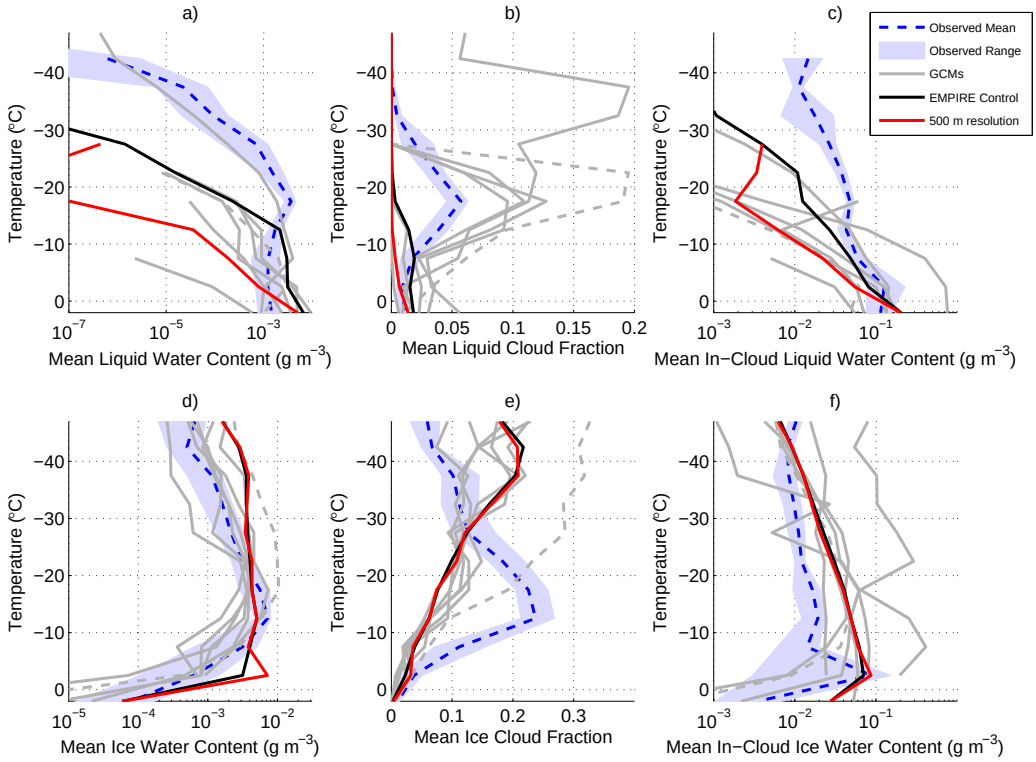

Figure 4.9 As figure 4.1, showing liquid and ice water contents and cloud fractions from EMPIRE experiments where the vertical resolution has been changed. The control simulation has a vertical resolution of 50 metres whilst 500 metres is nearer the resolution of a typical GCM.

EMPIRE is also sensitive to the vertical resolution at which it is run. The default resolution is a grid-spacing of 50 metres in the vertical. However, changing this to 500 metres, a resolution more representative of GCM vertical resolutions in the mid-troposphere, results in a marked decrease in the mean liquid water content and cloud fraction of the simulations. For temperatures between -10 °C and -30 °C the mean liquid water content falls from 4.60×10^{-4} g m^{-3} to 7.68×10^{-6} g m^{-3} as the resolution changes from 50 to 500 metres. This loss of 98.3% of the liquid in this temperature range has a number of causes that are further addressed in chapter 5. Such a large change in the liquid water content with changing resolution, with almost no change in the ice water properties of the cloud, is likely a key reason why current GCMs and NWP models fail to simulate these mixed-phase clouds as their resolution is at best 300 metres in the vertical in the state-of-the-art weather forecasting models and much less in global models, climate models or less sophisticated models constrained by a lack of computing time.

4.3.6 Summary of model sensitivities

So far in this chapter a large number of processes and parameterizations to which mixed-phase clouds are sensitive in some way have been identified. In this section greater detail about the nature of the changes is given and the magnitudes of the changes in liquid and ice water content are compared as well as an estimate of the albedo of the cloud.

For the comparison, only clouds that exist between -10 °C and -30 °C in the simulations are included. In this temperature range the mean liquid and ice water contents and mean albedo of the clouds are calculated. The albedo is estimated using the approximate relationship from Cahalan et al. (1994)

$$\alpha = \frac{\tau}{\tau + 10}, \tag{4.2}$$

where α is the albedo and τ is the optical depth of the cloud condensate, whether liquid or ice. This allows a comparison of the radiative impact of the changes in cloud properties to be made that is independent of the time of day or year and also unaffected by clouds, whether correctly forecast or not, outside of this temperature range.

These summaries are presented in table 4.2 and the modifications to EMPIRE are ordered by the mean liquid water content in the simulations. The modifications that produce the largest

Table 4.2 Summary of the control and modified simulations with EMPIRE showing the mean water contents and albedos for liquid and ice clouds separately. Only clouds in the temperature range of -10 °C to -30 °C are included. Modified simulations show quantities as a percentage of the value in the control simulations and ordered by their mean liquid water content.

	Mean liquid water content	Mean ice water content	Mean liquid albedo	Mean ice albedo
Control	4.60 x 10^{-4} g m^{-3}	2.82 x 10^{-3} g m^{-3}	0.127	0.0434
Modification		Percentage of control		
N_0 x 0.1	274	69	206	72
Growth rate x 0.5	256	98	197	99
N_0 x 0.2	232	78	183	80
RH_{crit} = 0.95	182	105	133	103
Fall speed x 1.5	176	71	148	74
Spheres	172	107	142	106
N_0 x 0.5	155	90	139	91
Liquid r_e = 2 μm	139	101	123	101
RH_{crit} = 0.90	134	101	120	100
Half non-local mixing	101	100	105	100
No entrainment	87	100	92	100
No non-local mixing	77	100	88	100
Radiation once per hour	77	99	83	99
RH_{crit} = 0.80	66	99	78	100
RH_{crit} = 0.75	39	102	58	103
Radiation once per 3 hours	35	100	53	100
Growth rate x 1.5	30	101	39	101
No moisture turb. mixing	27	102	44	101
Fall speed x 0.5	24	162	35	148
Radiation never	6.02	79	13	80
Resolution 500 m	1.67	100	3.92	102
Hexagonal plates	0.50	155	1.31	142

changes of mean liquid water content in the -10 °C and -30 °C temperature range are those that reduce the intercept parameter of the ice particle size distribution, half the ice particle growth rate, increase the critical relative humidity required to form clouds and increase the fall speed of ice particles. Aside from the change to RH_{crit} all of these modifications affect the ice growth rate, either directly or indirectly by means of altering the duration of liquid and ice particle coexistence. In the case of altering the size distribution both of these changes occur.

The modifications with the lowest liquid water content are where the ice particle habit is changed to hexagonal plates, the resolution is coarsened to 500 metres and the radiation scheme is not used. The hexagonal plates fall more slowly than the standard assumed habit and grow by diffusion more rapidly. The effect of resolution involves many processes and is investigated

in chapter 5 and the lack of radiation scheme prevents the clouds cooling from cloud top and preventing liquid clouds from maintaining themselves.

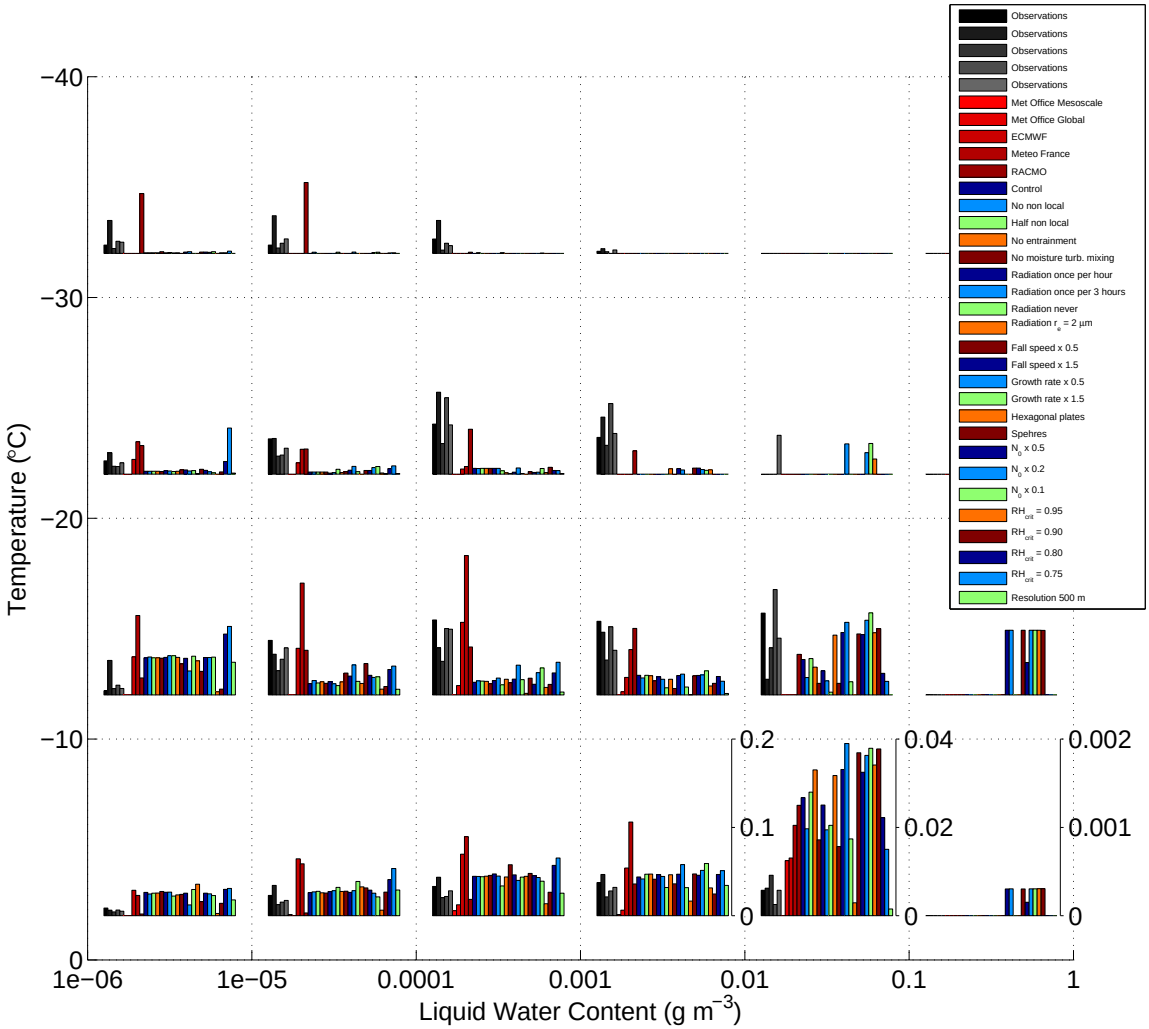

Figure 4.10 Frequencies with which the grid-box mean liquid water content falls between the extreme values of each box, shown for 4 temperature ranges. The values represent the fraction of grid-boxes in that temperature range that have liquid water content values in the appropriate range. The scale for liquid water contents below 0.01 g m^{-3} is shown in the fourth column. The scale of the two right-hand columns have been expanded for clarity by a factor of 5 and 100 respectively, relative to the remainder of the figure, as illustrated by the scales shown at the bottom of the columns. The five different observations are those on model grids, shown in the same order as the models subsequently shown.

To further understand the changes caused by the modifications to EMPIRE, PDFs of liquid water content in certain temperature ranges are created in four temperature ranges, each spanning 10 °C between 0 °C and −40 °C. The PDFs are split in figure 4.10 to allow comparison

between the different modified simulations. The values represent the fraction of grid-points in that temperature range that have liquid water content in the range shown.

The frequency of liquid water contents below 0.01 g m^{-3} is well represented in the 0 to -10 °C temperature range; however, the high bias in EMPIRE is a result of excessive frequency at which liquid water contents above 0.01 g m^{-3} are predicted. At temperatures colder than -10 °C there are too few points with liquid water content less than 0.01 g m^{-3}.

There is evidence that modified EMPIRE simulations that more closely match observed mean liquid water contents, particularly at temperatures between -20 and -30 °C is a result of an increase in the number of high liquid water content values, with almost all modifications showing very little variation in the number of lower liquid water contents. The exception to this is the increased number of small liquid water contents where RH_{crit} has been reduced. As hypothesised earlier, these simulations allow part of the grid-box to reach saturation more easily, however, when they do so only a small amount of liquid water is produced.

Whilst EMPIRE is seemingly unable to reproduce the observed frequency of low liquid water contents, it is producing significantly more liquid at colder temperatures than the Met Office models do. As the only prognostic models included in this comparison, this suggests that EMPIRE is performing better but that none of the modifications made are able to capture a realistic distribution of liquid water contents at colder temperatures.

4.4 Improvements to the physical parameterizations in EMPIRE

4.4.1 Ice cloud fraction

In the previous chapter it was identified that the parameterized ice cloud fraction used by current GCMs is not representative of the true relationship between ice cloud fraction and ice water content found from observations. The corrected relationship based on observations was applied to the NWP models in the previous chapter and found that this explained the difference in the predicted and observed ice cloud fraction. However, this change was made on the model output and it was not possible to change the cloud fraction used in the models and understand how this

change would affect the model simulations.

Here the parameterization used in EMPIRE is changed to the one defined in the last chapter based on the observed relationship between ice water content and cloud fraction. The change of the mean ice water content and cloud fraction shown by the model is analysed as is the change in the liquid cloud properties, if any.

Implementing the parameterization in EMPIRE (figure 4.11) has similar effects to the post-processing change to the GCMs from the earlier chapter and brings the predicted cloud fraction to better agree with the observed cloud fraction, except at cold temperatures where the high bias in ice water content exists that causes an excess cloud fraction. This improvement is as expected from the earlier change and it is encouraging to see that this change does not significantly change the simulated cloud properties other than increasing the cloud fraction.

Interestingly, the increase in ice cloud fraction from using this new parameterization also

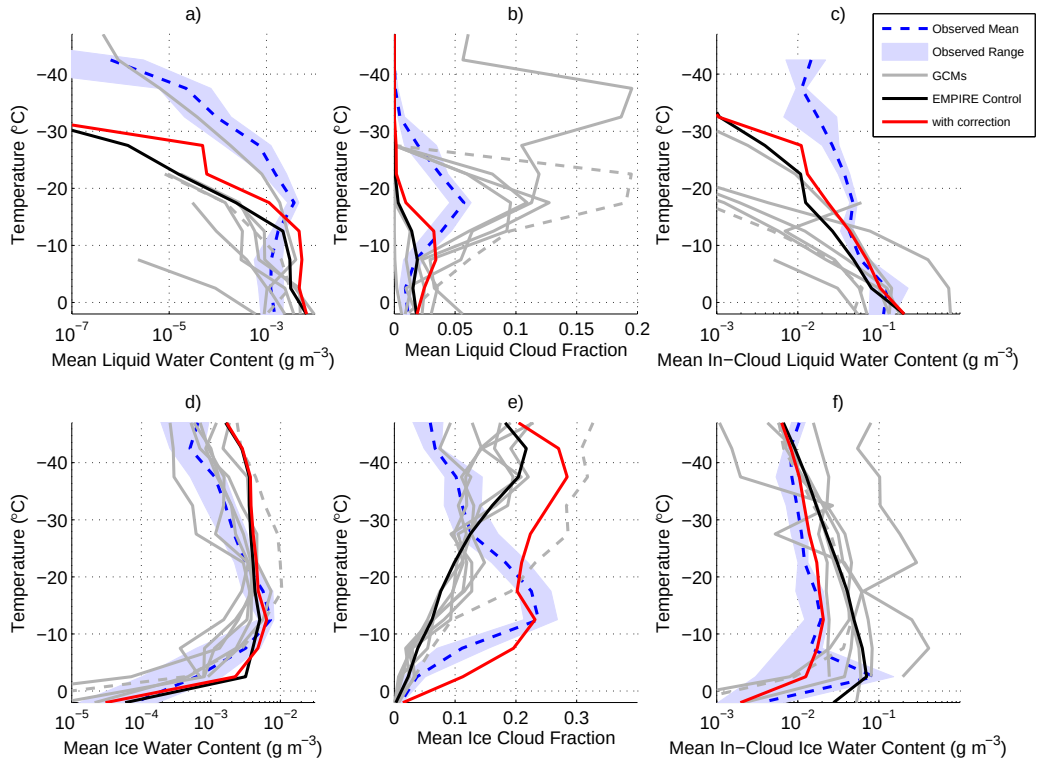

Figure 4.11 As figure 4.1, showing liquid and ice water contents and cloud fractions from EMPIRE experiments where the ice cloud fraction parameterization has been changed. The control simulation uses the standard parameterization whilst corrected parameterization uses the relationship described in chapter 3.

increases the liquid water content and liquid cloud fraction. The reason for this is not immediately apparent; however, investigation identifies the calculation of the supersaturation with respect to ice as the source of the change. This change may be specific to EMPIRE, and the Unified Model upon which it is based, as the calculation of the supersaturation involves splitting the grid-box in to 4 regions and calculating the vapour content of each. The four regions are liquid cloud, ice cloud, mixed-phase cloud and clear sky, with the size of each dependent on the cloud fraction of liquid and ice and the overlap between the two (assumed to be minimum overlap in both EMPIRE and the Unified Model). By increasing the ice cloud fraction, the fraction of the grid-box with no cloud has been reduced. The mean vapour mixing ratio in the clear portion of the grid-box is proportional to the total cloud fraction, equalling $\mathrm{RH}_{\mathrm{crit}} q_{si}$ once the grid-box becomes completely cloud-filled. Therefore, increasing the cloud fraction has also increased the vapour in the clear part of the grid-box and consequently reduced the vapour content of the ice cloud partition to maintain a constant water vapour content in the whole grid-box. This reduction of the water vapour content in the ice cloud partition reduces the calculated supersaturation and hence the depositional growth rate decreases. This results in liquid water cloud that glaciates more slowly and therefore the liquid cloud persists longer before being glaciated.

In summary, the change of the relationship between ice water content and cloud fraction has shown obvious benefits. Primarily the simulated ice cloud fraction is improved, as expected, but this does not change the overall ice water content notably. At the same time, at least in this model setup, the mean liquid water content is increased as liquid clouds persist longer due to a reduced depositional growth rate for ice.

4.4.2 Ice particle size distribution

As shown earlier both the ice particle growth rate and the mean ice particle fall velocity have significant impact on the amount of supercooled liquid remaining in the simulations. Each ice particle has a particular growth rate depending on its size and shape (its capacitance), but of equal importance is the assumed ice particle size distribution. The size distribution describes the sizes of numerous ice particles within a volume of air and whether the ice water content is comprised of many small particles or a few large ones. Changing the size distribution will result in a change in the mean growth rate and fall velocity of all the ice particles in the sample volume.

4.4.2.1 The ice particle size distribution construct

The size distribution describes how many large and small ice particles exist within the volume of air in question, in this case the model grid-box, and is important in the model as many micro-physical process rates depend upon it. Observed distributions (e.g. Houze et al., 1979; Field et al., 2005; Delanoë et al., 2005) demonstrate a wide variety of the concentrations of small and large particles. Whilst typical distributions are largely variable and do not generally fit inverse exponential distribution used by some models it should be possible to estimate different moments of the distribution reasonably using an inverse exponential, that is, the number of ice particles within a given size interval decreases exponentially as the ice particle size increases. More complex, and more simple, formulations of the ice particle size distribution exist, and the scheme used within the UK Met Office Unified Model is an inverse exponential with a modification for temperature similar to Wilson and Ballard (1999) which is apparently based on the observations of Houze et al. (1979). The size distribution is given below:

$$N(D) = N_0 \exp(-0.1222T) \exp(-\Gamma D), \tag{4.3}$$

where T in temperature in degrees Celsius, $N_0 \exp(-0.1222T)$ is the intercept parameter and Γ is the slope parameter. By default N_0 has a value of 2×10^6 m^{-4} so the intercept parameter changes from 2×10^6 m^{-4} at 0 °C to 2.6×10^8 m^{-4} at -40 °C. The slope parameter is calculated such that the ice water content, calculated from the integral of the size distribution, matches that predicted by the prognostic ice mixing ratio. This means that the number of small ice particles is nearly unchanged from small to large ice water contents, with the change being mainly a result of an increased number of larger particles.

The ice particle growth rate is dependent on the shape and size (capacitance) of the ice particle and the mass of an ice particle of a given size is known from the Brown and Francis (1995) relationship. Using these two pieces of information it is found that the ice particle growth rate is largest for the largest ice particles; however, the fastest growing particles in terms of a percentage change are the smaller particles, which have a much smaller initial mass. Therefore, for a given ice water content, a cloud volume of small ice particles will grow more rapidly than one containing only a few larger particles. In addition, the smaller particles will have a smaller terminal velocity and therefore remain within the cloud for a longer time. This increases the particles

ability to remove liquid water from the cloud. It is therefore important to adequately represent the distribution of ice particles within the grid-box.

Earlier in this chapter it was shown that EMPIRE has a significant sensitivity to the value of the intercept parameter, N_0, chosen by default. Reducing N_0 by an order of magnitude increased the amount of supercooled liquid present in the simulations by an order of magnitude between -10 °C and -30 °C. The physical interpretation of this is a reduction in the number of small ice particles and therefore an increase in the number of large ice particles. As discussed earlier it is the small ice particles that contribute most to the growth rate and also fall more slowly. Therefore, decreasing the number of small ice particles will lead to an increase in the number of large particles and a decrease in the amount of liquid water removed by depositional growth. As there is substantial sensitivity to the choice of N_0 in mixed-phase clouds it is therefore important to understand if the values currently used in models are suitable.

4.4.2.2 Comparison of observed and parameterized size distributions

To evaluate whether the parameterized size distribution used in the Met Office Unified Model is physically realistic, the parameterization is compared to the size distributions from aircraft observations.

Aircraft observations of the size of ice particles in mid-latitude clouds from the EUCREX field campaign in the early 1990s are used. More than 10000 size distributions (each a 5 second average) are used and these size distributions and their total ice water content are compared the mean ice growth rate and fall velocity calculated from the parameterized size distributions of equal ice water content.

4.4.2.3 Small ice particles concentrations

Small ice particles concentrations are hard to measure for two reasons: firstly because the particles are small and appear near-spherical to the cloud particle imaging instrument and therefore become difficult to identify the difference between them and liquid cloud droplets. Secondly, the measured volume of the cloud is often contaminated by shattering of larger ice particles on the aircraft or

on the tips of the instrument themselves (Korolev and Issac, 2005). This results in a number of larger particles not being detected and a very large increase in the number concentration of the small particles. It has been shown by comparison to Doppler lidar measurements that these small ice particles are an artifact of aircraft measurements (Westbrook and Illingworth, 2009). This problem has recently been addressed in part with specially designed tips on the instrument which deflect the shattered ice particle fragments away from the sensor, but is still a source of error in current measurements. Software detection algorithms can also identify small shattered particles as they often appear in clusters (e.g. Field et al., 2006) and can therefore be identified and discounted. These advances have improved the quality for aircraft observations recently, however, much of the earlier data still contain these problems and therefore need to be addressed.

The data are from the EUCREX field campaign in early 1990s and therefore likely suffers from the problems identified above. Therefore the concentrations for the small ice particles are likely to be unreliable. In the coming comparison the data used are the same as in Hogan et al. (2006). The number of small particles in this dataset is modified from the original EUCREX observations due to problems with undercounting by the 2D-C probe (Heymsfield and Baumgardner, 1985; Francis et al., 1998; Strapp et al., 2001) and shattering. The sub-100-μm particles are represented by a gamma function of solid ice spheres with a modal diameter of 6 μm and such that the 100 μm concentration is unchanged from that measured but the 25 μm concentration is a factor of 2 larger than measured (Hogan et al., 2006). This change increased the total ice water content by 5% on average.

4.4.2.4 Calculation of growth rates, fall velocities and parameterized size distribution

Information about the number and size of ice particles at high temporal resolution are available from the aircraft observations. This information is from 5 second subsets of the aircraft data, which equates to a horizontal distance of approximately 1 km. For each subset the total growth rate and the mass weighted mean fall velocity of the ice particles are calculated. The total growth rate is calculated using

$$\frac{dq_i}{dt} = \frac{1}{\rho}\int_0^\infty \frac{dM(D)}{dt} N(D)\, dD, \tag{4.4}$$

and the mass weighted fall velocity by

$$\overline{v_m} = \frac{\int_0^\infty V(D)M(D)N(D)\,dD}{\int_0^\infty M(D)N(D)\,dD}. \tag{4.5}$$

In both of the above equations $M(D)$ is the mass of an ice particle with diameter D, $V(D)$ is the fall velocity of the particle, $N(D)$ is the number of particles of that size per unit volume and ρ is the air density. $\frac{dM(D)}{dt}$ is calculated using equation (2.49), the other values are calculated as in EMPIRE using:

$$V(D) = 25.2D^{0.527};\;\; M(D) = 0.0185D^{1.9};\;\; N(D) = N_0\exp(-0.1222T)\exp(-\Gamma D); \tag{4.6}$$

where D is the diameter in metres and $N_0 = 2\times10^6$ m^{-4} following Wilson and Ballard (1999), but with the mass-diameter relationship from Brown and Francis (1995). They apply equally to the observed and the parameterized ice particles, other than the size distribution from the aircraft is used in place of the parameterized $N(D)$ above for the observations. The growth rate and mean fall velocity values are compared between the observed and parameterized size distributions for each 5 second subset of data. A consistent bias is found in both the growth rate and fall velocity which varies as a function of ice water content. The ratio of the parameterized value to the true value obtained from the observed size distribution are plotted in figure 4.12a, d as a function of the total ice water content in the sample and the temperature of that sample is denoted by the colour of the dot. For small ice water contents ($\leq 10^{-4}$ g m^{-3}) the Wilson and Ballard (1999) parameterization overestimates the total growth rate by a factor of two or more. Additionally, the mass weighted mean fall velocity is half or less of the true mean fall velocity. There is spread amongst the data, but the sign and magnitude of the biases are consistent across many samples and a range of temperatures and there is no apparent temperature dependent bias. The magnitude of the bias decreases as the ice water content increases and the sign of the bias changes for ice water contents greater than 10^{-2} g m^{-3} in both the growth rate and fall velocity.

The nature of the bias with excessive ice growth and decreased fall velocity is symptomatic of an error in the number of small ice particles. The small particles are most efficient at depositional growth and fall most slowly, and an increased number of small particles in the parameterization would give the biases found. This excess of small particles could also be described as N_0 being too large.

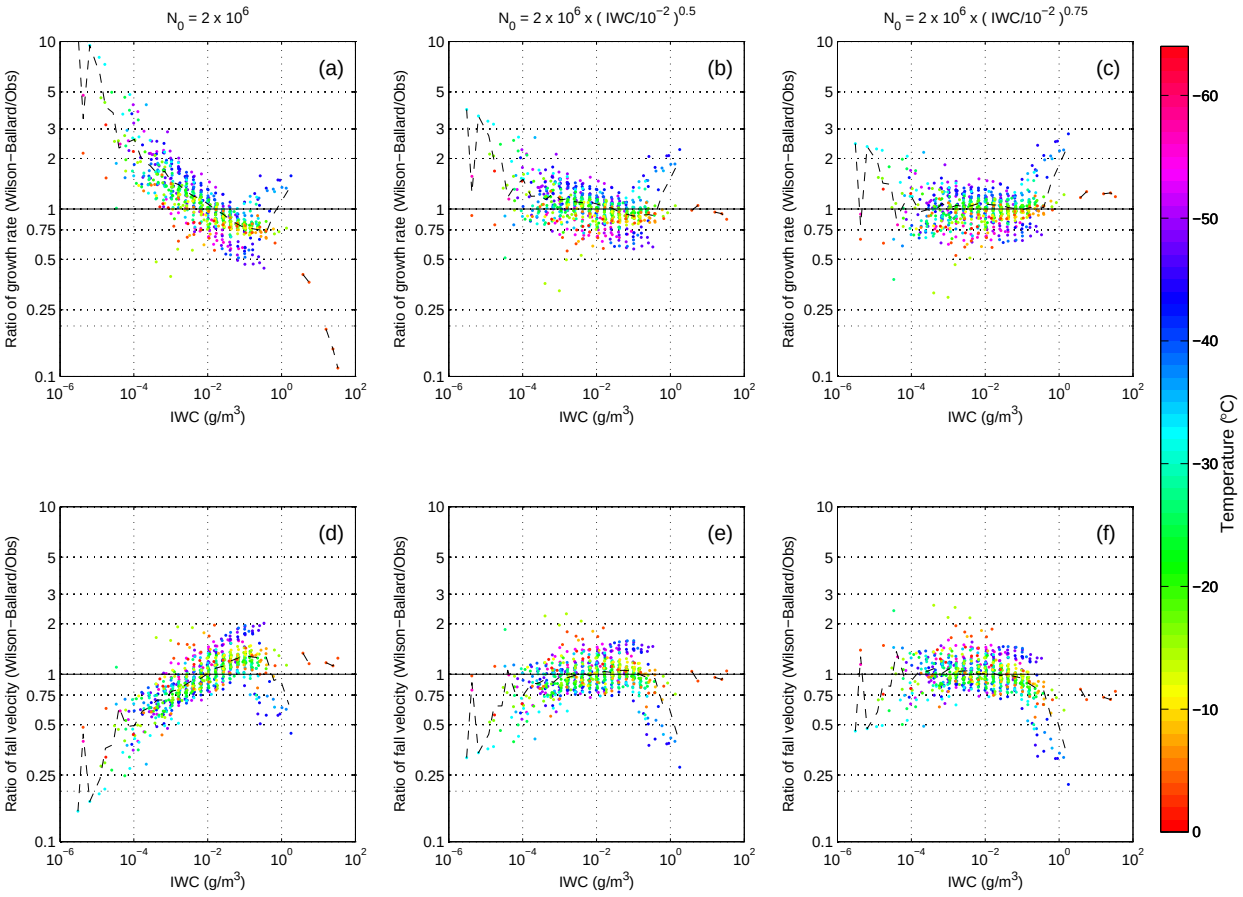

Figure 4.12 The parameterized process rates from Wilson and Ballard (1999) plotted as a fraction of the true growth rate calculated using size distributions observed during EUCREX. Panels a-c show the growth rates and panels d-f show fall velocities. This is shown as a function of ice water content (x-axis) and temperature (colour) for the standard parameterization (panels a and d) and two modifications of N_0 based on the ice water content (panels b, c, e and f).

The literature on size distributions suggests that formulations of the particle size distribution with more variables than the exponential fit are not required to devise accurate values of ice water content and radar reflectivity (Heymsfield et al., 2008) and that there is some dependence of N_0 on the ice water content (Houze et al., 1979; Delanoë and Hogan, 2008; Morrison et al., 2011b). Using the information from these papers a correction is applied to N_0 such that it becomes a function of both ice water content and temperature, rather than just temperature as described in Wilson and Ballard (1999). Two different functions for N_0 are tested, based on the observed relationships in Delanoë and Hogan (2008) and Morrison et al. (2011b). The relationship in Delanoë and Hogan (2008) is approximately $N_0 \sim \mathrm{IWC}^{0.5}$ whilst Morrison et al. (2011b) analysed

aircraft observations of Arctic mixed-phase clouds during SHEBA and found a slightly stronger relationship of $N_0 \sim \text{IWC}^{0.627}$. The first alteration changes N_0 in (4.6) to be expressed as

$$N_0 = 2 \times 10^6 \left(\frac{\text{IWC}}{10^{-2}} \right)^{0.5} \quad \text{m}^{-4} \tag{4.7}$$

where IWC has units of g m^{-3}, based on the approximate relationship between N_0 and IWC in Delanoë and Hogan (2008). The second change gives an even stronger relationship between N_0 and IWC of

$$N_0 = 2 \times 10^6 \left(\frac{\text{IWC}}{10^{-2}} \right)^{0.75} \quad \text{m}^{-4}. \tag{4.8}$$

This relationship gives a stronger dependence of N_0 on IWC than the $N_0 \sim \text{IWC}^{0.627}$ found in Morrison et al. (2011b) and has been chosen due to the small biases found when this dependence is implemented. The effect of changing the value of N_0 can be seen in panels b,c,e,f of Figure 4.12 when compared to panels a and d. By changing N_0 to that in (4.7) a considerable improvement in the calculated growth rates and fall velocities is seen across the range of ice water contents (Figure 4.12 b, e). The magnitude of the bias at both small and large values is greatly reduced and gives satisfactory results when compared to the samples obtained by aircraft observations.

By further increasing the dependence of N_0 on the ice water content and using (4.8), the fit with observations is even better. There is now almost no bias in the parameterized growth rates across 4 orders of magnitude of ice water content and may prove reasonable beyond this range although the observed data are too sparse to allow any reasonable comparison. This change is larger than justified by current observations but gives an excellent prediction of the total growth rate and mass weighted mean fall velocity, which is essentially the role of the size distribution in numerical models.

Our observations of mixed-phase clouds using radar and lidar shown earlier in figure 4.10 show that the majority of mixed-phase clouds analysed have ice water contents between 10^{-4} and 10^{-2} g m^{-2} which correspond to growth rates 2.5 and 1.1 times larger than observations and fall velocities a factor of 0.5 and 1 times the observations when using a constant value for N_0. So whilst the calculated growth rates and fall velocities are acceptable for the highest observed ice water contents, at the lower end considerable biases exist that act to remove liquid from mixed-phase clouds too rapidly. With the smaller of the two corrections (4.7) applied, the mean bias is reduced to a factor of 1.5 for growth rates and 0.75 for fall velocity where ice water content is 10^{-4} g m^{-2} and these two values improve further to 1.1 and 0.95 using the larger correction (4.8).

4.4.2.5 Impact of ice particle shattering

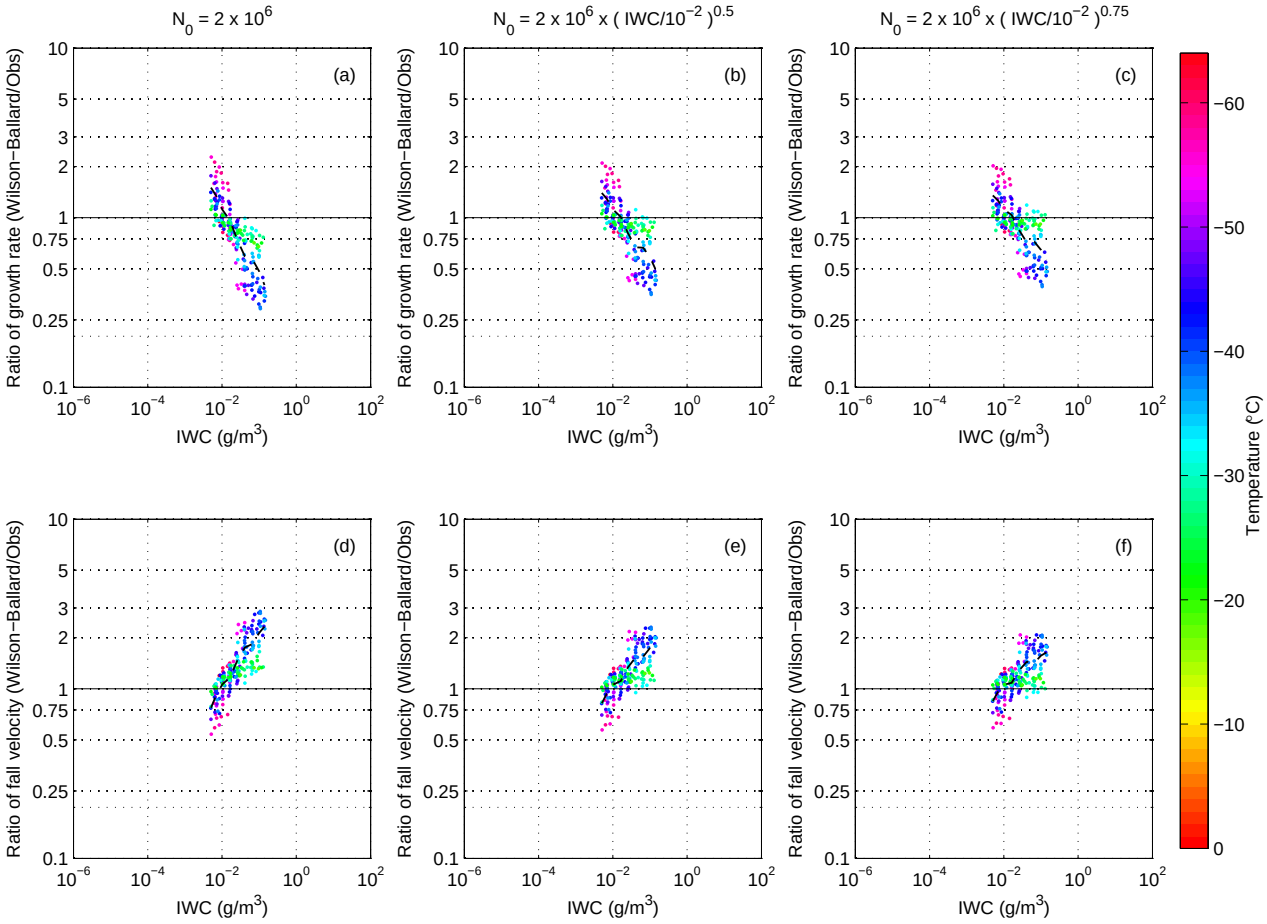

Figure 4.13 As 4.12 but using data from CONSTRAIN, which has been processed to remove the effects of ice particle shattering on the observing instrument.

As mentioned in section 4.4.2.3, the EUCREX data from the early 1990s may be subject to ice particle shattering artifacts in the data. The data was collected before the issue of ice shattering was properly identified and understood. Therefore, if any shattering has occurred on the instrument prior to sampling, there have been no efforts to remove the shattered particles from the dataset. In order to ensure that the results obtained here are not as a result of shattered particles the results have been tested with a second, more recent dataset. The data are from the 2010 CONSTRAIN project, which consisted of flights over the UK, mainly studying cirrus clouds. A different set of instruments was used to create the size distributions, these included 2D-C, 2D-S and cip-100 instruments which each measure a different size range of particles and have been combined to make a single composite size distribution for each 10 second sample (Cotton

et al., 2012). The data is processed to remove the effects of shattering by using a time of arrival algorithm (Field et al., 2006) and only samples with greater than 0.3 g m^{-3} of ice are included to ensure reasonable agreement between the instruments in the overlapping size bins.

Performing the same analysis on this data shows a similar result as for the EUCREX data (figure 4.13). There is still an ice water content dependent bias in the parameterized growth rate and fall speed, and the intercept with the 'correct' one-to-one line is not significantly changed. The slope of the data points and therefore the magnitude of the bias is increased, particularly for the colder temperatures, however, a similar magnitude effect is observed at warmer temperatures around -20 °C where mixed-phase clouds are typically observed. This is what is expected if some shattering were present in the EUCREX dataset. Unfortunately samples with small ice water contents have been removed from this dataset due to quality issues. The size distributions of small ice water contents typically contains more smaller particles and is therefore less prone to shattering, suggesting that the EUCREX data may be more reliable for the smaller ice water contents.

This new evidence supports the original conclusions that there is an ice water content dependent bias in the parameterized growth rates and fall speeds of ice particles, both of which act to reduce the amount of supercooled liquid water in mixed-phase clouds. The modifications to N_0 in the size distribution reduce this bias, particularly for warmer temperatures where mixed-phase clouds are found, in agreement with the results obtained from the EUCREX data.

4.4.2.6 Applying corrections in EMPIRE

Applying the corrections to EMPIRE (figure 4.14) gives an increase in the liquid water content of simulated clouds, particularly in the -10 °C to -30 °C temperature range, of 162% ($IWC^{0.5}$) and 189% ($IWC^{0.75}$); a change of similar magnitude to halving the intercept parameter N_0 everywhere. This is the expected change of both reducing the glaciation rate and increasing the fall velocity of the ice particles and results in supercooled liquid layers that have an increased lifetime as they do not glaciate as quickly. This increase in the liquid cloud lifetime also allows for more ice in the simulations, with the mean ice water content increasing by 5% and 8% for the $IWC^{0.5}$ and $IWC^{0.75}$ corrections respectively and increases the total albedo of the clouds by more than 85%

in both cases.

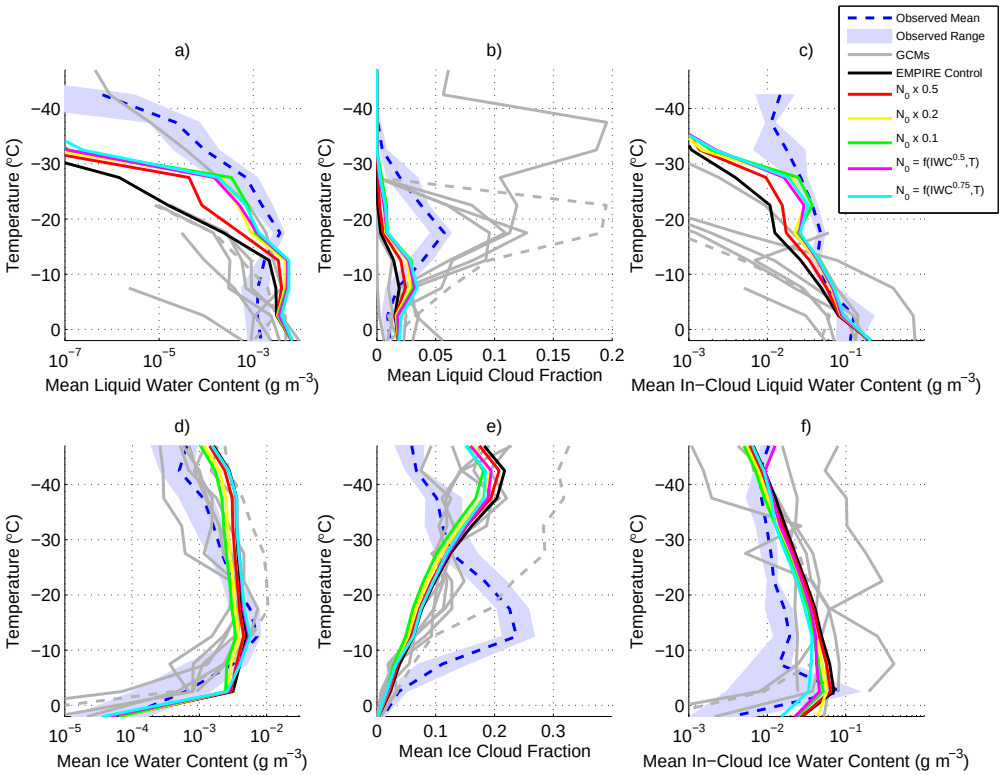

Figure 4.14 As figure 4.1, showing liquid and ice water contents and cloud fractions from EMPIRE experiments where the ice particle size distribution specifications have been changed. The experiments are: (red) N_0 in ice particle size distribution scaled by 0.5, (yellow) N_0 scaled by 0.2, (green) N_0 scaled by 0.1, (magenta) N_0 parameterized as a function of IWC$^{0.5}$ and (cyan) N_0 parameterized as a function of IWC$^{0.75}$.

4.4.3 Combination of parameterization changes

Whilst the above sections have highlighted that a number of different processes all contribute to varying degrees to the maintainence of mixed-phase clouds, no single change has enabled the mean supercooled liquid water content or cloud fraction to match or exceed the observed quantities for these cases. A further simulation has been run to assess the maximum amount of supercooled liquid possible if all parameterizations are setup to favour the existence of supercooled liquid. This means using the corrected ice particle size distribution with $N_0 \sim \text{IWC}^{0.75}$, the corrected ice cloud fraction relationship from observations, reducing the growth rate of ice particles by 50% and increasing the fall velocity by 50% and additionally changing the ice particle habit to spheres, the slowest growing and fastest falling particle shape. A change to the radiation

scheme, setting the liquid effective radius to 2 μm, increases the optical depth of liquid and increases both the longwave cooling and amount of reflected solar radiation. This is a combination of all the changes that give an increase to the amount of supercooled liquid water in the previous experiments, summarised in table 4.2, with the exception of changing RH_{crit}.

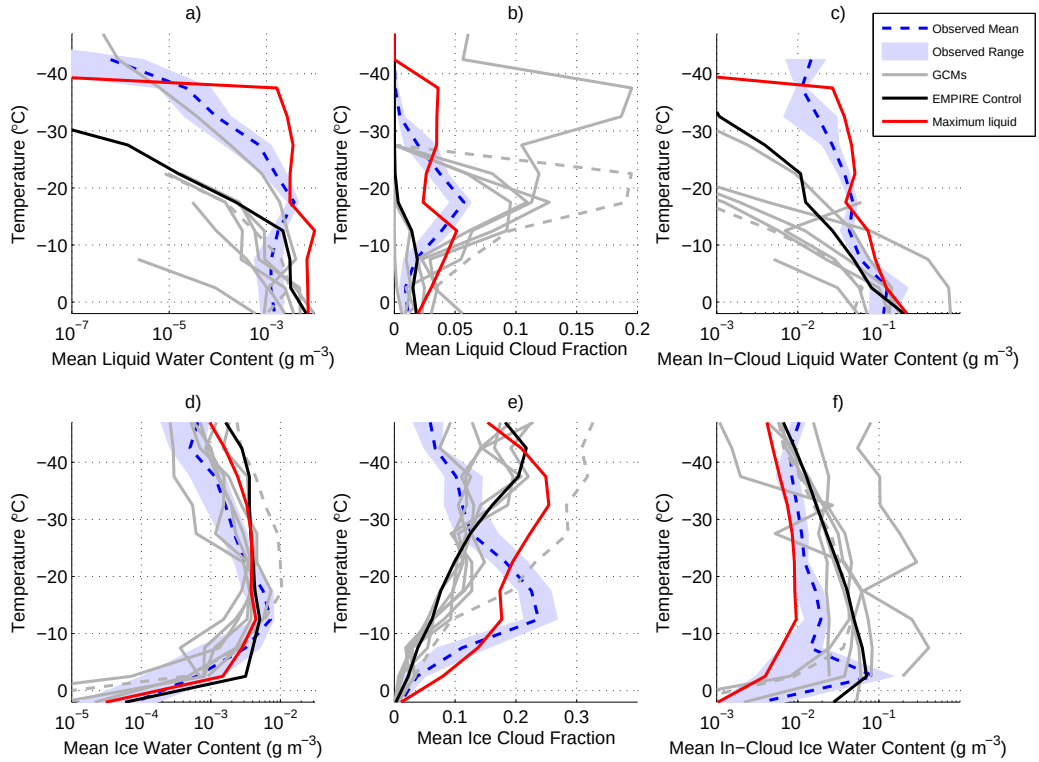

Figure 4.15 As figure 4.1, showing liquid and ice water contents and cloud fractions from EMPIRE experiments where all parameterizations are changed to maximise the amount of supercooled liquid water in the simulations.

The results, shown in figure 4.15, show a large increase in the total amount of supercooled liquid water which exceeds the observed values for all temperatures between 0 and -40 °C, except at -17 °C where the simulated value is within the range of observations. The total liquid water content in the temperature range -10 °C to -30 °C is 649% of that in the control simulation and 47% larger than the mean observed liquid water content in that temperature range. A similar increase is also seen in the liquid cloud fraction, but is still underestimated by a factor of 2 at -17 °C despite overestimating at temperatures warmer than -10 °C and between -30 and -40 °C. The mean ice water content decreases slightly (8% between -10 °C and -30 °C) as a result of the reduced growth rate and increased fall speed but the cloud fraction increases due to the change in the cloud fraction parameterization.

4.5 Conclusions

In this chapter, EMPIRE has been used as a tool to develop an understanding on the important processes in maintaining mixed-phase clouds. Initially the ability of EMPIRE to simulate thin, single-layer mixed-phase clouds is assessed and compared to observations and other numerical models. EMPIRE has a similar behaviour to the GCMs in general, with the amount of supercooled liquid at temperatures colder than $-15\ ^{\circ}$C being underestimated. Biases similar to GCMs were also observed in the mean ice water content, ice cloud fraction and in-cloud liquid and ice water contents. The liquid cloud fraction was most similar to the GCMs with prognostic ice water content although had more cloud fraction and liquid water content than these GCMs.

The contributions of the processes to liquid water content tendency is calculated and it is found that the supercooled liquid water layer at the cloud top is maintained in the simulation by radiative cooling at the cloud top. The turbulent mixing acts to reduce the production of liquid water from radiative cooling by transporting the cooled air to lower in the cloud. The net tendency throughout most of the depth of the cloud was a small decrease in the liquid water content with time but at the cloud top the liquid water content is increasing because the radiative cooling extends to higher in the cloud than the turbulent mixing does.

Through a number of different modifications to EMPIRE the importance of each physical parameterizations and processes in the model is assessed. The largest sensitivities to changes are those affecting the ice production mechanisms. The reason for an underestimate in the supercooled liquid water content is largely because the ice growth rate is too large (due to a number of causes) rather than too little liquid being produced by the model; however, both will have an effect here. Changing the growth rate of ice particles directly, or the assumed size distribution of ice particles, their fall speed or their habit all have a large effect on the amount of supercooled liquid present in the simulations.

Many of the modifications that effect the amount of liquid water in the simulations do not significantly change the mean amount of ice (see table 4.2). In particular, reducing only the growth rate by 50% increases the mean liquid water content by over 150% but reduces the ice water content by less than 2%. Reducing the frequency of the radiation scheme to values found in GCMs had a detrimental affect on the liquid water content, reducing the mean by 65% when only

used every 3 hours (rather than every 15 minutes). Reducing the number of vertical grid-points in the model, to more closely match GCM resolutions removed almost all (98.3%) of the liquid water in the simulations, this will have severe implications for the ability of the current GCMs to simulate mixed-phase clouds, even in an otherwise perfect model.

Finally, possible improvements to the physical parameterizations in EMPIRE and GCMs are identified. The ice cloud fraction parameterization as a function of ice water content is modified based on radar observations. This was identified in the previous chapter as being incorrect and that post-processing the ice water content gave a much improved cloud fraction prediction from the GCMs. This was tested in EMPIRE to evaluate the changes of making this correction within the model. It resulted in an increase in the ice cloud fraction to better agree with observations, as also found in the previous chapter. Also it gave an increase in the amount of supercooled liquid and liquid cloud fraction because of the way the grid-box is partitioned in the calculation of the supersaturation with respect to ice. The net result was to decrease the rate at which ice grows and sustain longer lived liquid water clouds.

The modifications to EMPIRE that showed the most sensitivity to change - the fall speed and growth rate of ice - are together affected by the ice particle size distribution. By testing the parameterized size distribution against aircraft observations from the EUCREX campaign a bias was identified in both growth rate and fall speed of the total population of ice particles within a grid-box. This resulted in ice particles both growing too quickly and falling too slowly, combining to rapidly remove the supercooled liquid from the cloud. The bias was evidently dependent on the ice water content but not on the temperature and therefore a correction based on the ice water content was made that removed much of the bias across many orders of magnitude of ice water content. This was shown to increase the liquid water content, particularly at temperatures colder than -10 °C, to agree better with observations.

It is notable from all of the modifications made to EMPIRE that mixed-phase clouds are sensitive to a number of different processes to a varying degree. However, no single modification was able to increase the liquid water content or liquid cloud fraction of EMPIRE enough to match or exceed the observed values, although a combination of all beneficial changes is able to exceed the observed liquid water content. At temperatures warmer than -10 °C the mean liquid water content and cloud fraction exceed the observations in all simulations, largely caused by a small

number of clouds that had a very large water content. This suggests that there is not a simple model bias that can be corrected to permit GCMs to simulate mixed-phase clouds correctly. Indeed attempts to correct model biases such as the ice particle size distribution did improve the liquid water content, but the liquid cloud fraction was less easily manipulated. This suggests that the changes to the model were able to change the properties of the existing simulated clouds but were unable to change the frequency with which supercooled liquid clouds occur. This may be due to a bias in the humidity of the forcing dataset or a lack of updrafts strong enough to bring the air to saturation preventing clouds from forming at all.

CHAPTER 5:

VERTICAL RESOLUTION SENSITIVITY

As was shown in the previous chapter, EMPIRE demonstrates a sensitivity to vertical resolution. Thin liquid water layers are able to persist longer in simulations which have higher vertical resolution. All GCMs and NWP models currently run on a much coarser vertical grid than the default 50 metre spacing of EMPIRE and this suggests that resolution could be one of the reasons why current models are not correctly simulating mixed-phase clouds. Understanding this resolution dependence is important to infer the potential effect resolution is having on GCM simulations of mixed-phase clouds. In this chapter the following questions are addressed:

1. How large an effect is resolution having on simulations of mixed-phase clouds?
2. What vertical resolution can be considered good enough for a convergent solution?
3. What is the cause of the resolution dependence?
4. How well can the sub-grid physics be parameterized to remove the resolution dependence?

To further explore this resolution dependence, EMPIRE is used in an idealised configuration; this is explained in section 5.1. Experiments using this setup are used to answer the questions above. Attempts are made to correct the model by adding a parameterization specifically to capture mixed-phase clouds in low resolution models and analyse how well it performs compared to the high resolution simulations.

5.1 Idealised simulation

To investigate the resolution dependence previously discovered, an idealised version of EMPIRE is used throughout this chapter. The idealised model uses the full physics of the model described in

chapter 2. However, there is no advective forcing applied to the model and there are no tendencies to adjust the model fields. The simulation is initiated from a radiosonde sounding from Larkhill (5 September 2003, 0600 UTC) and after that it is completely free running with vertical velocity set to zero everywhere. An idealised model is used to investigate the resolution dependence because this allows the effects of resolution on the simulation to be isolated. Efforts to maintain realism within the simulation are made as the model is initialised from a radiosonde sounding and includes all the physical processes that are included within EMPIRE.

The model is initialised using a radiosonde sounding launched from Larkhill, UK at 06 UTC on 05 September 2003. At this time a stratiform mixed-phase cloud was observed to be forming over the Chilbolton radar facility, approximately 28 km to the East of Larkhill. This cloud was observed to exist for approximately 10 hours with cloud top initially around 6 km increasing gradually throughout this time to about 7.5 km. This is consistent with the sounding which shows a liquid-saturated layer at 6 km altitude. The model was initialised using this sounding and then run for 60 minutes to allow the model to spin-up and for radiation, turbulent mixing and microphysics to come in to equilibrium. At the end of the 60 minute spin-up, the model variables are output and these are used in the initialisations of the variable resolution simulations. The liquid water content is calculated as the difference between q_t and $\mathrm{RH}_{\mathrm{crit}} q_{sl}$ and the ice water content is initially zero. Linear interpolation is used to calculate model variables on grid levels not explicitly calculated from the 25 m resolution simulation. The initial profile can be seen in figure 5.1 and shows an almost well-mixed profile between altitudes of 5500 m and 6100 m. The initial profile has a supercooled liquid-saturated layer which is initially ice free. The model is then allowed to run freely and see how the liquid and ice profiles evolve and how they differ with changing resolution. The model is integrated forward in time for a period of 6 hours and includes all physical processes but no vertical velocities or advective tendencies.

5.2 Effect of vertical resolution

Initially the idealised version of EMPIRE is run at two vertical resolutions; high resolution with a vertical grid spacing of 50 m and a low resolution with 500 m grid spacing. The low resolution has a grid spacing that is similar to GCM and NWP models' vertical resolution in the mid-troposphere.

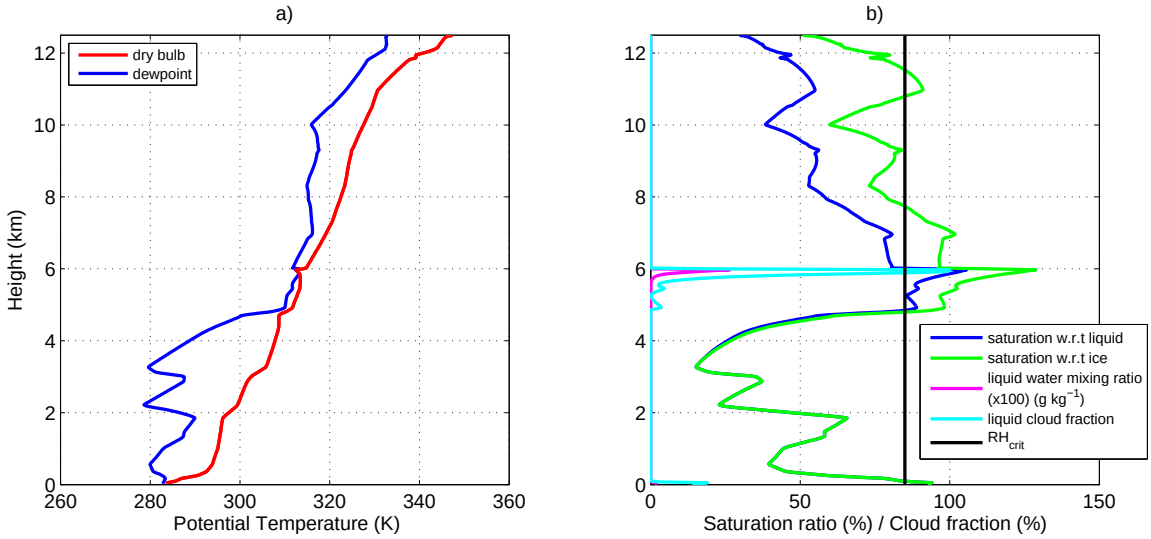

Figure 5.1 Initial model profile of a) potential temperature and "dewpoint potential temperature" ($T_{\text{dew}} \times \left(\frac{p_0}{P}\right)^{\frac{R}{c_p}}$) and b) saturation ratio with respect to liquid and ice and cloud fraction and $q_l \times 100$.

These two resolutions are equivalent to those used in the sensitivity tests in chapter 4. Results from these two model integrations can be seen in figure 5.2. The contoured colour in panels a and c represents the model ice water mixing ratio and panels b and d show the liquid water mixing ratio. The difference in the liquid and ice water content evolution is clear, with a layer of liquid water persisting in the high resolution model simulation, whilst in the low resolution simulation the liquid water content is continually decreasing before the cloud becomes completely glaciated after about 1 hour.

A difference in the evolution of the ice water mixing ratio is noted, with larger values found in the 500 metre resolution simulation for the first 2 hours of the simulation whilst the liquid layer is still present. This difference is particularly noticeable at and near the cloud top and is particularly important as this is also where the liquid water is present in the largest concentrations. Because the rate of ice growth is dependent on the ice mixing ratio, these large values near cloud top significantly increase the growth rate. This allows the high ice water mixing ratios to be sustained at cloud top whilst the liquid evaporates to maintain the vapour source. The absence of the liquid water layer at cloud top beyond 1 hour and the reduction in the ice water mixing ratio lower in the cloud as a result will together have a profound effect on the solar radiation able to penetrate the cloud and potentially reach the Earth's surface.

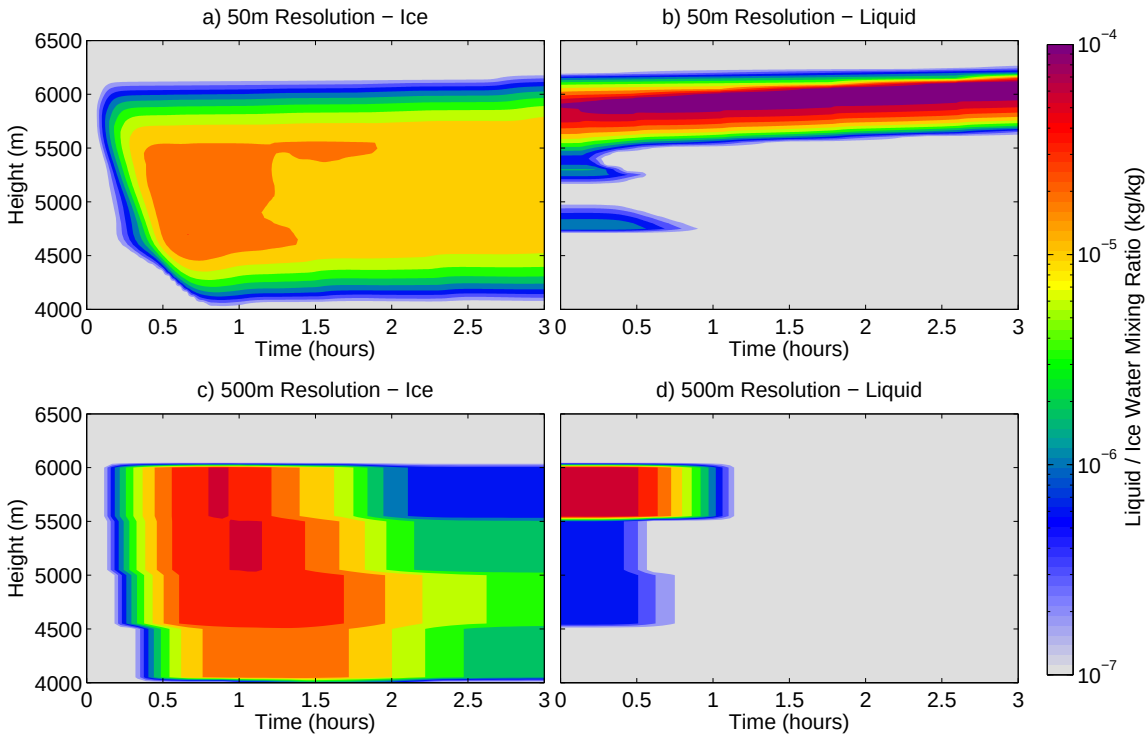

Figure 5.2 Idealised simulation at vertical resolutions of 50 m (a-b) and 500 m (c-d). Ice water mixing ratio is shown in the left hand panel and liquid water mixing ratio in the right hand panel. The colour bar is applicable to both liquid and ice.

Whilst the difference between these two resolutions is stark, an understanding of the behaviour across a large range of resolutions is required. To determine this, EMPIRE is run at a number of different vertical resolutions and the liquid water in the simulations is compared. Figure 5.3 shows the simulated liquid water path at hourly intervals from the simulations. The liquid water path is near constant when the model is initialised; however, at coarser resolutions there is a reduction in the initial liquid water path due to a poorly resolved vertical structure of the cloud. As the simulations evolve in time, the coarser resolution simulations glaciate most quickly but after 1 hour even the 500 m simulation has a liquid water path in excess of 0.1 g m^{-2}. After two hours only simulations with resolution finer than 350 m have a liquid water path in excess of this threshold, and in the coarser resolution simulations the liquid cloud has already dissipated. This continues with finer resolutions being affected further into the simulations.

As the vertical grid spacing increases the total liquid water path decreases, most notably for grid spacings larger than 250 metres. For resolutions of 200 metres or finer the simulations start

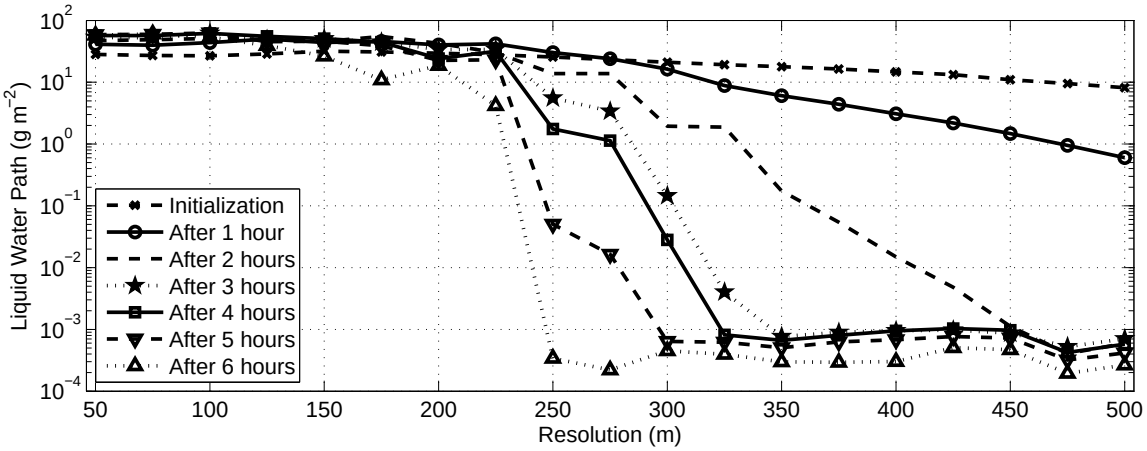

Figure 5.3 Liquid water path from plotted at hourly intervals from model simulations of varying resolution. For model vertical resolutions greater than 250 metres liquid water path decreases with time into the model simulation; however, for finer resolutions the model maintains the liquid water path throughout the simulation.

to converge. These results are particularly concerning as typical GCM resolutions are 500–1000 m in the middle troposphere. Even the state-of-the-art operational forecast models have mid-tropospheric vertical resolutions of 250–400 m (see figure 5.4) and the total liquid water path at these resolutions is significantly less than that of the high resolution simulations. Vertical resolutions on the order of tens of metres throughout the troposphere are unattainable in GCMs due to the computational time that would be required to run over such large domains. This implies that GCMs may never be able to capture mixed-phase clouds in their current configuration.

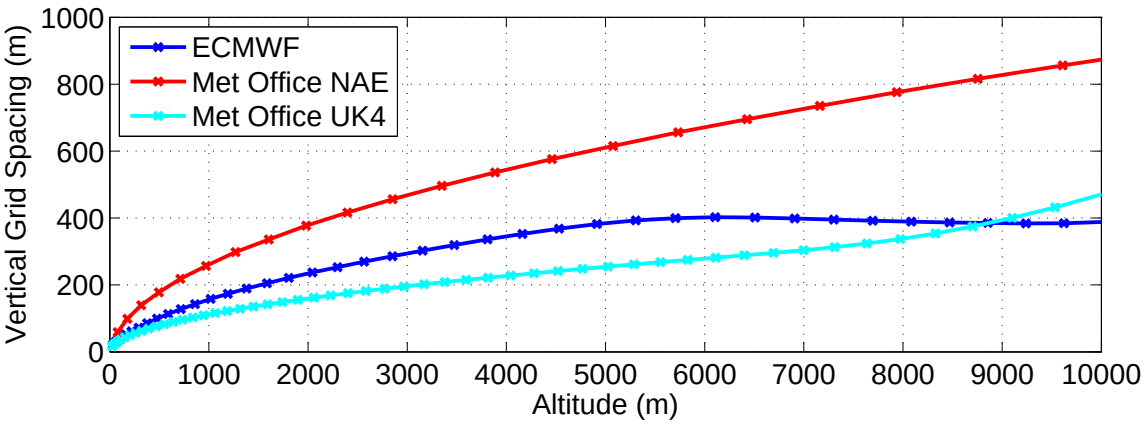

Figure 5.4 Vertical spacing of model levels in the ECMWF and UK Met Office Unified Models plotted against altitude for operational model configurations as of 1 January 2010.

5.3 Causes of resolution dependence

5.3.1 Process rates

Figure 5.2 shows a marked difference in the liquid and ice mixing ratios at two different resolutions. Notably, the ice water mixing ratio at cloud top is substantially higher in the coarse resolution simulation. To understand why the model shows this difference the sources and sinks of ice in the top 500 metres of the two simulated mixed-phase clouds are analysed. The process rates for each simulation are shown in figure 5.5. The deposition growth rate of ice and the rate of loss due to sedimentation are significantly smaller in the 50 metre simulation, to such an extent that the y-axis of figure 5.5a is a factor of 10 smaller than 5.5b.

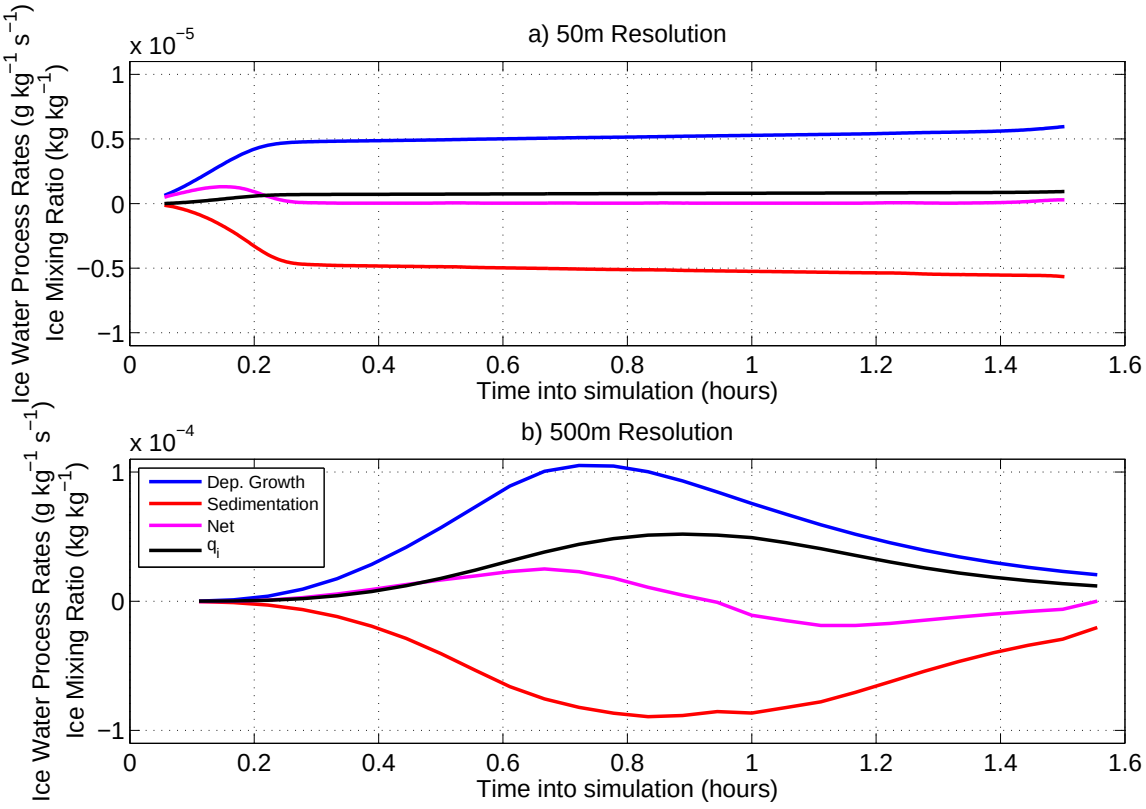

Figure 5.5 Time series of the model source terms for ice at resolutions of a) 50 m and b) 500 m. Note the factor of 10 difference in the y-axis scale of panel a) and b) and that the ice growth and sedimentation rates in the 50 m simulation reach an equilibrium which never occurs in the 500 m simulation.

The most significant difference between the two sets of process rates is that in the 50 metre simulation the growth rate and sedimentation rate reach an equilibrium so that there is no net change in the ice mixing ratio near the cloud top. In the 500 metre simulation this never occurs and the growth rate increases with time until all of the available water has been used up and the liquid water has evaporated. The sedimentation rate increases as the larger mass of cloud ice falls more quickly; however, the rate of loss does not match the growth rate until the liquid has all evaporated and therefore the cloud never reaches equilibrium as occurs in the 50 metre simulation.

5.3.2 Resolution dependent processes

Of the processes that are either a source or sink of liquid water, at least one must change significantly as the model vertical resolution changes to explain the observed difference. The only sink of liquid water of concern is the evaporation of liquid caused by growth of ice particles from vapour. Other sinks such as warming by radiation or large scale descent are negligible in our idealised simulation. The main sources of water are longwave radiative cooling at the cloud top and the supply of vapour from lower in the cloud due to turbulent mixing.

The rate of ice growth within a grid-box is strongly dependent on the mean ice water content and therefore the sources and sinks of cloud ice are also important. These are simply the growth of ice from water vapour and the sedimentation of ice into and out of the model level. This indicates the importance of the ice growth rate as, not only is it the primary sink of liquid but also, it determines the ice water content of the model grid-box at later timesteps that in turn will affect the rate of liquid depletion. Therefore, increasing the ice growth rate but keeping the sedimentation rate constant even for only a single timestep, will increase the liquid depletion rate throughout the simulation until such a time as the liquid has completely evaporated. Similarly, reducing the sedimentation rate but keeping the growth rate constant will have the same effect.

In addition to these processes, the vertical structure of the cloud is also important - with the liquid present at the top and falling ice beneath. As the model resolution becomes coarser information is lost about the vertical structure of the cloud and therefore become less likely to identify a liquid-saturated layer at cloud top.

The rate at which liquid is generated or removed from the cloud layer due to these processes is

dependent on quantities which vary in the vertical near cloud top. Before understanding why these processes are resolution dependent, the vertical profile of these quantities at the top of the cloud need to be considered. Figure 5.6 shows the vertical profile of temperature, q_i and supersaturation with respect to ice near the cloud top from the 50 m vertical resolution simulation discussed above and, for comparison, the same quantities once averaged over a 500 m layer. When looking at this, it is important to remember that numerical models do not account for sub-grid structure in the vertical. The mean quantity for a layer is assumed to be applicable to the layer as a whole when calculating the process rates.

5.3.2.1 Resolving cloud vertical structure

EMPIRE has only 5 prognostic variables: θ_l, q_t, q_i, u and v. All the other variables are calculated using these prognostic variables. The three most important of these prognostic variables for describing the cloud structure are θ_l, q_t and q_i. Typically the top of the cloud is well-mixed, with profiles of θ_l and q_t constant with height due to the turbulent mixing driven from cloud top. The ice water mixing ratio, q_i, tends to increase with increasing distance from cloud top as can be seen

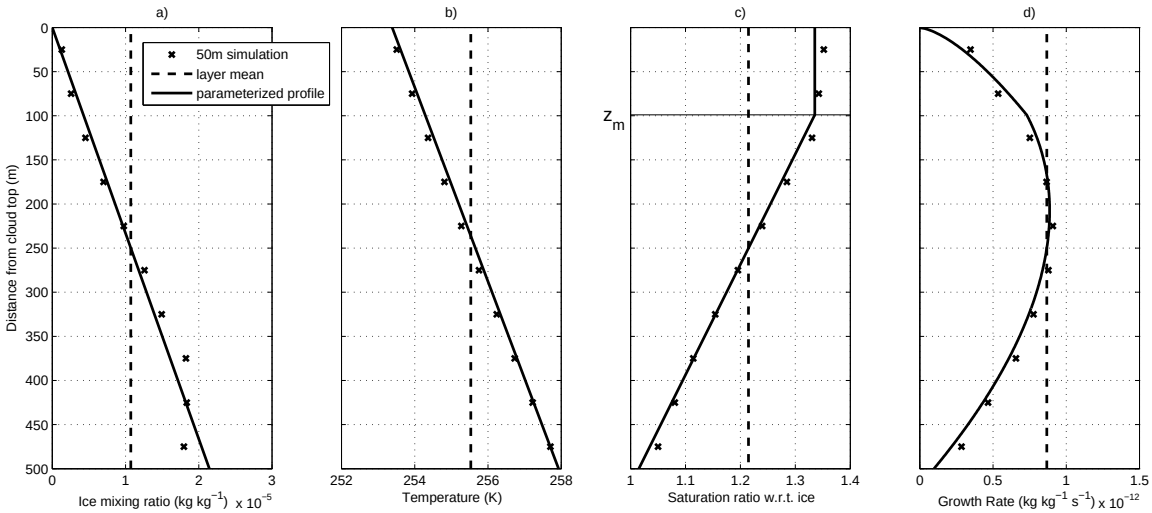

Figure 5.6 Vertical profiles of ice water mixing ratio, temperature, saturation with respect to ice and ice depositional growth rate in the top 500 m of an EMPIRE simulated mixed-phase cloud. The crosses are from a 50 m resolution EMPIRE simulation, the dashed line represents the quantities as calculated using mean values of q_i, θ_l and q_t over the 500 m layer. The solid line shows the parameterized sub-grid profile for use in coarse resolution models.

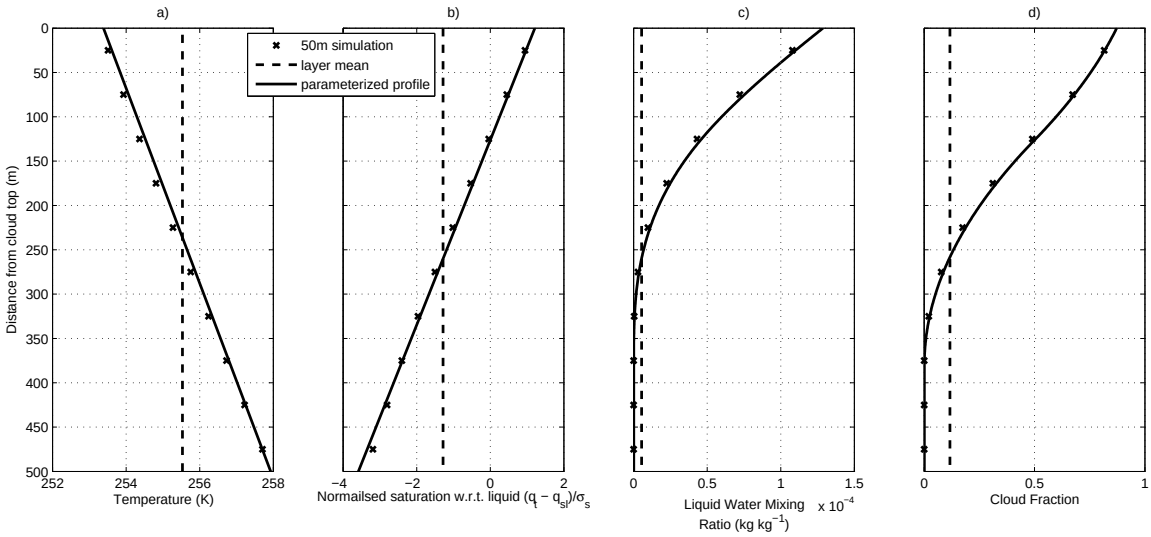

Figure 5.7 Vertical profiles of temperature, the normalised saturation with respect to liquid, $(q_t - q_{sl})/\sigma_s$, as used in the cloud scheme, liquid water mixing ratio and liquid cloud fraction in the top 500 m of an EMPIRE simulated mixed-phase cloud. The crosses are from a 50 m resolution EMPIRE simulation, the dashed line represents the quantities as calculated using mean values of q_i, θ_l and q_t over the 500 m layer. The solid line shows the parameterized sub-grid profile for use in coarse resolution models.

in figure 5.6, and the value of q_i is an almost linear function of distance from cloud top. Whilst θ_l and q_t may be well-mixed throughout the cloud layer the vertical structure in T is still important due to the change of pressure with height. In a layer of 500 m depth, with θ_l and q_t constant with height, it would be expected that the temperature differ by $\pm 2.5^{\circ}$C from the layer-mean temperature due to the pressure change across the layer. The lower pressure at the top of the layer means that the potential temperature translates to a colder air temperature. As a result, the saturation mixing ratio is also lower at the layer top and therefore liquid may exist at the top of this layer as q_t is well-mixed and could exceed the saturation mixing ratio. Using the layer-mean potential temperature, mixing ratio and pressure will correctly calculate the layer-mean temperature but may fail to capture the correct liquid water mixing ratio.

5.3.2.2 Evolution of cloud ice

The ice in mixed-phase clouds is almost always produced in the liquid water regions of the cloud (Westbrook and Illingworth, 2011). Once the ice crystal forms it grows in size through vapour

deposition and falls towards the ground. The net result of these two processes is an increase in ice water mixing ratio away from the top of the cloud, as seen in figure 5.6.

Using the Wilson and Ballard (1999) microphysics scheme and integrating the growth rate of each ice particle over the size distribution of ice particles within the grid-box gives a growth rate term for q_i:

$$\frac{\mathrm{d}q_i}{\mathrm{d}t} = \frac{2\pi SS_i}{A+B}\left(\frac{N_0 \exp(-0.1222T)}{\rho}\right)^{1-\frac{2}{b+1}}\left(\frac{q_i}{a\Gamma(b+1)}\right)^{\frac{2}{b+1}}, \tag{5.1}$$

where the time rate of change of the ice water mixing ratio (q_i) is given in terms of the supersaturation with respect to ice (SS_i), the intercept parameter of the ice crystal size distribution (N_0), the air temperature (T) and density (ρ), a and b from the ice mass-diameter relationship ($m = aD^b$), A and B together form the denominator of the ice particle growth equation (2.49). The most significant terms in equation 5.1 are SS_i and q_i. The value of these two terms change significantly with height in the top few hundred metres of the cloud (figure 5.6a,c). The ice water mixing ratio increases nearly linearly with distance down from cloud top whilst the supersaturation decreases with distance down from cloud top. The product of these two terms is at a maximum when both the ice mixing ratio and supersaturation have intermediate values, which results in the fastest growth rates in the middle of the cloud (figure 5.6d). Failure to resolve these vertical structures and instead using the mean values for both ice water content and supersaturation gives these fastest growth rates through the whole depth of the layer. As a result, the coarse resolution model growth rates are higher than the equivalent growth rates from the fine resolution model (dashed line in figures 5.6 and 5.7) purely as a result of using these averaged values.

5.3.2.3 Ice sedimentation

The transfer of ice from one grid-box to the next due to sedimentation of the ice particles can simply be quantified as

$$\left.\frac{dq_{i\,j}}{dt}\right|_{\text{sedimentation}} = \frac{q_{i\,j+\frac{1}{2}}v_{j+\frac{1}{2}} - q_{i\,j-\frac{1}{2}}v_{j-\frac{1}{2}}}{\Delta z} \tag{5.2}$$

where q_i and v are the ice water mixing ratio and the mass-weighted fall velocity for ice particles falling into and out of grid-box at model level j, with level $j+1$ being above level j and Δz being the grid-box depth.

This sedimentation equation describes the sedimentation used in many microphysics schemes and requires only a method for calculating the mean fall velocity of the ice particles; all other quantities are known from the model. This simplistic approach does cause some changes as the vertical resolution is changed. The change in our simulations occurs because, again, the vertical structure of the cloud is not captured. As shown in figure 5.6 the ice water mixing ratio increases approximately linearly with distance from cloud top; however, the coarse model only has information about the layer mean and assumes this to be applicable to the whole layer. This difference is largest in the uppermost cloudy model level, where at cloud top the ice water content is zero. In this case, as the ice water content increases approximately linearly down from cloud top, then the ice water content at the base of the grid-box must be twice the layer mean. When the structure is resolved, there is approximately double the flux of ice out of the bottom of the model layer than when calculated using the mean as the ice water mixing ratios are larger here which affects both the amount and mean fall velocity of the ice particles. In the coarse resolution, where this structure is not resolved, too little ice is being transported out of the bottom of the layer. As a result the ice water content starts to build up in the uppermost cloudy model layer and will further increase the ice growth rate in the following timestep and amplify the difference between the coarse- and fine-resolution simulations.

5.3.2.4 Radiative cooling

The radiative heating and cooling rates are calculated using the Edwards and Slingo (1996) radiation code. For cloudy regions the heating and cooling rates are dependent on the cloud properties (cloud fraction, water content and hydrometeor size, shape and phase). The hydrometeor size and shape are constant in the radiation scheme for ice and liquid phase respectively so only the water contents and cloud fraction from the model affect the radiation calculations. As mentioned above in section 5.3.2.1, as the model resolution coarsens, our ability to resolve the liquid cloud and peak liquid water content reduces. As a result of this the peak radiative cooling at cloud top associated with the liquid water layer is reduced and lessens the rate at which the highest cloudy model level is cooled. Less cooling of the model layer, all else being equal, results in a higher saturation mixing ratio and therefore less liquid water. This positive feedback may explain our lack of liquid water in coarse resolution simulations. However, the cloud-top cooling is balanced

by turbulent heat flux, so the mixing scheme needs to be considered as well.

5.3.2.5 Turbulent mixing

The turbulent mixing scheme is adapted from Lock et al. (2000) to allow mixed-phase clouds to be mixed by turbulence generated from radiative cooling at cloud top and the resulting destabilisation of the cloud layer. This scheme depends heavily on the radiation scheme in two ways. Firstly, it requires the radiation scheme to cool the cloud top layer sufficiently so as to destabilise the layer and allow turbulent mixing. Secondly, the magnitude of turbulent mixing prescribed is also determined by the cloud-top radiative flux divergence. Both of these will show a resolution dependence if the radiation scheme is showing a resolution dependence as might be expected. Additionally, the Lock scheme requires that a negatively buoyant air parcel at cloud top is able to descend more than one grid-level. As the model grid-spacing becomes coarser this requirement means a greater physical depth of instability is required, and without a well resolved thermal structure this is unlikely to be achieved. The reduction in turbulent mixing that might be expected as a result of this will inhibit the upward transport of moisture to the cloud top, but it may also inhibit the downward transport of colder temperatures from cloud top. It is not clear whether changing the model vertical resolution will increase or decrease the cloud liquid water content through turbulent mixing processes.

5.3.3 Identifying importance of each process

To understand which of the processes discussed above is having the largest impact on our simulations as the resolution is changed, each process is tested individually using the idealised EMPIRE model framework. Using the model setup described earlier in section 5.1, EMPIRE is run with a vertical resolution of 50 metres. Multiple simulations with EMPIRE are conducted and in each case one process is changed so that it acts as if it has a vertical resolution of 500 metres. This may involve, for instance, averaging over 10 model levels and using the 10-level average value from these layers as the input to calculate process rates in each of the individual model levels. This has the result of giving equal process rates to blocks of 50 metre model levels, as would be calculated in a 500 metre simulation, but allowing other processes to have effect at 50 metre resolution.

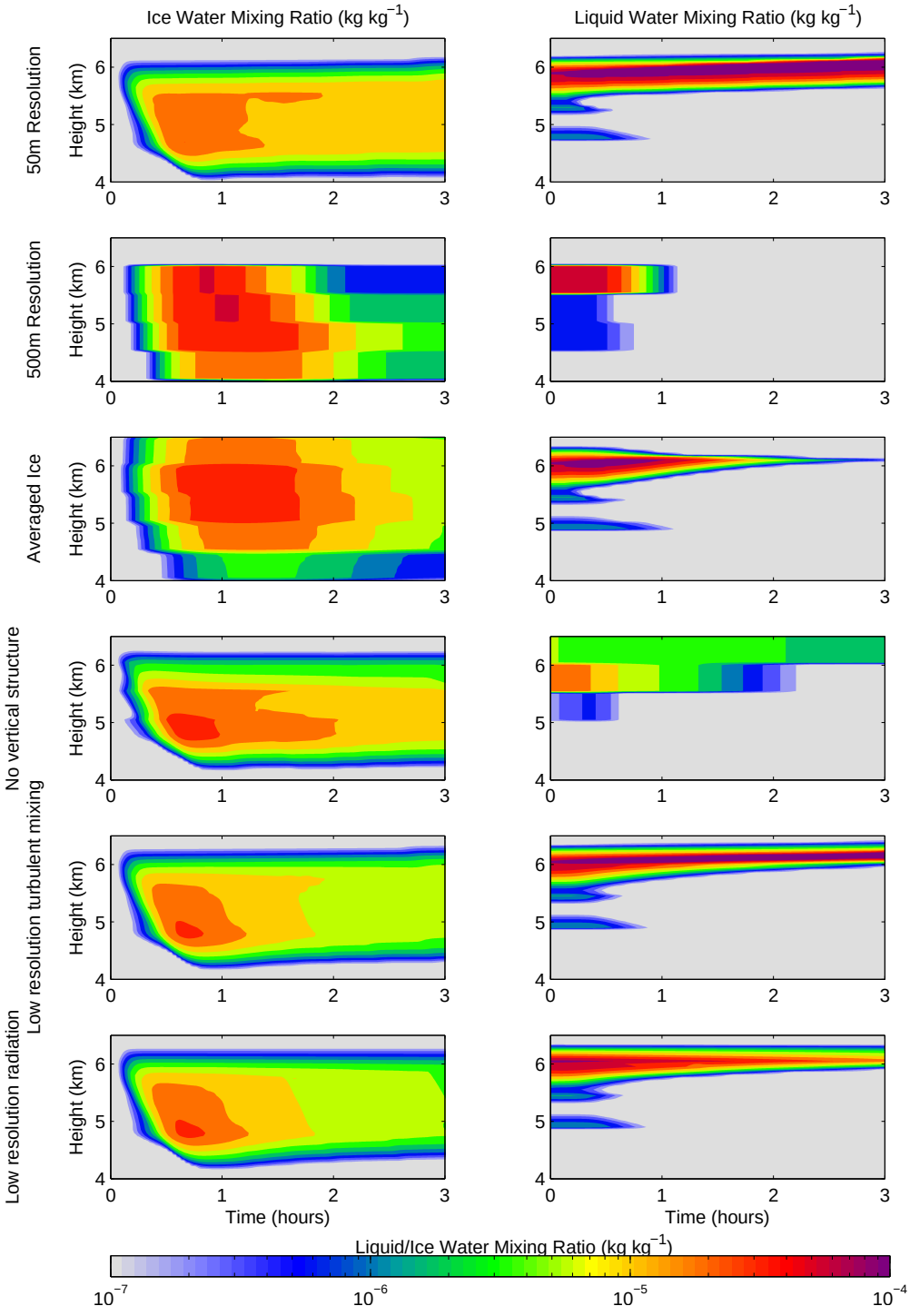

Figure 5.8 Liquid and ice water mixing ratios from six idealised EMPIRE simulations. The simulations from top to bottom are: 50 m resolution, 500 m resolution, 50 m resolution with ice averaged across 10 model levels, 50 m resolution where the vertical structure of temperature is not resolved, 50 m resolution with turbulent mixing on 500 m grid and 50 m resolution with radiation scheme using 500 m averaged quantities.

The processes that are coarsened in the simulations are: a) ice growth and sedimentation, b) resolving sub-grid vertical profile of T (and therefore q_l), c) turbulent mixing (both diagnosis of the diffusivity profile and solving of the diffusion equation) and d) radiation (both temperature and cloud inputs and applying heating and cooling to model levels). The ice growth and sedimentation changes are combined into one simulation as separating these two effects from each other becomes very difficult in practice, largely because they both depend on and change the value of q_i within a timestep.

The liquid and ice water mixing ratios from these simulations are shown in figure 5.8. The first two rows show the same data as figure 5.2, the other four rows show experiments where one processes is coarsened, a-d in the same order as above. This shows that when using coarse resolution for one process only, the simulated cloud can change to closely match that of the 500 metre simulation. This is particularly the case for the simulations where the ice water content has been averaged when calculating the depositonal growth and sedimentation rates and where the vertical structure of the temperature profile is not resolved. In fact, combining these two processes gives us a simulation which is qualitatively very similar to the 500 metre simulation (not shown). The simulations with coarsened radiation or turbulent mixing do not show such a marked difference from the 50 m simulation and this indicates that these processes are less important to resolve fulls and are not the major cause of the resolution dependence. The ice growth and sedimentation processes are most important together with resolving the vertical structure of the temperature (and therefore cloud) within the model grid level; these processes are the focus of the rest of this chapter.

5.4 Correcting for resolution dependence

The sensitivity of EMPIRE to vertical resolution is caused by processes changing their behaviour with changing vertical resolution. The processes which are most important in this change are the ice sedimentation and ice growth by deposition. It is also important to represent the vertical structure of temperature at the cloud top so as to correctly identify when part of a model layer is liquid saturated even though the grid-box mean mixing ratio and temperature suggest the layer is below saturation.

These three important processes all show such a dependence because there is no sub-grid structure within the model layer. All current numerical models assume that the grid-box mean values are representative of the depth of that model level. Whilst there have been attempts to address the horizontal variability within a grid-box, for instance the Smith (1990) cloud scheme, currently no information about the vertical structure is included in the models.

When the process rates are calculated using information about the vertical profile of the quantities (as in the high resolution simulation) then the depositional growth rate is reduced and the sedimentation rate is increased, on average. In addition, the liquid water content diagnosed by the model increases as the model resolution becomes finer. If the sub-grid vertical profile of these quantities can be accurately described in the coarse resolution models and these profiles used to calculate the process rates then this may allow mixed-phase clouds to be more accurately modelled in coarse resolution models.

5.4.1 Vertical structure of mixed-phase clouds

The vertical structure of mixed-phase clouds can be assessed from various sources to understand how to implement a sub-grid vertical profile in low resolution models. Vertical profile data from the top of mixed-phase clouds has been combined from various sources including high resolution EMPIRE model simulations, other modelling simulations, radiosonde soundings, aircraft observations and remote sensing observations.

High resolution EMPIRE simulations show that the cloud top is very turbulent and as a result of this turbulent mixing, the mean profiles of potential temperature and of total water mixing ratio are well mixed. This is backed up by radiosonde observations which show well mixed layers beneath mid-level liquid saturated layers. Additionally, aircraft observations (e.g. Fleishauer et al., 2002) show that the profile of liquid water content is nearly adiabatic, as would be expected with a well-mixed layer. Knowing that both θ_l and q_t are well-mixed then the profile of temperature, supersaturation, liquid water content and cloud fraction can all be calculated. The profile of ice water content is more difficult to define precisely and there are very few reliable observations of ice water content near the top of mixed-phase clouds. Observations of ice at the top of mixed-phase clouds from aircraft observations (e.g. Fleishauer et al., 2002; Carey et al., 2008; Lawson

and Zuidema, 2009) show ice water content increasing with distance down from cloud top, although often this is based on only a small number of highly averaged data points in the vertical or on a very noisy profile of ice water content. This pattern is supported by modelling studies using large eddy simulations (LES, Smith et al., 2009) and single-column models and cloud resolving models (Klein et al., 2009) and for a number of different particle habits (Avramov and Harrington, 2010). The shape of the vertical profile of ice at cloud top is very variable from cloud to cloud but simulations by Smith et al. (2009) and EMPIRE give high enough resolution to suggest an approximately linear increase from cloud top, which does not disagree with the other observed and simulated profiles.

5.4.2 Parameterization of sub-grid vertical structure

5.4.2.1 Fundamental assumptions

The parameterization to correct for the resolution dependence is designed such that it can be applied to the top grid-level of a mixed-phase cloud layer. The following assumptions are made:

1. The grid level is well mixed in the conserved prognostic variables θ_l and q_t.
2. The ice water mixing ratio (q_i) increases linearly from 0 at the cloud top to twice the layer mean value at the base of the model layer.
3. Except for liquid water content and cloud fraction, other derived variables are a linear function of height.

This parameterization is only applied to the uppermost grid-level in a cloud layer that contains non-zero values for both q_l and q_i. In most cases this is sufficient to cover the depth of the well-mixed and liquid-saturated layer when applied at resolutions typical of GCM mid-troposphere.

5.4.2.2 Correcting ice growth rate

The model equation to calculate the depositional growth of ice is given earlier in equation 5.1, where all the quantities are assumed to be constant with height within a grid-box. An attempt to

correct for this is made by assuming a vertical profile for horizontally averaged SS_i and q_i (see figure 5.6). Whilst the temperature also changes with height, and will affect A, B, T and ρ, the fractional changes in these terms are much smaller than for SS_i and q_i. This allows us to simplify this equation to

$$\frac{dq_i}{dt} = \alpha SS_i q_i^{\frac{2}{b+1}}, \tag{5.3}$$

where

$$\alpha = \frac{2\pi}{A+B}\left(\frac{N_0 \exp(-0.1222T)}{\rho}\right)^{1-\frac{2}{b+1}}\left(\frac{1}{a\Gamma(b+1)}\right)^{\frac{2}{b+1}} \tag{5.4}$$

is constant with height under our assumption. If all terms in equation 5.3 are constant with height, with a value equal to their grid-box mean (denoted by an overbar), then the calculated growth rate is

$$\frac{d\hat{q}_i}{dt} = \alpha \overline{SS_i}\,\overline{q_i}^{\frac{2}{b+1}}, \tag{5.5}$$

However, the profiles of ice water mixing ratio and supersaturation can be defined to improve our estimate of the growth rate:

$$q_i = \frac{2z}{\Delta z}\overline{q_i}, \tag{5.6}$$

$$SS_i = \frac{\Delta z - 2z}{\Delta z}\,\Delta SS_i + \overline{SS_i}, \tag{5.7}$$

where

$$\Delta SS_i = (SS_i)_{\text{top}} - (SS_i)_{\text{base}} \tag{5.8}$$

is the difference between the supersaturation at the top and base of the grid-box. In these equations z is the distance below cloud top and Δz is the depth of the grid-box in which the parameterization is being applied. From figure 5.6c, the SS_i profile changes from near constant close to the cloud top to a linear decrease in the lower part of the layer. The height below cloud top, z_m at which this changes is calculated as

$$z_m = \Delta z \frac{\overline{SS_i} + 0.5\Delta SS_i - (SS_i)_{\text{a}}}{\Delta SS_i} \tag{5.9}$$

where $(SS_i)_{\text{a}}$ is the supersaturation between z_m and the cloud top, calculated as

$$(SS_i)_{\text{a}} = \frac{q_{sl}}{q_{si}} + (1 - RH_{\text{crit}}) \tag{5.10}$$

Rewriting equation 5.7 and accounting for a different profile in the cloud top region where the air is at liquid saturation gives:

$$SS_i = \begin{cases} \left[\frac{\Delta z - 2z}{\Delta z}\beta + 1\right]\overline{SS_i} & \text{if } z \geq z_m \\ \gamma\overline{SS_i} & \text{if } z < z_m \end{cases} \tag{5.11}$$

where

$$\beta = \frac{\Delta SS_i}{\overline{SS_i}} \quad \text{if } \overline{SS_i} \neq 0, \tag{5.12}$$

and

$$\gamma = \frac{(SS_i)_a}{\overline{SS_i}} \quad \text{if } \overline{SS_i} \neq 0. \tag{5.13}$$

The parameterized profiles of q_i and SS_i are shown earlier in figure 5.6a) and c) respectively. Also plotted are data points from the 50 metre simulation, which show a good agreement between the high resolution data and the parameterized profiles.

The strength of parameterizing q_i and SS_i as multiples of $\overline{q_i}$ and $\overline{SS_i}$ is that later the correct growth rate can be calculated from the standard calculated growth rate by a simple multiplicative factor. A problem is encountered if SS_i is zero, however, this is not able to happen in a grid-box which is liquid saturated at the top unless the vertical resolution is extremely coarse and in this case the calculated grid-box mean growth rate would be zero.
The mean ice growth rate in this grid-box can be calculated by integrating equation 5.3 over the depth of the grid-box using profiles of q_i and SS_i from equations 5.6 and 5.11 respectively. As α is assumed to be constant with height, this can be written as

$$\overline{\frac{dq_i}{dt}} = \frac{\alpha}{\Delta z}\int_0^{\Delta z} SS_i q_i^{\frac{2}{b+1}}\, dz. \tag{5.14}$$

$$\overline{\frac{dq_i}{dt}} = \frac{\alpha}{\Delta z}\left(\int_0^{z_m} SS_i q_i^{\frac{2}{b+1}}\, dz + \int_{z_m}^{\Delta z} SS_i q_i^{\frac{2}{b+1}}\, dz\right). \tag{5.15}$$

$$\overline{\frac{dq_i}{dt}} = \frac{\alpha}{\Delta z}\left\{\int_0^{z_m} \gamma\overline{SS_i}\left(\frac{2z}{\Delta z}\overline{q_i}\right)^{\frac{2}{b+1}} dz + \int_{z_m}^{\Delta z}\left[\frac{\Delta z - 2z}{\Delta z}\beta + 1\right]\overline{SS_i}\left(\frac{2z}{\Delta z}\overline{q_i}\right)^{\frac{2}{b+1}} dz\right\}. \tag{5.16}$$

$$\overline{\frac{dq_i}{dt}} = \frac{\alpha}{\Delta z}\overline{SS_i}\,\overline{q_i}^{\frac{2}{b+1}}\left\{\int_0^{z_m} \gamma\left(\frac{2z}{\Delta z}\right)^{\frac{2}{b+1}} dz + \int_{z_m}^{\Delta z}\left[\frac{\Delta z - 2z}{\Delta z}\beta + 1\right]\left(\frac{2z}{\Delta z}\right)^{\frac{2}{b+1}} dz\right\}. \tag{5.17}$$

After integrating and simplifying terms, this leaves a relatively simple expression

$$\overline{\frac{dq_i}{dt}} = 2^{\frac{b}{b+1}}\left[\frac{b+1}{2b+1}\left((1+\beta-\gamma)\left(1-\frac{z_m}{\Delta z}^{\frac{2b+1}{b+1}}\right)+\gamma\right)+\beta\frac{2b+2}{3b+2}\left(\frac{z_m}{\Delta z}^{\frac{3b+2}{b+1}}-1\right)\right]\frac{d\hat{q}_i}{dt} \quad , \tag{5.18}$$

where $\frac{d\hat{q}_i}{dt}$ is the growth rate calculated by equation 5.5. As the parameterized growth rate is related to the regular growth rate by a factor, this allows us to correct the timestep change in ice mixing ratio by multiplying by this factor.

5.4.2.3 Correcting ice sedimentation rate

The calculation of the rate of change of ice mixing ratio due to sedimentation requires the fluxes of ice both into and out of the layer. These fluxes require values of q_i, and the mass weighted fall velocity at the interface between grid-boxes. It is common in simple numerical schemes to assume that the values at the edges of the grid-box are the grid-box mean values. This is how ice sedimentation in the Met Office Unified Model is calculated but as noted earlier this assumption does not hold near the top of mixed-phase clouds. More advanced (2nd order) schemes interpolate between the values in two grid-boxes to give the appropriate values at the interface. This gives a more accurate estimate of the flux through the bottom of the grid-box, especially where the linear increase of ice water content with depth down from cloud top continues through the top few grid-boxes. However, the depth of the layer over which the ice increases linearly is often 500 metres or less and therefore in coarse resolution models the grid-box mean values may not increase linearly with depth and the flux out of the uppermost model layer may also be underestimated by a 2nd order scheme. In some circumstances the 2nd highest cloudy model level may have a very little ice water content, particularly soon after cloud formation or if that model level is particularly dry and this may give a lower flux of ice than a simple upwind scheme. In order to give an accurate representation of the flux of ice from the uppermost cloudy grid-box the value of ice water content at the base of the layer is fixed at twice the grid-box mean quantity and the mass weighted fall velocity is calculated using this ice water content. This is the same as a 2nd order scheme would do if the increasing ice water content with depth continues beyond the uppermost grid-box but ensures the correct sedimentation of ice from the layer if the lower grid-box has a lower ice water content.

The rate of ice loss from a grid-box due to sedimentation can change by almost a factor of two when the sub-grid distribution of ice is considered. As the ice water mixing ratio is parameterized to increase linearly from cloud top through the uppermost grid-box, the ice water mixing ratio at the base of this grid-box is twice the mean value. This affects the sedimentation rate in two ways: firstly the amount at the base of the grid-box is increased by a factor of two and secondly the mean fall speed of the ice particles is increased. These two factors are easily accounted for using the existing calculation for the ice sedimentation rate by increasing the fall speed to account for

this. The equation for calculating the mean fall speed is

$$v = \frac{c\Gamma(b+d+1)\rho^{-0.4}}{\Gamma(b+1)\left(\frac{(aN_0\Gamma(b+1)e^{-0.1222T})}{\mathrm{IWC}}\right)^{\frac{d}{b+1}}} \tag{5.19}$$

so by increasing IWC to $2 \times$ IWC the correct mean fall speed for the ice water content found at the bottom of the grid-box can be calculated. Having corrected the fall speed, the factor of approximately 2 difference between the mean ice water mixing ratio and the value at the bottom of the model layer needs to be accounted for. The simplest way to add this effect is to increase the fall speed again such that the flux through the bottom of the grid-box is correct when using the grid-box mean ice mixing ratio. To do this the fall speed is increased by a factor,

$$\text{Correction Factor} = 2 - \frac{v\Delta t}{\Delta z}. \tag{5.20}$$

This correction factor includes the factor of 2 increase at the bottom of the grid-box but also accounts for the decrease of ice mixing ratio above this and therefore reduces the correction factor by the fraction of the grid-box from which ice can fall to the grid-box beneath in a single timestep.

5.4.2.4 Representing liquid cloud structure

Unlike the ice water content and supersaturation discussed so far in this chapter, the liquid water content and cloud fraction are not important for the calculation of any process rates, rather they are needed to calculate the grid-box mean correctly when only part of the layer contains liquid water. To represent the sub-grid vertical structure of the cloud, the assumption that the layer is well-mixed is used. This means that θ_l and q_t are constant with height and T decreases approximately linearly with increasing height. If it is assumed that the cloud is adiabatic and that the liquid water content linearly decreases from cloud top then the total liquid water content within the grid-box could be easily calculated. However, the inclusion of a cloud fraction scheme complicates this because nearer the cloud top there is both an increased (in-cloud) liquid water content and increased cloud fraction. Therefore, to correctly calculate the profile of liquid water use of the cloud scheme is required. EMPIRE uses the simple Smith (1990) cloud scheme as explained in chapter 2. It is fortunate that the Q_N (the grid-box mean saturation with respect to liquid normalised by the standard deviation of q_t within that grid-box) in this cloud scheme used to

calculate both liquid water content and cloud fraction is a linear function of height in a well-mixed layer. Q_N is defined as

$$Q_N = \frac{q_t - q_{sl}}{\sigma_s}, \tag{5.21}$$

where σ_s is the sub-grid standard deviation of q_t, defined as

$$\sigma_s = \frac{(1 - \mathrm{RH}_{\mathrm{crit}})\, q_{sl}}{\sqrt{6}}. \tag{5.22}$$

The values of Q_N can easily be calculated at the top and bottom of the grid-layer and therefore construct the function throughout the grid-box. Smith (1990) describes how the liquid water mixing ratio (q_l) and cloud fraction (CF) are a function of Q_N

$$\frac{q_l}{\sigma_s} = \begin{cases} 0 & \\ \frac{1}{\sqrt{6}}\left(1 + \frac{Q_N}{\sqrt{6}}\right)^3 & \\ Q_N + \frac{1}{\sqrt{6}}\left(1 - \frac{Q_N}{\sqrt{6}}\right)^3 & \\ Q_N & \end{cases} \qquad CF = \begin{cases} 0 & Q_N \le -\sqrt{6} \\ \frac{1}{2}\left(1 + \frac{Q_N}{\sqrt{6}}\right)^2 & -\sqrt{6} < Q_N \le 0 \\ 1 - \frac{1}{2}\left(1 - \frac{Q_N}{\sqrt{6}}\right)^2 & 0 < Q_N < \sqrt{6} \\ 1 & \sqrt{6} \le Q_N \end{cases} \tag{5.23}$$

Using this relationship it is then possible to calculate the amount of liquid water within the grid-box and the correct grid-box mean liquid water content and similarly for cloud fraction.

5.5 Testing the parameterization

5.5.1 Idealised simulation

Applying the parameterization to the low resolution model allows us to see how much of an improvement it provides. First, its performance is checked in the 500 metre resolution simulation in which the resolution dependence was initially noticed. Figure 5.9 shows the 500 metre simulation with the parameterization and the 50 metre simulations without the parameterization included. The parameterization clearly increases the liquid water content and the duration of the liquid cloud. The total liquid water content has not increased to match that of the 50 metre simulation, but is a large improvement on the unmodified 500 metre simulation. The parameterization is not expected to fully correct the low resolution simulation as it does not attempt to correct for all of the resolution dependent processes, but just the main three. The small changes in the radiation

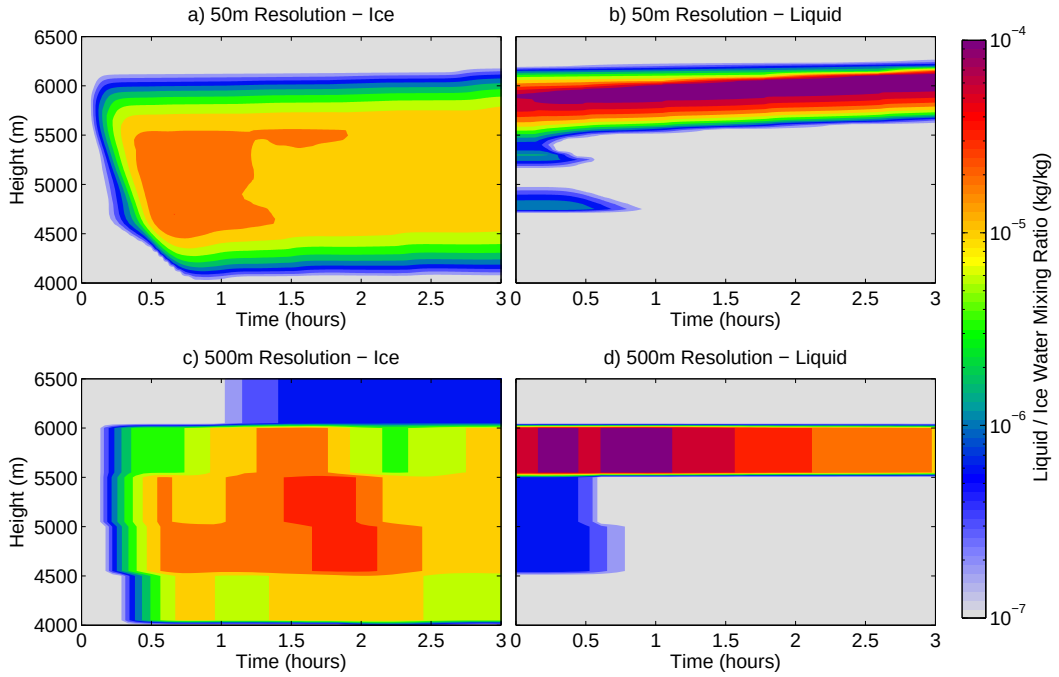

Figure 5.9 Same as figure 5.2 but 500 m resolution simulation includes the parameterization of the sub-grid vertical structure. Ice water mixing ratio is shown in the left hand panel and liquid water mixing ratio in the right hand panel. The colour bar is applicable to both liquid and ice.

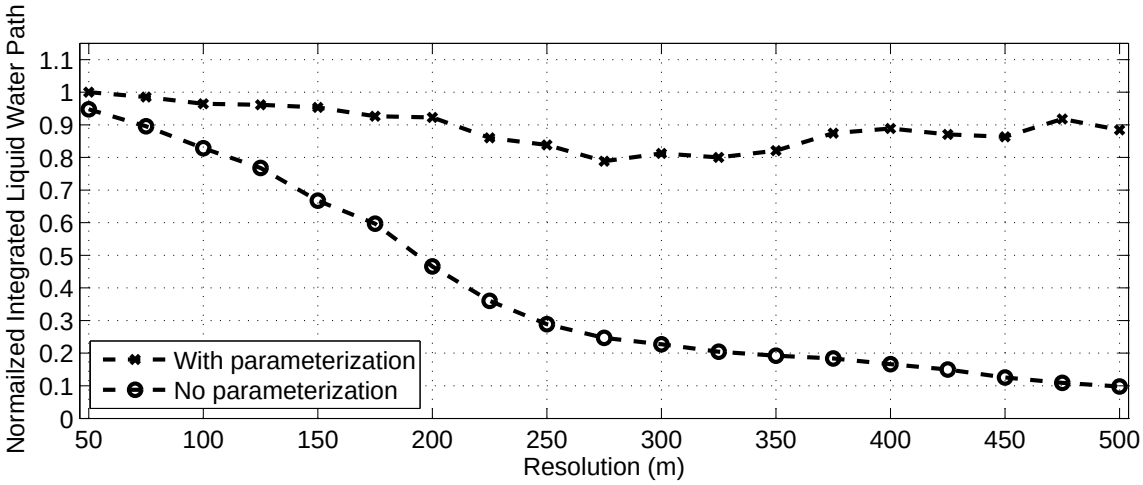

Figure 5.10 Normalised Integrated Liquid Water Path (NILWP) from idealised simulations with no radiation or turbulent mixing, with and without the vertical resolution parameterization. The NILWP is normalised such that the simulation with the parameterization and a resolution of 50 metres gives a value of 1. The NILWP in simulations with the parameterization included are larger than without it and are nearly constant across a large range of resolutions.

and turbulent mixing processes with resolution are preventing the liquid water content reaching the values from the 50 metre simulation.

To check that the parameterization is working correctly, EMPIRE is run with the radiation and turbulent mixing processes turned off. Figure 5.10 shows the normalised integrated liquid water path from simulations with and without the resolution parameterization. The simulations with the parameterization included do not show the same decline in NILWP with resolution as the simulations without the parameterization do. The NILWP values are nearly constant with resolution up to resolutions of about 200 metres.

Figure 5.11 shows the liquid water path at hourly intervals for the first 6 hours of the idealised simulation with and without the resolution parameterization. Again it is noted that the simulations with the parameterization included has an almost constant liquid water path at each time interval, regardless of model resolution. In comparison, the standard simulation initially show a gradual decrease in liquid water path with increasing resolution. This decrease becomes more marked as the simulation evolves, with the coarsest resolutions becoming completely glaciated. These parameters can also be assessed for the model including the full physics. The NILWP in this case (figure 5.12) shows a decrease with increasing resolution for simulations both with and without the parameterization. However, for a given resolution the liquid water path is much higher if the parameterization is active and the resolution required to achieve a fixed value of liquid water path is coarser and therefore may be more attainable in GCMs. This suggests that this parameterization should enable GCMs to capture long lived mixed-phase clouds in their current setup. Obviously there is still a resolution dependence shown, even with the parameterization, as the effects of the radiation and turbulent mixing processes changing with resolution are not accounted for. Nevertheless, the improvements can clearly be seen in figure 5.13 where the liquid water path is maintained at substantial levels in simulations where the parameterization is included as opposed to those without it, particularly for the coarsest resolutions. This improvement in the liquid characteristics of the cloud should have a substantial impact on the radiative properties of the cloud.

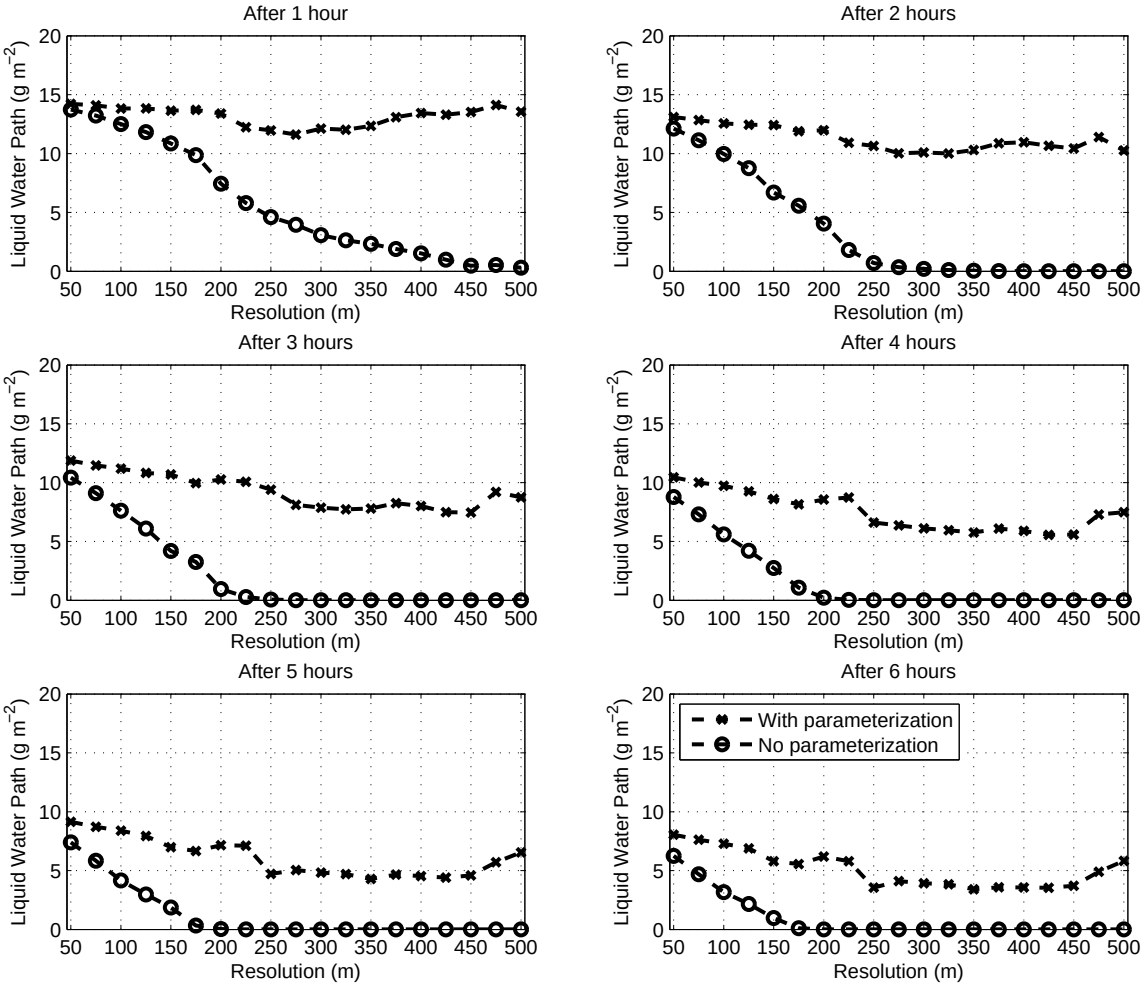

Figure 5.11 Liquid Water Path from idealised simulations with no radiation or turbulent mixing, with and without the vertical resolution parameterization plotted at hourly intervals.

5.5.2 Testing over many cases

To understand the potential impact this parameterization may have if it were included in GCMs, EMPIRE is run over the cases from chapter 4 at 500 metre resolution with the parameterization active. This is then compared with the 50 m resolution simulations and 500 m resolution simulations without the parameterization. Figure 5.14 shows water contents and cloud fraction for both liquid and ice as a function of temperature for the three sets of simulations. As found before there is a large difference in the liquid water content and cloud fraction between the 50 metre and 500 metre simulations. Panel a shows that with the parameterization included in the low resolution simulation, the mean liquid water mixing ratio increases to near that of the high resolution sim-

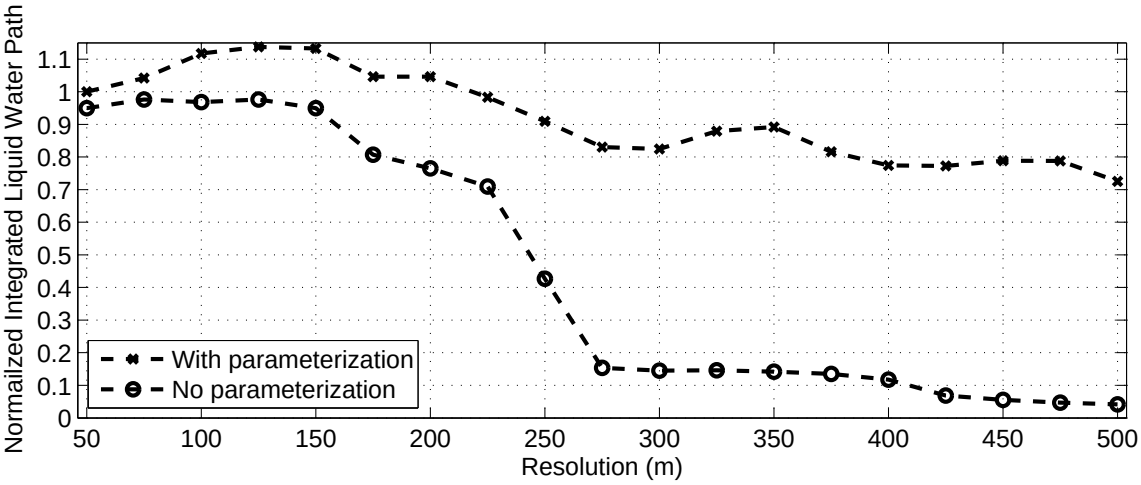

Figure 5.12 Normalised Integrated Liquid Water Path (NILWP) from idealised simulations with full model physics including radiation and turbulent mixing, with and without the vertical resolution parameterization. The NILWP normalised such that the simulation with the parameterization and resolution of 50 metres gives a value of 1. Again, the NILWP is larger when the parameterization is included and more constant across a large range of resolutions.

ulation. Between temperatures of -15 and -25°C this represents a correction of two orders of magnitude. However, the simulation including the parameterization only has 21% of the water in the high resolution control simulation between -10 and -30°C largely due to the lack of liquid clouds at temperatures colder than -20°C which may be because EMPIRE fails to bring air close enough to saturation to form clouds initially, so the parameterization has no chance to make a difference. The liquid cloud fraction (panel b) correction is similar for temperatures colder than -15 $^{\circ}$C but warmer than this the parameterization produces an increased cloud fraction. The ice cloud properties are nearly unchanged by the parameterization; this is a sign that the ice water content and cloud fraction at the top of mixed-phase clouds represent only a small part of the ice cloud layer as a whole. Overall this parameterization produces a marked improvement in the properties of liquid water clouds simulated by the coarse resolution model and produces mean liquid water contents and cloud fractions similar to those produced by higher resolution models. This adds further weight to the argument that the inclusion of this parameterization in low resolution GCMs would significantly improve their representation of mixed-phase clouds.

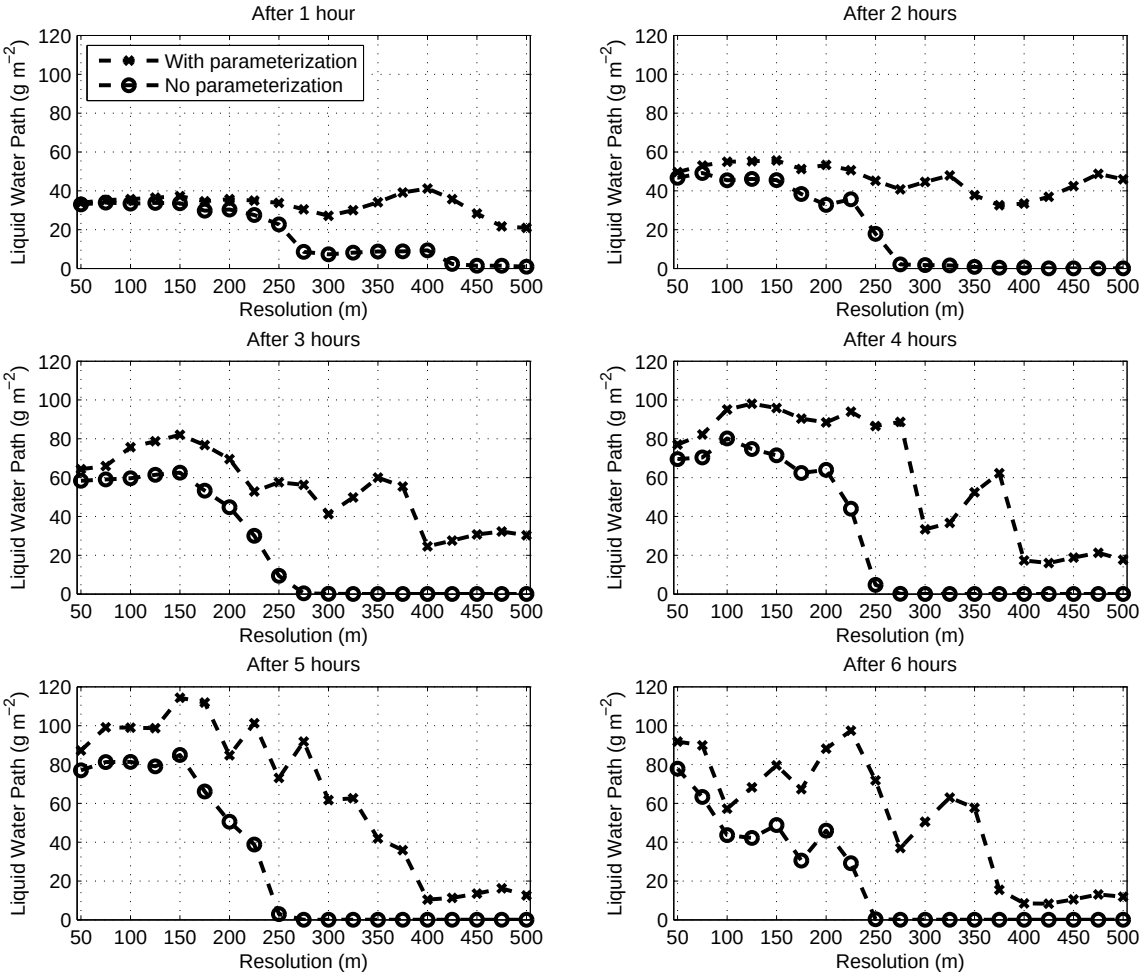

Figure 5.13 Liquid Water Path from idealised simulations with full model physics including radiation and turbulent mixing, with and without the vertical resolution parameterization plotted at hourly intervals.

5.6 Conclusions

In this chapter the vertical resolution dependence in EMPIRE has been explored and is discovered to be having a large effect on the simulations in chapter 4. The difference in simulations becomes particularly noticeable where vertical grid spacing is greater than 200 metres and the difference becomes larger as the resolution becomes coarser.

A number of reasons why this resolution dependence is present were explored, and whilst they all are having some effect on the simulations, the largest sources of error come from the ice growth and sedimentation processes and the failure of the coarse model to resolve the vertical

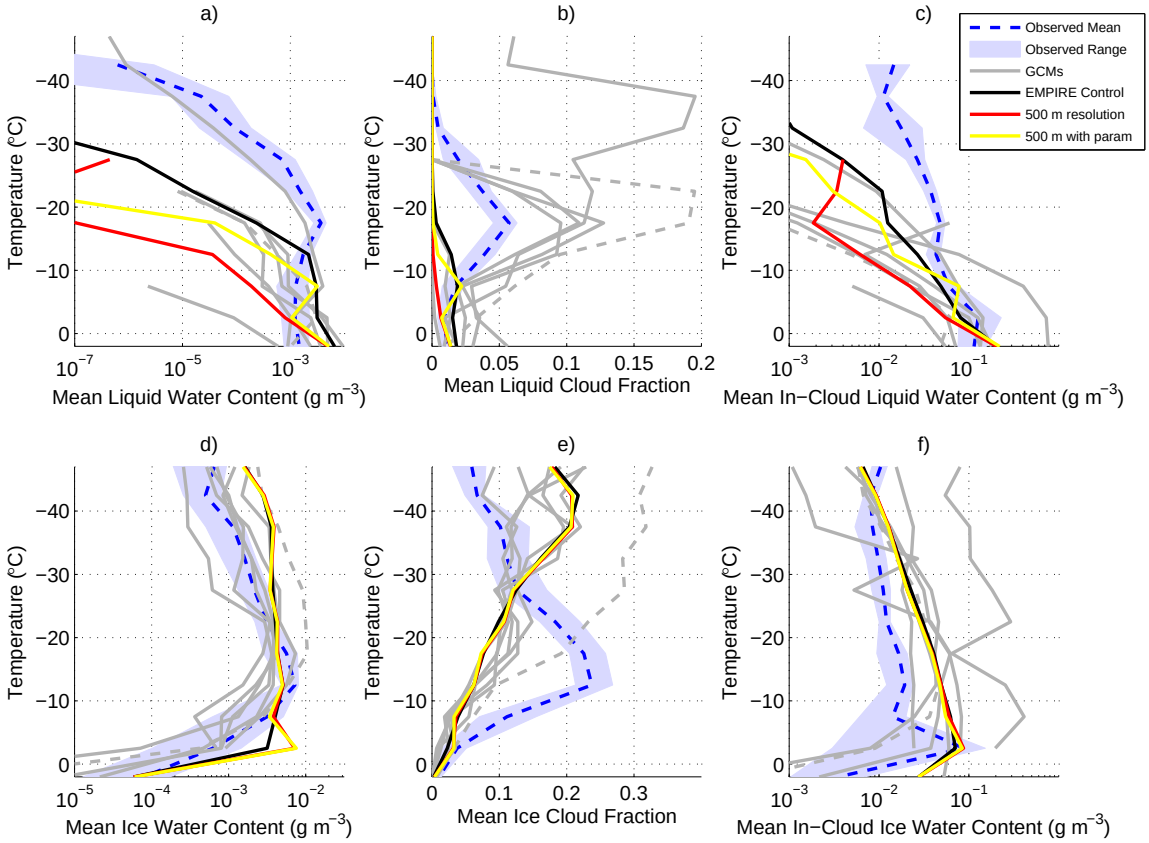

Figure 5.14 As figure 4.1, showing liquid and ice water contents and cloud fractions from EMPIRE experiments where the vertical resolution specification has been changed. The experiments are: (black) 50 metre vertical resolution, (red) 500 metre vertical resolution and (yellow) 500 metre vertical resolution with the sub-grid parameterization of cloud vertical structure active in the uppermost mixed-phase model level.

structure of the liquid and ice water contents within a grid-box.

A relatively simple, physically based parameterization to correct for this resolution dependence has shown some very encouraging results. The normalised integrated liquid water path is shown to be more nearly constant with resolution in simulations that include the parameterization. This is most true for model simulations that do not include radiation and turbulent mixing processes because the resolution dependent processes remaining in the model have all been corrected for. In the full physics model simulations the correction is not as large as in the simulations with no radiation or turbulent mixing. This is because these resolution dependent processes are included in the model but their resolution dependence is not corrected for.

The parameterization can increase the liquid water path by many orders of magnitude in the

coarsest models which will have a profound effect on the radiative properties of the modelled mixed-phase clouds. This suggests that were this parameterization to be included in GCMs it may substantially affect the radiation balance of the model.

CHAPTER 6:

CONCLUSIONS AND FUTURE WORK

This thesis has attempted to answer the question "Why can't models simulate mixed-phase clouds correctly?". The aim was to quantify, understand and attempt to fix the poor representation of mixed-phase clouds in operational NWP models. This has been achieved by careful analysis of observations and models to determine the degree to which mixed-phase clouds are misrepresented by models and using a new single column model (EMPIRE) to determine the model processes important to maintain mixed-phase clouds. Amongst many sensitivities the analysis highlighted a particularly strong sensitivity to the model vertical resolution hindering the performance of NWP models and attempts to understand and correct for this are made in chapter 5. The main reasons models are unable to correctly simulate mixed-phase clouds are:

1. Models with a temperature dependent split of cloud condensate into liquid and ice are unable to represent the vertical structure of mixed-phase clouds, as reported by Marsham et al. (2006). However, models with more advanced microphysics schemes containing a separate prognostic variable for ice and physically based parameterizations of the conversion of liquid to ice perform worse than models with a single variable for both ice and liquid condensate.

2. The conversion from cloud liquid to cloud ice is too rapid. This may be as a result of an error in one of the many microphysical parameterizations that exhibit a significant sensitivity (e.g. ice particle growth rate, fall velocity, number concentration, habit).

3. The parameterized ice growth rate is too large in grid-boxes with low ice water contents. This is due to the steepness of the ice particle size distribution, giving a larger number of particles that observed and acting as a too rapid sink of liquid.

4. A strong sensitivity to the model vertical resolution artificially increases the growth rate of ice particles near cloud top which further exacerbates the problem of rapid ice growth.

6.1 Summary of results

Careful comparison of the models with observations was performed ensuring that the horizontal and vertical resolution are the same and that model clouds are sampled in the same way as observed clouds through the use of forward models. After selecting 21 days based on the presence of mixed-phase clouds that are well observed by ground based remote sensors, comparisons with models revealed a systematic underestimate of supercooled liquid water content for all models at temperatures below -10 °C with all models underestimating the liquid water content at temperatures between -10 °C and -30 °C by a factor of 2 or more. The two models with the largest underestimate of supercooled liquid water content were the two versions of the Met Office Unified Model with the higher resolution mesoscale version having no liquid at temperatures below -10 °C on the days analysed. This is of particular interest as these are the only two models studied where the ice water content is a prognostic variable separate from liquid and therefore calculates the growth of ice (and therefore the depletion of liquid) explicitly using a series of physically based parameterizations. In agreement with previous studies (Vaillancourt et al., 2003) the ice water content is better predicted by models than the liquid water content with the model mean ranging from 57–104% of the observed mean. Despite this, the predicted ice cloud fraction is underestimated by all models for temperatures warmer than -20 °C and most notably the observed peak of 23.4% at -12 °C is not seen in models where the ice cloud fraction is only 5.5–9.5%. A new cloud fraction parameterization was developed based on 2 years of radar observations of clouds which largely removed this bias in EMPIRE and could be easily implemented in GCMs in place of the current erroneous one.

As has been identified before, the observed structure of mixed-phase clouds with a layer of liquid water above a thicker ice layer cannot be represented correctly by models that use temperature alone to determine the ratio of liquid and ice condensate in the cloud (Marsham et al., 2006). This is demonstrated in chapter 3 where the only models able to correctly simulate mean structure of observed mixed-phase clouds, with the larger liquid water contents at cloud top, were the two versions of the Unified Model which both include a separate prognostic variable for ice. The Unified Model better represents the structure, but as noted above the mean supercooled liquid water content is significantly underestimated in both these models. As a result of the errors in these two types of models the radiation calculations are incorrect. Calculations using the Edwards

and Slingo (1996) radiation scheme showed that the observed mixed-phase clouds had a cooling effect on the climate system, in agreement with Hogan et al. (2003a), with a mean cloud radiative forcing of -8.14 W m^{-2}. However, when the phase of the cloud condensate is calculated as a function of temperature using the same relationship as the ECMWF model then the mixed-phase clouds cause a warming, of 1.79 W m^{-2} on average, although the effect of clouds outside this temperature range was strong enough that the total cloud radiative forcing was negative. This warming effect was increased further if all liquid was converted to ice, as may be the case in the Unified Model, with the mean cloud radiative forcing from clouds between 0 and -40 °C being a warming of 2.42 W m^{-2}. In practice, the Unified Model would not produce as much ice as observed if the liquid did not exist and the estimated warming effect is an overestimate as a result.

To determine the reasons for the significant underestimate of supercooled liquid water in predictions made by most NWP models, a single column model (EMPIRE) was created based around the Unified Model but with the option to include additional processes, run at higher resolution and alter physical parameterizations. When tested, EMPIRE compared well with observations of the time evolution of mixed-phase clouds and with the physical process rates of large-eddy simulations of mixed-phase clouds. This model was then used to assess which of the physical processes are most important in maintaining mixed-phase clouds. Changes to any process or parameterization that affected the rate at which ice grows by vapour deposition or the speed at which it falls from the cloud strongly affects the amount of supercooled liquid water in the simulations. The most sensitive parameter in the model was the ice particle size distribution intercept parameter (N_0); by reducing this by a factor of 10 the mean liquid water content in the simulations increased by 174% and the ice water content reduced by 31%. The large sensitivity arises because it changes the relative number of smaller and larger ice particles affecting both the total growth rate and mean fall speed of the ice particles within a grid-box. It is also notable that changing the growth rate of ice particles can have a large impact of the mean amount of liquid water but leaves the mean ice water content almost unchanged. Therefore it is possible to adjust the growth rate to improve the representation of supercooled liquid water in the simulations without having an adverse affect on the simulated ice water contents.

Due to the large sensitivity to the ice particle size distribution intercept parameter, an attempt to evaluate the Unified Model value against observations was made. Comparing with aircraft ob-

servations of ice particle size distributions revealed that, for a given ice water content, the Unified Model produces ice that both grows too quickly (by up to a factor of 2.5) and falls too slowly (by as much as 50%) and that these biases are worst for small ice water contents, those that are typically found in mixed-phase clouds. These biases in growth rate and fall speed were removed by adjusting N_0 to be a function of ice water content as well as temperature and simulations using this adjusted N_0 increased the supercooled liquid water content by 189% and ice water content by 8%. This has implications beyond the Unified Model for all models with a separate prognostic variable for ice. Both the Deutscher Wetterdienst (DWD) LME model and the latest ECMWF model have a separate prognostic for ice. The DWD-LME model has a lower, fixed value of N_0 (4×10^5) than the Unified Model ($2 \times 10^6 \exp(-0.1222T)$) which will result in a slower growth rate of ice particles and a faster fall velocity, in better agreement with observations and may be related to the fact that this is the only model not to underestimate the mid-level cloud fraction in the study of Illingworth et al. (2007). The ECMWF model ice microphysics is based on Rotstayn et al. (2000) and has ice particles that are all the same size within a grid-box and is therefore not obvious whether this will suffer from the same biases, although the model initially suffered a significant underestimate of supercooled liquid water content (Richard Forbes, personal communication).

Another important factor is the value of $\mathrm{RH}_{\mathrm{crit}}$ used in the cloud scheme, representing the degree of variability of the specific humidity within a grid-box. Increasing the grid-box mean relative humidity required to form cloud makes it more difficult for the model to form cloud, but when the model is able to form cloud the associated liquid water content and cloud fraction were higher, resulting in longer lived mixed-phase clouds that form less often and on average resulting in more supercooled liquid water in the simulations.

It was striking that the ice cloud fraction predicted by all of the models, including EMPIRE, fell well outside the range of the observed ice cloud fraction. In particular the observed peak in ice cloud fraction at around -12 °C was not captured by any model and the multi-model average predicted only 31% of the observed ice cloud fraction at this temperature. The models all agreed with each other quite strongly in both the amount of ice cloud fraction and the relationship with temperature, both of which were notably different from the observations suggesting a systematic bias in all models. Using the radar observations from Chilbolton it was possible to define a relationship between grid-box mean ice water content and ice cloud fraction, and whilst the cloud

fraction for individual grid-boxes is highly variable for constant ice water content, the mean cloud fraction for each ice water content range calculated does not change with temperature. Applying this relationship to the GCM model output notably improved the representation of ice cloud fraction in the models when compared to observations, with the multi-model mean increasing to 71% of the observations. The improvement was most notable for the Unified Model where the ice cloud fraction is already a function of ice water content with this relationship increasing the cloud fraction by 219% for the mesoscale model and 287% for the global model. The addition of this relationship to EMPIRE showed a similarly large improvement in the representation of ice cloud fraction and additionally an increase in the mean supercooled liquid water content.

By changing a number of parameterizations within EMPIRE such that they are all more favourable for the formation and maintainence of supercooled liquid water the mean liquid water content in the simulated cases exceeds or matches the observed liquid through the whole mixed-phase temperature range analysed. This shows that there is scope for the models to produce mixed-phase clouds with sufficient liquid water without the need for prognostic ice nuclei that would be depleted and therefore limiting the ice nucleation (and growth) rate. However, the values chosen in these parameterizations are all towards the extreme end of the observed uncertainty and it is unlikely that all of these parameterizations are incorrect by this degree generally, although there may be specific cases where mixed-phase clouds are not adequately represented by the general parameterization used in GCMs.

Lastly, the large resolution sensitivity of EMPIRE was investigated. Model simulations with 500 metre resolution contained less than 2% of the liquid water content present in the 50 metre simulations at temperatures between -10 °C and -30 °C. It is concerning that with EMPIRE having a vertical resolution of 500 metres, similar to that of GCMs, the liquid water content of mixed-phase clouds is so vastly underestimated. The reason for the underestimate is that the vertical structure of the cloud in the region near the cloud top is not resolved and therefore not only is the liquid water profile not correctly predicted, but also the growth rate of ice is overpredicted and the rate of sedimentation out of the grid-box to the grid-box below is underpredicted (particularly with simplistic 1st order upwind schemes but also with more sophisticated schemes such as the TVD scheme used in EMPIRE). This resolution dependence can be corrected for by the inclusion of a parameterization of the sub-grid vertical structure of the cloud top. The profiles of ice water

content and supersaturation are modelled based on a combination of observations and high resolution simulations using EMPIRE. With the parameterization included the resolution dependence of the model is reduced and coarse resolution models at 500 metre grid-spacing can simulate long lived mixed-phase clouds.

Having identified a number of reasons why operational models are unable to simulate mixed-phase clouds correctly and suggested corrections or improvements to a number of problems then there is scope for improving the representation of mixed-phase clouds in GCMs as per the aims of this thesis. The sensitivity to resolution is likely the most significant reason models are underestimating the supercooled liquid water content with current GCM mid-troposphere resolutions towards the coarsest end of our sensitivity tests, although other problems with too rapid glaciation of clouds also exist. By implementing the improvements to these problems, models will be better able to predict mixed-phase clouds and their important radiative impact which should benefit both numerical weather and climate prediction.

6.2 Future Work

Whilst the differences between model simulations and observations of liquid and ice water contents and cloud fractions is large, it is only based on 21 days of data due to the restriction of days chosen having good observations of mixed-phase clouds from ground based sensors. Future work could focus on extending this type of analysis to a larger, more representative dataset. Careful thought would be required to ensure that a fair comparison is made in light of the difficulty in observing mixed-phase clouds from the ground, particularly in the presence of low-level liquid clouds or multiple layers of liquid. One solution would be to use CloudSat and CALIPSO to retrieve properties about mixed-phase clouds from space, which would negate the problem caused by low level liquid water clouds, but a method of determining the liquid water content of the cloud would be required. This would also have the advantage of providing a global perspective rather than just from a single site.

To further test the models, the inclusion of Doppler measurements from both the radar and lidar can be used. This would allow for more rigorous testing of the model parameterizations, for example ice particle fall velocity, than has currently been performed. Assessing the model

representation of fall velocity would allow an assessment of why the model exhibits bias which is not possible by comparing model and observed mean liquid and ice water contents and cloud fraction alone, as has been done here.

The large difference of the model relationship between ice cloud fraction and ice water content, and that derived from radar observations is a concern for models, particularly the Unified Model. By correcting the parameterization the error in predicted ice cloud fraction is significantly reduced suggesting that further work to better understand this is necessary. Initially it would be required to analyse similar observations from other sites, possibly those used as part of Cloudnet or ARM and additionally the use of CloudSat could prove useful for a global perspective. If this relationship is robust across all sites then it could very easily replace the current parameterization of ice cloud fraction in the models and may even remove or reduce the bias in modelled mid-level cloud fraction highlighted by Illingworth et al. (2007). It should be noted that even though the mean ice cloud fraction is well predicted as a function of the ice water content that a very large spread of values for individual clouds exists and that the reason for this is also in need of investigation. Nevertheless, the current parameterization used in the Met Office Unified Model leads to considerable bias in the ice cloud fraction and this could be removed with the use of the new cloud fraction parameterization, even if the cloud to cloud variability still remains undetermined.

Clearly there is a large spread in the possibilities of simulated mixed-phase clouds that are all within the realms of the uncertainties of many microphysical parameters and processes, as explored in chapter 4. It is therefore important that further work to obtain and interpret observations of clouds from both aircraft and remote sensing equipment are conducted. It is also required that further modelling studies are carried out to test our understanding of the microphysical properties and processes within cloud. This is essential if models are to ever simulate clouds realistically enough to simulate future climate accurately. At present the contrasting representation of clouds in different climate simulations is the primary source of inter-model differences in the climate models (Dufresne and Bony, 2008; Andrews et al., 2012).

There is also significant uncertainty in a number of model parameterizations. Some of these processes are better constrained by observations than others and there is promise that future observations will help constrain these further and provide a more general understanding making some parameterizations less location specific. Ice fall velocity and critical relative humidity are

two examples of fairly poorly constrained parameters that there is a large sensitivity to when modelling mixed-phase clouds. Because of this, and in the absence of further observational constraint, it may be useful to parameterize these stochastically. Stochastic parameterizations choose a random number within the range of uncertainty for a model value and apply this for a fixed amount of time before choosing another value, again randomly, although possibly using information about the previous value. This could potentially lead to improved performance of the model by, for example, allowing cloud to form where it would otherwise not have which may then be maintained by radiative cooling. This has already been implemented in some models (e.g. Met Office MOGREPS regional models, Bowler et al., 2008) for some properties such as the convective entrainment rate, RH_{crit} and ice particle fall speed. This could be applied to the RH_{crit} in the cloud scheme as well as the fall speeds, growth rates and other microphysical properties of clouds in EMPIRE to determine the overall effect and potential benefit of such a scheme.

The large sensitivity to the model vertical resolution and the reduction in this sensitivity by including the parameterization described in chapter 5 indicates further work is required on solving this problem in GCMs. The obvious next step would be to apply this resolution parameterization to a GCM and assess the change on a global scale of the predicted mixed-phase clouds and the radiation budget. The direction of the change (to reduce the ice growth rate at the top of the cloud) is the same as that made by Richard Forbes in the ECMWF model, although not based on physical reasoning, and results from his experiments suggested that the global mean surface temperature error is reduced as a result of this change. It may be that further development of the parameterization yields better results — for example a better fit of the ice water content profile with height than the linear one used may improve the calculation of the growth rate and yield better results.

Given the significant deficiencies identified in this thesis of the simulation of mixed-phase clouds by operational numerical models then the implementation of changes leading to an improved simulation is a must together with additional work to better constrain microphysical parameterizations and further improve the physical representation of mixed-phase clouds. This is particularly important given their potentially large radiative impact which is likely to be lacking from many operational weather and climate models.

Bibliography

Andrews, T., J. M. Gregory, M. J. Webb, and K. E. Taylor, 2012: Forcing, feedbacks and climate sensitivity in CMIP5 coupled atmosphere-ocean climate models. *Geophys. Res. Lett.*, in press.

Avramov, A. and J. Y. Harrington, 2010: Influence of parameterized ice habit on simulated mixed phase arctic clouds. *J. Geophys. Res.*, **115**, D03 205.

Avramov, A., et al., 2011: Towards ice formation closure in Arctic mixed-phase boundary layer clouds during ISDAC. *J. Geophys. Res.*, **116**, D00T08.

Bender, F. A., 2008: A note on the effect of GCM tuning on climate sensitivity. *Env. Res. Lett.*, **3**, 014 001.

Bergeron, T., 1935: *On the physics of clouds and precipitation in Proces Verbaux de l'Association de Meteorologie*. Int. Union of Geodesy and Geophys., Paris, 156-178 pp.

Betts, A. K., 1973: Non-precipitating cumulus convection and its parameterization. *Q. J. R. Meteorol. Soc.*, **99**, 178–196.

Bodas-Salcedo, A., M. J. Webb, M. E. Brooks, M. A. Ringer, K. D. Williams, S. F. Milton, and D. R. Wilson, 2008: Evaluating cloud systems in the Met Office global forecast model using simulated CloudSat radar reflectivities. *J. Geophys. Res.*, **113**, D00A13.

Bony, S., et al., 2006: How well do we understand and evaluate climate change feedback processes? *J. Clim.*, **19**, 3445–3482.

Bouniol, D., et al., 2010: Using continuous ground-based radar and lidar measurements for evaluating the representation of clouds in four operational models. *J. Appl. Meteorol. Climatology*, **49**, 1971–1991.

Bowler, N. E., A. Arribas, K. R. Mylne, K. B. Robertson, and S. E. Beare, 2008: The MOGREPS short-range ensemble prediction system. *Q. J. R. Meteorol. Soc.*, **134**, 703–722.

Brown, B. G., G. Thompson, R. T. Bruintjes, R. Bullock, and T. Kane, 1997: Intercomparison of in-flight icing algorithms. Part II: Statistical verification results. *Wea. Forecasting*, **12**, 890–914.

Brown, P. R. A. and P. N. Francis, 1995: Improved measurements of the ice water content in cirrus using a total-water probe. *J. Atmos. Oceanic Technol.*, **12**, 410–414.

Cahalan, R. F., W. Ridgway, W. J. Wiscombe, T. L. Bell, and J. B. Snider, 1994: The albedo of fractal stratocumulus clouds. *J. Atmos. Sci*, **51**, 2434–2455.

Carey, L. D., J. Niu, P. Yang, J. A. Kankiewicz, V. E. Larson, and T. H. Vonder Haar, 2008: The vertical profile of liquid and ice water content in midlatitude mixed-phase altocumulus clouds. *J. Appl. Meteorol. Climatology*, **47**, 2487–2495.

Cober, S. G., G. A. Issac, A. V. Korolev, and J. W. Strapp, 2001: Assessing cloud phase conditions. *J. Appl. Meteorol.*, **40**, 1967–1983.

Cotton, R. J., et al., 2012: The effective density of small ice particles obtained from in situ aircraft observations of mid-latitude cirrus. *Q. J. R. Meteorol. Soc.*, **DOI: 10.1002/qj.2058**.

Crosier, J., et al., 2011: Observations of ice multiplication in a weakly convective cell embedded in supercooled mid-level stratus. *Atmos. Chem. Phys.*, **11**, 257–273.

Curry, J. A. and E. E. Ebert, 1992: Annual cycle of radiative fluxes over the Arctic Ocean: Sensitivity to cloud optical properties. *J. Clim.*, **5**, 1267–1280.

de Boer, G., E. W. Eloranta, and M. D. Shupe, 2009: Arctic mixed-phase stratiform cloud properties from multiple years of surface-based measurements at two high-latitude locations. *J. Atmos. Sci*, **66**, 2874–2887.

de Boer, G., H. Morrison, M. D. Shupe, and R. Hildner, 2011: Evidence of liquid dependent ice nucleation in high-latitude stratiform clouds from surface remote sensors. *Geophys. Res. Lett.*, **38**, L01 803.

Dee, D. P., et al., 2011: The ERA-Interim reanalysis: configuration and performance of the data assimilation system. *Q. J. R. Meteorol. Soc.*, **137 (656)**, 553–597.

Delanoë, J. and R. J. Hogan, 2008: A variational scheme for retrieving ice cloud properties from combined radar, lidar and infrared radiometer. *J. Geophys. Res.*, **113**, D07 204.

Delanoë, J., R. J. Hogan, R. M. Forbes, A. Bodas-Salcedo, and T. H. M. Stein, 2011: Evaluation of ice cloud representation in the ECMWF and UK Met Office models using CloudSat and CALIPSO data. *Q. J. R. Meteorol. Soc.*, **137**, 2064–2078.

Delanoë, J., A. Protat, J. Testud, D. Bouniol, A. J. Heymsfield, A. Bansemer, P. R. A. Brown, and R. M. Forbes, 2005: Statistical properties of the normalized ice particle size distribution. *J. Geophys. Res.*, **110**, D10 201.

Dessler, A. E., 2010: A determination of the cloud feedback from climate variations over the past decade. *Science*, **330**, 1523–1527.

Dufresne, J.-L. and S. Bony, 2008: An assessment of the primary sources of spread of global warming estimates from coupled atmosphere-ocean models. *J. Clim.*, **21**, 5135–5144.

ECMWF, 2010: IFS documentation - cy36r1, part IV: Physical processes. *http://www.ecmwf.int/research/ifsdocs/CY36r1/PHYSICS/IFSPart4.pdf*, 92.

Edwards, J. M. and A. Slingo, 1996: Studies with a flexible new radiation code. I: Choosing a configuration for a large-scale model. *Q. J. R. Meteorol. Soc.*, **122**, 689–719.

Field, P. R., A. J. Heymsfield, and A. Bansemer, 2006: Shattering and particle interarrival times measured by optical array probes in ice clouds. *J. Atmos. Oceanic Technol.*, **23**, 1357–1371.

Field, P. R., R. J. Hogan, P. R. A. Brown, A. J. Illingworth, T. W. Choularton, and R. J. Cotton, 2005: Parametrization of ice-particle size distributions for mid-latitude stratiform cloud. *Q. J. R. Meteorol. Soc.*, **131**, 1997–2017.

Field, P. R., R. J. Hogan, P. R. A. Brown, A. J. Illingworth, T. W. Choularton, P. H. Kaye, E. Hirst, and R. Greenaway, 2004: Simultaneous radar and aircraft observations of mixed-phase cloud at the 100 m scale. *Q. J. R. Meteorol. Soc.*, **130**, 1877–1904.

Findeisen, W., 1938: Kolloid-meteorologische vorgange bie neiderschlags-bildung. *Meteorol. Z.*, **55**, 121–133.

Fleishauer, R. P., V. E. Larson, and T. H. Vonder Haar, 2002: Observed microphysical structure of midlevel, mixed-phase clouds. *J. Atmos. Sci*, **59**, 1779–1804.

Fletcher, N. H., 1962: *The physics of rainclouds*. University Press, Cambridge.

Francis, P. N., P. Hignett, and A. Macke, 1998: The retrieval of cirrus cloud properties from aircraft multi-spectral reflectance measurements during eucrex'93. *Q. J. R. Meteorol. Soc.*, **124**, 1273–1291.

Fridlind, A. M., A. S. Ackerman, G. McFraquhar, G. Zhang, M. R. Poellot, P. J. DeMott, A. J. Prenni, and A. J. Heymsfield, 2007: Ice properties of single-layer stratocumulus during the Mixed-Phase Arctic Cloud Experiment (M-PACE): Part II: Model results. *J. Geophys. Res.*, **112**, D24 202.

Fridlind, A. M., B. van Diedenhoven, A. S. Ackerman, A. Avramov, A. Mrowiec, H. Morrison, P. Zuidema, and M. D. Shupe, 2012: A FIRE-ACE/SHEBA case study of mixed-phase Arctic boundary-layer clouds: Entrainment rate limitations on primary ice nucleation processes. *J. Atmos. Sci*, **69**, 365–389.

Gaussiat, N., R. J. Hogan, and A. J. Illingworth, 2007: Accurate liquid water path retrieval from low-cost microwave radiometers using additional information from a lidar celiometer and operational forecast models. *J. Atmos. Oceanic Technol.*, **24**, 1562–1575.

Gregory, D. and D. Morris, 1996: The sensitivity of climate simulations to the specification of mixed phase clouds. *Clim. Dyn.*, **12**, 641–651.

Gunn, K. L. S. and J. S. Marshall, 1958: The distribution with size of aggregate snowflakes. *J. Meteor.*, **15**, 452–461.

Hallett, J. and S. C. Mossop, 1974: Prodoction of secondary ice particles during the riming process. *Nature*, **249**, 26–28.

Harrington, J. Y., T. Reisin, W. R. Cotton, and S. M. Kreidenweis, 1999: Cloud resolving simulations of arctic stratus. Part II: Transition-season clouds. *Atmos. Res.*, **51**, 45–75.

Heymsfield, A. J. and D. G. Baumgardner, 1985: Summary of workshop on processing 2-d probe data. *Bull. Amer. Metoer. Soc.*, **66**, 437–440.

Heymsfield, A. J., P. R. Field, and A. Bansemer, 2008: Exponential size distributions for snow. *J. Atmos. Sci*, **65**, 4017–4031.

Heymsfield, A. J. and M. Kajikawa, 1987: An improved approach to calculating terminal velocities of plate-like crystals and graupel. *J. Atmos. Sci*, **144**, 1088–1099.

Hobbs, P. V. and A. L. Rangno, 1985: Ice particle concentrations in clouds. *J. Atmos. Sci*, **42**, 2523–2549.

Hogan, R. J., 2006: Fast approximate calculation of multiply scattered lidar returns. *Applied Optics*, **45**, 5984–5992.

Hogan, R. J., M. D. Behera, E. J. O'Connor, and A. J. Illingworth, 2004: Estimate of the global distribution of stratiform supercooled liquid water clouds using LITE lidar. *Geophys. Res. Lett.*, **31**, L05 106.

Hogan, R. J., P. R. Field, A. J. Illingworth, R. J. Cotton, and T. W. Choularton, 2002: Properties of embedded convection in warm-frontal mixed-phase cloud from aircraft and polarimetric radar. *Q. J. R. Meteorol. Soc.*, **128**, 451–476.

Hogan, R. J., P. N. Francis, H. Flentje, A. J. Illingworth, M. Quante, and J. Pelon, 2003a: Characteristics of mixed-phase clouds: Part I: Lidar, radar and aircraft observations from CLARE'98. *Q. J. R. Meteorol. Soc.*, **129**, 2089–2116.

Hogan, R. J., P. N. Francis, H. Flentje, A. J. Illingworth, M. Quante, and J. Pelon, 2003b: Characteristics of mixed-phase clouds: Part II: A climatology from ground-based lidar. *Q. J. R. Meteorol. Soc.*, **129**, 2117–2134.

Hogan, R. J., C. Jakob, and A. J. Illingworth, 2001: Comparison of ECMWF winter-season cloud fraction with radar derived values. *J. Appl. Meteorol. Climatology*, **40**, 513–525.

Hogan, R. J., M. P. Mittermaier, and A. J. Illingworth, 2006: The retrieval of ice water content from radar reflectivity factor and temperature and its use in evaluating a mesoscale model. *J. Appl. Meteorol.*, **45**, 301–317.

Houze, R. A., P. V. Hobbs, P. H. Herzegh, and D. B. Parsons, 1979: Size distribution of precipitation particles in frontal clouds. *J. Atmos. Sci*, **36**, 156–162.

Illingworth, A. J., et al., 2007: Cloudnet - continuous evaluation of cloud profiles in seven operational models using ground-based observations. *Bull. Amer. Metoer. Soc.*, **88**, 885–898.

Jiang, H., W. R. Cotton, J. O. Pinto, J. A. Curry, and M. J. Weissbluth, 2000: Cloud resolving simulations of mixed-phase arctic stratus observed during base: Sensitivity to concentration of ice crystals and large-scale heat and moisture advection. *J. Atmos. Sci*, **57**, 2105–2117.

Klein, S. A., et al., 2009: Intercomparison of model simulations of mixed-phase clouds observed during the ARM Mixed-Phase Arctic Cloud Experiment. I: Single-layer cloud. *Q. J. R. Meteorol. Soc.*, **135 (641)**, 979–1002, doi:10.1002/qj.416.

Korolev, A., 2007: Limitations of the Wegener-Bergeron-Findeisen mechanism in the evolution of mixed-phase clouds. *J. Atmos. Sci*, **64**, 3372–3375.

Korolev, A. and P. R. Field, 2008: The effect of dynamics on mixed-phase clouds: Theoretical considerations. *J. Atmos. Sci*, **65**, 66–86.

Korolev, A. and G. A. Issac, 2003: Phase transformations in mixed-phase clouds. *Q. J. R. Meteorol. Soc.*, **129**, 19–38.

Korolev, A. and G. A. Issac, 2005: Shattering during sampling by OAPs and HVPS. Part I: Snow particles. *J. Atmos. Oceanic Technol.*, **22**, 528–542.

Korolev, A. V., G. A. Issac, S. G. Cober, J. W. Strapp, and J. Hallett, 2003: Microphysical characterization of mixed-phase clouds. *Q. J. R. Meteorol. Soc.*, **129**, 39–65.

Korolev, A. V., G. A. Issac, J. W. Strapp, S. G. Cober, and H. W. Barker, 2007: In situ measurements of liquid water content profiles in mid-latitude stratiform clouds. *Q. J. R. Meteorol. Soc.*, **133**, 1693–1699.

Lawson, R. P. and P. Zuidema, 2009: Aircraft microphysical and surface-based radar observations of summertime arctic clouds. *J. Atmos. Sci*, **66**, 3505–3529.

Liu, X., S. Xie, and S. J. Ghan, 2007: Evaluation of a new mixed-phase cloud microphysics parameterization with CAM3 single-column model and M-PACE observations. *Geophys. Res. Lett.*, **34**, L23 712.

Locatelli, J. D. and P. V. Hobbs, 1974: Fall speeds and masses of solid precipitation particles. *J. Geophys. Res.*, **79**, 2185–2197.

Lock, A., 2007: *UM Version 6.3, Documentation Paper 24 The parametrization of boundary layer processes*. Met Office.

Lock, A. P., A. R. Brown, M. R. Bush, G. M. Martin, and R. N. B. Smith, 2000: A New Boundary Layer Mixing Scheme. Part I: Shceme Description and Single-Column Model Tests. *Mon. Wea. Rev.*, **128**, 3187–3199.

Lopez, P., 2002: Implementation and validation of a new prognostic large-scale cloud and precipitation scheme for climate and data-assimilarion purposes. *Q. J. R. Meteorol. Soc.*, **128**, 229–257.

Louis, J.-F., 1979: A parametric model of vertical eddy fluxes in the atmosphere. *Bound.-Layer. Meteor.*, **17**, 187–202.

Lynch, D. K., K. Sassen, D. O. Starr, and G. Stephens, (Eds.) , 2002: *Cirrus*. Oxford University Press, New York.

Marshall, J. S. and W. M. Palmer, 1948: The distribution of raindrops with size. *J. Meteor.*, **5**, 165–166.

Marsham, J. H., S. Dobbie, and R. J. Hogan, 2006: Evaluation of a large-eddy model simulation of a mixed-phase altocumulus cloud using microwave radiometer, lidar and Doppler radar data. *Q. J. R. Meteorol. Soc.*, **132**, 1693–1715.

Meyers, M. O., P. J. DeMott, and W. R. Cotton, 1992: New primary ice-nucleation parameterization in an explicit cloud model. *J. Appl. Meteorol.*, **129**, 2089–2116.

Mitchell, D. L., 1996: Use of mass and area-dimensional power laws for determining precipitation particle terminal velocities. *J. Atmos. Sci*, **53**, 1710–1723.

Mitchell, J. F. B., C. A. Senior, and W. J. Ingram, 1989: CO_2 and climate: a missing feedback? *Nature*, **341**, 132–134.

Morrison, A. E., S. T. Siems, and M. J. Manton, 2011a: A three year climatology of cloud-top phase over the southern ocean and north pacific. *J. Clim.*, **24**, 2405–2418.

Morrison, H., G. de Boer, G. Feingold, J. Harrington, M. D. Shupe, and K. Sulia, 2012: Resilience of persistent arctic mixed-phase clouds. *Nature Geoscience*, **5**, 11–17.

Morrison, H., M. D. Shupe, J. O. Pinto, and J. A. Curry, 2005: Possible roles of ice nucleation and ice nuclei depletion in the extended lifetime of arctic mixed-phase clouds. *Geophys. Res. Lett.*, **32**, L18 801.

Morrison, H., P. Zuidema, G. M. McFarquhar, A. Bansemer, and A. J. Heymsfield, 2011b: Snow microphysical observations in shallow mixed-phase and deep frontal arctic cloud systems. *Q. J. R. Meteorol. Soc.*, **137**, 1589–1601.

Moss, S. J. and D. W. Johnson, 1994: Aircraft measurements to validate and improve numerical model parameterizations of ice to water ratios in clouds. *Atmos. Res.*, **34**, 1–25.

O'Connor, E. J., A. J. Illingworht, and R. J. Hogan, 2004: A technique for autocalibration of cloud lidar. *J. Atmos. Oceanic Technol.*, **21**, 777–786.

Pinto, J. O., 1998: Autumnal mixed-phase cloudy boundary layers in the arctic. *J. Atmos. Sci*, **55**, 2016–2038.

Platt, C. M. R., 1973: Lidar and radiometric observations of cirrus clouds. *J. Atmos. Sci*, **30**, 1191–1204.

Probert-Jones, J. R., 1962: The radar equation in meteorology. *Q. J. R. Meteorol. Soc.*, **88**, 485–495.

Pruppacher, H. R. and J. D. Klett, 1978: *Microphysics of clouds and precipitation*. D. Reidel Publishing Company, Boston, USA.

Rauber, R. M. and A. Tokay, 1991: An explaination for the existence of supercooled water at the top of cold clouds. *J. Atmos. Sci*, **48**, 1005–1023.

Riihimaki, L. D., S. A. McFarlane, and J. M. Comstock, 2012: Climatology and formation of tropical midlevel clouds at the Darwin ARM site. *J. Clim.*, **25(19)**, 6835–6850.

Rogers, R. R. and M. K. Yau, 1988: *A Short Course in Cloud Physics*. Pergamon Press.

Rotstayn, L. D., B. F. Ryan, and J. J. Katzfey, 2000: A scheme for calculation of the liquid fraction in mixed-phase stratiform clouds in large-scale models. *Mon. Wea. Rev.*, **128**, 1070–1088.

Ryan, B. F., 2000: A bulk parameterization of the ice particle size distribution and the optical properties in ice clouds. *J. Atmos. Sci*, **57**, 1436–1451.

Senior, C. A. and J. F. B. Mitchell, 1993: Carbon dioxide and climate: The impact of cloud parameterization. *J. Clim.*, **6**, 393–418.

Shupe, M. D., 2011: Clouds at arctic atmospheric observatories. part II: Thermodynamic phase characteristics. *J. Appl. Meteorol. Climatology*, **50**, 645–661.

Shupe, M. D., P. Kollias, P. O. G. Persson, and G. M. McFarquhar, 2008a: Vertical motions in arctic mixed-phase stratiform clouds. *J. Atmos. Sci*, **65**, 1304–1321.

Shupe, M. D., S. Y. Matrosov, and T. Uttal, 2006: Arctic mixed-phase cloud properties derived from surface-based sensors at SHEBA. *J. Atmos. Sci*, **63**, 697–711.

Shupe, M. D., et al., 2008b: A focus on mixed-phase clouds. *Bull. Amer. Metoer. Soc.*, **89**, 1549–1562.

Simpson, J., C. Kummerow, W. K. Tao, and R. F. Adler, 1996: On the Tropical Rainfall Measuring Mission (TRMM). *Meteorology and Atmospheric Physics*, **60**, 19–36.

Smith, A. J., V. E. Larson, J. Niu, J. A. Kankiewics, and L. D. Carey, 2009: Processes that generate and deplete liquid water and snow in thin midlevel mixed-phase clouds. *J. Geophys. Res.*, **114**, D12 203.

Smith, R. N. B., 1990: A scheme for predicting layer clouds and their water content in a general circulation model. *Q. J. R. Meteorol. Soc.*, **116**, 435–460.

Stephens, G. L., et al., 2002: The CloudSat mission and the A-Train. *Bull. Amer. Metoer. Soc.*, **83**, 1771–1790.

Stokes, G. M. and S. E. Schwartz, 1994: The atmospheric radiation measurement (arm) program: Programmatic background and design of the cloud and radiation test bed. *Bull. Amer. Metoer. Soc.*, **75**, 1201–1221.

Strapp, J. W., F. Albers, A. Reuter, A. V. Korolev, U. Maixner, E. Rashke, and Z. Vukovic, 2001: Laboratory measurements of the response of a pms oap-2dc. *J. Atmos. Oceanic Technol.*, **18**, 1150–1170.

Sun, Z. and K. P. Shine, 1994: Studies of the radiative properties of ice and mixed-phase clouds. *Q. J. R. Meteorol. Soc.*, **120**, 111–137.

Sun, Z. and K. P. Shine, 1995: Parameterization of ice cloud radiative properties and its application to the potential climatic importance of mixed-phase clouds. *J. Clim.*, **8**, 1874–1888.

Sweby, P. K., 1984: High-resolution schemes using flux limiters for hyperbolic conservation-laws. *SIAM J. Numer. Analysis*, **21**, 995–1011.

Thuburn, J., 1997: TVD schemes, positive schemes, and the universal limiter. *Mon. Wea. Rev.*, **125**, 1990–1993.

Tompkins, A. M., 2002: A prognostic parameterization for the subgrid-scale variability of water vapor and clouds in large-scale models and its use to diagnose cloud cover. *J. Atmos. Sci*, **59**, 1917–1942.

Tripoli, G. J. and W. R. Cotton, 1981: The use of ice-liquid water potential temperature as the thermodynamic variable in deep atmospheric models. *Mon. Wea. Rev.*, **109**, 1094–1102.

Tselioudis, G. and C. Jakob, 2002: Evaluation of midlatitude cloud properties in a weather and a climate model: Dependence on dynamic regime and spatial resolution. *J. Geophys. Res.*, **107**, D244 781.

Tsushima, Y., et al., 2006: Importance of the mixed-phase cloud distribution in the control climate for assessing the response of clouds to carbon dioxide increase: a multi-model study. *Clim. Dyn.*, **27**, 113–126.

Vaillancourt, P. A., A. Tremblay, S. G. Cober, and G. A. Issac, 2003: Comparison of aircraft observations with mixed-phase cloud simulations. *Mon. Wea. Rev.*, **131**, 656–671.

van Diedenhoven, B., A. M. Fridlind, A. S. Ackerman, E. W. Eloranta, and G. M. McFarquhar, 2009: An evaluation of ice formation in large-eddy simulations of supercooled Arctic stratocumulus using ground-based lidar and cloud radar. *J. Geophys. Res.*, **114**, D10 203.

van Leer, B., 1974: Towards the ultimate conservative difference scheme. II: Monotonicity and conservation combined in a second order scheme. *J. Comput. Phys.*, **14**, 361–370.

Vidaurre, G. and J. Hallett, 2009: Ice and water content of stratiform mixed-phase cloud. *Q. J. R. Meteorol. Soc.*, **135**, 1292–1306.

Wandinger, U., 2005: Introduction to lidar. *Lidar: range resolved optical remote sensing of the atmosphere*, C. Weitkamp, Ed., Elsevier.

Warren, S. G., C. J. Hahn, J. London, R. M. Chervin, and R. L. Jenne, 1986a: Global distribution of total cloud cover and cloud type amounts over land. *NCAR Tech. Note, NCAR/TN-273+STR*.

Warren, S. G., C. J. Hahn, J. London, R. M. Chervin, and R. L. Jenne, 1986b: Global distribution of total cloud cover and cloud type amounts over the ocean. *NCAR Tech. Note, NCAR/TN-317+STR*.

Wegener, A., 1911: *Thermodynamik der Atmosphare*. J. A. Barth, Leipzig, Poland.

Westbrook, C. D., R. J. Hogan, and A. J. Illingworth, 2008: The capacitance of pristine ice crystals and aggregate snowflakes. *J. Atmos. Sci*, **65**, 206–219.

Westbrook, C. D. and A. J. Illingworth, 2009: Testing the influence of small crystals on ice size spectra using doppler lidar observations. *Geophys. Res. Lett.*, **36**, L12 810.

Westbrook, C. D. and A. J. Illingworth, 2011: Evidence that ice forms primarily in supercooled liquid clouds at temperatures $> -27^{\circ}$C. *Geophys. Res. Lett.*, **38**, L14 808.

Wilson, R. W. and S. P. Ballard, 1999: A microphysically based precipitation scheme for the UK Meteorological Office Unified Model. *Q. J. R. Meteorol. Soc.*, **125**, 1607–1636.

Winker, D., M. Vaughan, A. Omar, Y. Hu, K. Powell, Z. Lie, W. Hunt, and S. Young, 2002: Overview of the CALIPSO mission and CALIOP data processing algorithms. *J. Atmos. Oceanic Technol.*, **26**, 2310–2323.

Wood, R. and P. R. Field, 2000: Relationships between total water, condensed water and cloud fraction in stratiform clouds examined using aircraft data. *J. Atmos. Sci*, **57**, 1888–1905.

Yuan, J., Q. Fu, and N. McFarlane, 2006: Tests and improvements of gcm cloud parameterizations using cccma scm with the sheba data set. *Atmos. Res.*, **82**, 222–238.

Zhang, D., Z. Wang, and D. Liu, 2010: A global view of midlevel liquid-layer topped stratiform cloud distribution and phase partition from calipso and cloudsat measurements. *J. Geophys. Res.*, **115**, D00H13.

Zhang, M. H., et al., 2005: Comparing clouds and their seasonal variations in 10 atmospheric general circulation models with satellite measurements. *J. Geophys. Res.*, **110**, D15S02.